Contact Guidance During Breast Cancer Cell Dissemination

by

Kristen Elise Loesel

A dissertation submitted in partial fulfillment
of the requirements for the degree of
Doctor of Philosophy
(Cancer Biology)
in the University of Michigan
2023

Doctoral Committee:

Professor Ryoma Ohi, Chair
Associate Professor Brendon M. Baker
Professor Pedro Lowenstein
Professor Carole A. Parent

Kristen Elise Loesel

kloesel@umich.edu

ORCID iD: 0000-0002-5916-8460

Dedication

This dissertation is dedicated to my father and mother. I am continually grateful to have you as my parents.

Acknowledgements

First, thank you to all the mentors who have guided me throughout this journey. I am grateful to Carole for accepting me into her research lab and giving me the opportunity to work on this project. I would also like to thank my committee members: Ryoma Ohi, Brendon Baker, and Pedro Lowenstein. Thank you all for the valuable advice and guidance you have provided during my graduate training. I am also grateful for my undergraduate research mentors: Jay Scott, Costas Lyssiotis, and Luigi Franchi. Thank you all for taking me into your labs and encouraging me to continue pursuing research in graduate school.

I am very grateful to the current and past members of my lab: Dr. Shuvasree SenGupta, Dr. Cosmo Saunders, Dr. Song Chen, Dr. Subhash Arya, Peilin Shen, Dr. Fatima Javed, Dr. Lauren Hein, Yang Xu, Samantha Bebel, Emma Theisen, Ila Ghoshal, Nicole Zambrana-García, Christina Zheng, Rachael Baliira, Sam Collie, Megan Schafer, Joseph Serrenho, Dajia Wang, and Debatrayee Sinha. Sree, you welcomed me into the lab and always helped me when I needed advice. Thank you for your feedback on countless documents, experiments, and presentations, but more importantly thank you for being such a warm and supportive friend in and out of the lab. Peilin, thank you for your friendship and being such a light in our lab. Lauren and Fatima, thank you for your support and friendship. I am so grateful for all the advice and guidance throughout this journey. Sam, I am so grateful you joined our lab. Thank you for all the coffee walks and your friendship, especially in these last six months. Megan, thank you for all your help in the lab in the

last two years. You are such an enthusiastic and kind person, and I am so grateful to have had the opportunity to mentor you.

I would also like to thank the current and past administrators and directors of the Cancer Biology graduate program: Dawn Storball, Chanise Holmes, Sam Wilhelmi, Beth Lawlor, David Lombard, and Costas Lyssiotis.

Also, I am very grateful to Brendon Baker for allowing me to work in his lab and for helping me troubleshoot problems with the fiber mats. In addition, I would like to thank Harrison Hiraki, a graduate student in the Baker lab, for teaching me to electrospin and with Chapter 2 of this thesis. To am also grateful for the extensive advice and insight from Pierre Coulombe on the work in Chapter 3 of this thesis.

I would like to thank all my friends who have supported me in this journey. I am continually grateful to have started graduate school with five amazing scientists: Rachael Baliira, Daniel Salas-Escabillas, Brittany Salazar, Katelyn Donahue, and Catherine Redmond. Rachael, thank you for all of the laughter and love. You have taught me so much, and I am so thankful to have you in my life. Brittany, thank you for hosting so many gatherings and for your continued friendship. Katelyn, thank you for always being there for me and making me smile. Daniel, you are one of the kindest and most supportive people I have ever met. Thank you for coordinating so many get together and for being such a wonderful friend.

Lastly, I am continually grateful to my family for their support and love. I am so thankful to my parents, Lisa and Phil, for everything they have taught me and always being there for me. Thank you to my siblings Jeremy, Jennifer, David, and Michelle. Thank you for all the get-togethers and phone calls. I am grateful to have such a close family. I am so grateful to also be a part of the Maurer family. I am especially thankful to Carol and Kevin for welcoming me into their

family. I want to end by thanking my husband Ethan for always supporting me in my goals. Ethan, you are the most selfless, kind, funny, smart, loving person I have ever met. I cannot thank you enough for your support on this journey. I am forever grateful to have you by my side.

Table of Contents

List of Figures

Abstract

Cancer invasion and metastasis are major life-threatening events in patients with cancer, yet the mechanisms by which cancer cells invade neighboring tissues remain poorly understood. It has been demonstrated that physical features of the dysregulated tumor extracellular matrix (ECM), such as fiber alignment, influence invasion phenotypes. Cells can polarize and migrate along aligned architectures, such as collagen fibers, through a process called contact guidance. In this dissertation, we investigate the mechanisms by which collectively migrating cancer cells sense and respond to fiber alignment.

This dissertation examines how collectively migrating breast cancer cells sense fibrous topographies. Chapter 2 details an adaptable collective cell migration assay we developed to study the effects of synthetic, electrospun fibers on collective migration behaviors. First, we described how to fabricate electrospun fiber mats using dextran vinyl sulfone (DexVS). Next, we describe a collective migration assay using cancer cell spheroids and DexVS fiber matrices. To quantify the migration phenotypes, we outlined the MATLAB code we developed to track cell migration over time. To demonstrate the capabilities of our system, we analyzed the collective migration behavior of an invasive breast cancer cell line on fibers oriented parallel to each other or randomly distributed. We explained how to calculate several migration parameters including cell speed, distance traveled, and directionality. In addition, we calculated the dispersal of individual cells from the migrating sheet and compared the migration phenotypes between individual cells and collectively migrating cells. Lastly, we report how to determine protein localization and expression after migration on fiber mats.

In chapter 3, we investigated the role of RhoA GTPase, a key regulator of the cytoskeleton and actomyosin contractility, during collective contact guidance. Our studies demonstrate that RhoA is crucial in the control of contact guidance in collectively migrating breast cancer cells by regulating cell-ECM and cell-cell adhesions. Using the methods outlined in Chapter 2, we found that the loss of RhoA resulted in decreased contact guidance and fractured cell-cell junctions in collectively migrating cells. We identified ROCK, a well-characterized RhoA effector, as being partially responsible for these effects. Notably, we determined that RhoA was dispensable for contact guidance in single cell migration. Additionally, we found that the loss of RhoA resulted in decreased focal adhesion lifetime during collective migration. Lastly, we discovered that RhoA was crucial for proper formation of both adherens junctions and desmosomes, two types of epithelial cell junctions.

Together, this dissertation provides a novel understanding of how cancer cells sense biophysical cues during invasive migration and moreover, uncovers a novel role for RhoA GTPase signaling during collective contact guidance.

Chapter 1 Introduction

1.1 The extracellular matrix in normal and malignant tissue

The extracellular matrix (ECM) is a dynamic network of macromolecules surrounding cells within all tissues[1,2]. The ECM provides structural support within tissues while also playing a key role in regulating tissue homeostasis by influencing events such as proliferation, growth, and differentiation[3,4]. The ECM is composed of a complex network of structural proteins (including collagens and elastin), glycoproteins (including laminin, proteoglycans, and fibronectin), growth factors, and enzymes[5]. These components are abundantly spread throughout the ECM and often crosslinked to form the meshwork of the tissue. There are two main types of ECM matrices, the basement membrane and the interstitial matrix[6]. In healthy tissue, the basement membrane is a well-organized and dense matrix found on the basal side of epithelial sheets and is necessary for tissue polarity, whereas the interstitial matrix constitutes the majority of the tissue stroma providing structural support for cells. ECM organization and composition are tightly regulated to maintain tissue homeostasis, and thus dysregulated ECM remodeling is associated with many pathological conditions, including cancer and fibrosis[7].

Collagens constitute the majority of ECM proteins with over 30% of the ECM being composed of collagens, specifically collagen type I, II, and III[8,9]. A total of 28 types of collagen have been identified in vertebrates, and each type is made up of either homotrimers or heterotrimers[10,11]. Collagens can be broadly divided into two groups based on their supramolecular organization, fibrillar and nonfibrillar collagens. Fibrillar collagens (types I, II, III, V, XI, XXIV and XXVII) form elongated fibril structures that create 3D networks and

provide mechanical support to a tissue[12]. Type I collagen, a fibrillar collagen, makes up more than 90% of the collagen molecules in the body, and it is a principal component of interstitial matrices found in organs and connective tissues like skin, tendons, and mammary glands. Type IV collagen is a non-fibrillar collagen that is an essential component of the basement membrane. Collagens are produced and secreted into the ECM by fibroblasts, osteoblasts, chondrocytes, and some types of epithelial cells. The ECM undergoes continuous remodeling to ensure that tissues retain their structure and ability to function properly, including breaking down old collagens that need to be replaced with newly synthesized collagens[7].

The composition of the ECM varies from tissue to tissue and during tissue state transitions, such as during development or pathological progression[13,14]. During many diseases, including cancer, ECM components can have disrupted expression, altered turnover, or aberrant posttranslational modifications[7,15]. Many solid cancers, including pancreas and breast, are associated with a dense, fibrotic ECM, termed desmoplasia[16,17]. Desmoplasia is often due to an increased deposition of fibrous collagen, specifically type I collagen, which leads to an increase in tissue stiffness. In pancreatic cancer, chemoresistance is attributed to the highly desmoplastic tumor microenvironment which prevents the distribution of therapeutic agents[18,19].

In breast cancer, the ECM displays significant changes compared to healthy mammary tissue, including the upregulation of fibrillar collagens (I, III, V), hyaluronan, and matricellular proteins such as thrombospondin-1 and tenascin C (**Figure 1.1**). Additionally, during the progression of breast cancer there is a decreased expression of collagen IV, which is mainly due to the degradation of the basement membrane surrounding the breast epithelium by remodeling enzymes such as matrix metalloproteinases (MMPs)[20]. The heavy deposition of fibrous collagen within the ECM causes tissue stiffness to increase by over 10-fold compared to normal stroma[21].

Elastin and collagen molecules can be crosslinked by lysyl oxidase (LOX) and lysine hydroxylases, which are both frequently overexpressed in cancer, leading to an increase in ECM stiffness and promotion of cancer progression[22,23].

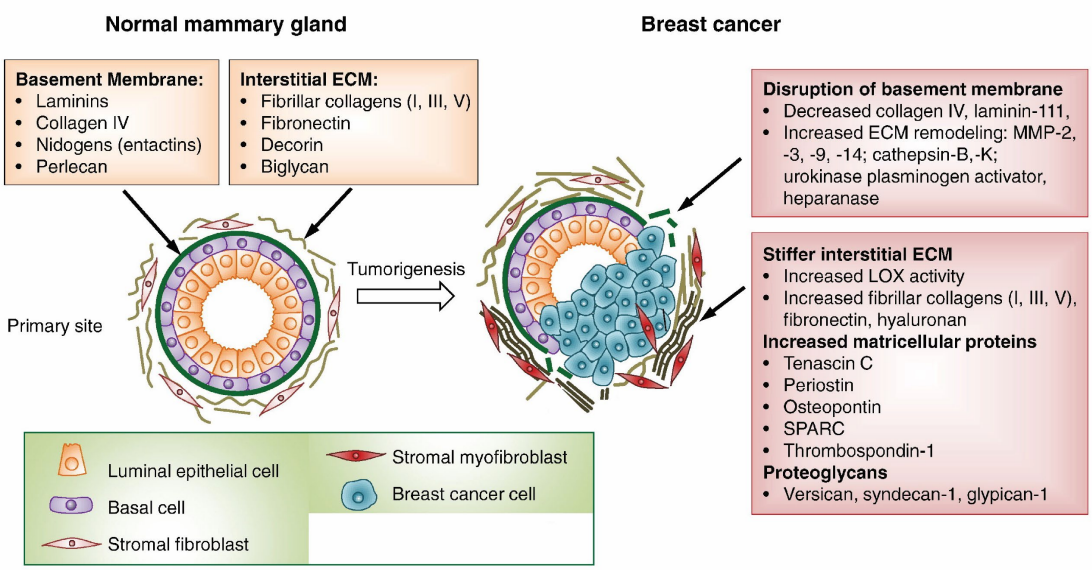

Figure 1.1 Extracellular matrix remodeling during breast cancer progression.

The normal mammary gland consists of two main types of epithelia, luminal and basal epithelium. The luminal epithelium forms the inner layer of the mammary ducts while the basal epithelium, consisting of myoepithelial cells, forms the outer layer of the duct. A basement membrane surrounds the ducts separating the stroma from the epithelium. During breast cancer progression, often the basement membrane is disrupted, and the interstitial matrix stiffness is greatly increased which promotes tumor aggressiveness. These ECM changes are often due to excessive fibrillar collagen and fibronectin deposition, decreased collagen IV deposition, and the upregulation of ECM remodeling enzymes such as lysyl oxidases (LOXs) and matrix metalloproteinases (MMPs). (Modified from Insua-Rodríguez *et al*., *Adv Drug Deliv Rev*, 2016.)

Desmoplasia not only increases tissue stiffness but also creates distinct structural patterns in the tumor microenvironment termed tumor-associated collagen signatures (TACS) [24,25]. TACS were originally observed in murine mammary carcinoma tissue to describe zones within a tumor that share distinct collagen architectures. TACS-1, characterized by dense collagen surrounding the tumor, are observed at small tumor regions, while TAC-2 and TACS-3 are indicative of invasive tumors (**Figure 1.2**). Specifically, TACS-2 describes collagen fibers which lie parallel to the tumor mass, while TACS-3 indicates the presence of radially aligned collagen fibers. These structural patterns help facilitate the directional invasion of cancer cells into and through the stroma, a critical first step in metastasis[24,26]. Since the identification of TACS features in

breast cancer, similar collagen architectures have been observed in melanoma[27], lung cancer[28], pancreatic cancer[29–31], and prostate cancer[32,33]. Additionally, TACS have been used clinically as an prognostic marker due to the now well-established association between prognosis and primary tumor architectures[34–38].

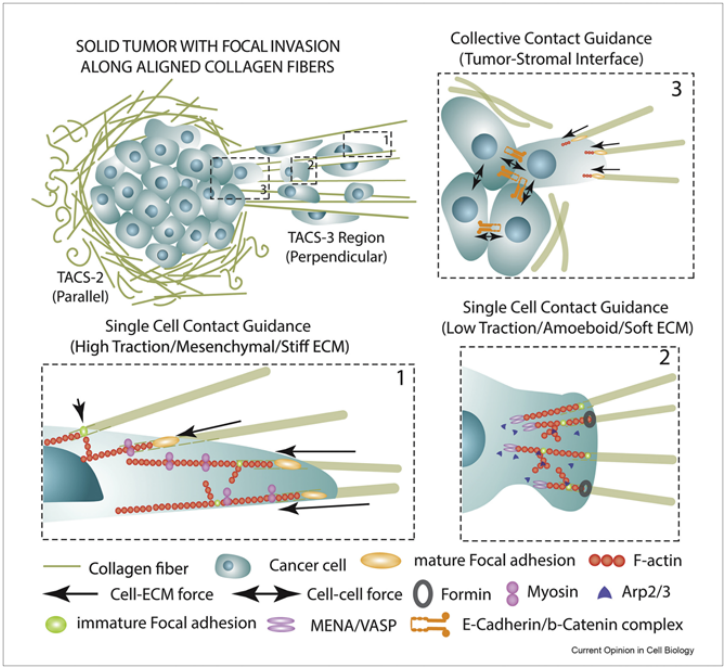

Figure 1.2 Tumor-associated collagen signatures (TACS) describe distinct collagen architectures often observed in invasive cancer tissue.

Schematic illustrates a solid tumor mass surrounded by both parallel collagen fibers (TACS-2) and perpendicularly aligned collagen fibers (TACS-3). Using the aligned collagen fibers, cancer cells are able to directionally migrate away from the primary tumor. Magnified region 1 shows a mesenchymal cancer cell migrating along an aligned fiber with constrained focal adhesions and a polarized actin cytoskeleton. Magnified region 2 depicts a cancer cell migrating using a low traction, amoeboid migration mode. Magnified region 3 illustrates collectively migrating cancer cells at the tumor-stroma interface intricately balancing cell-cell and cell-ECM interactions to navigate the complex fiber networks. (Modified from Ray et al., *Curr. Opin. Cell Biol.,* 2021.)

1.2 Contact guidance

Extracellular mechanical cues, such as stiffness and topography, are increasingly recognized as powerful signals that can drastically alter cell growth, differentiation, and migration[39]. Within the tumor ECM, collagen alignment has been shown to drive the directed migration of cancer cells along aligned ECM fibers in a process known as contact

guidance[24,40,41]. Contact guidance refers to the ability of cells to polarize and migrate along anisotropic architectures, such as aligned collagen fibers[42].To investigate the mechanisms of how cells sense contact guidance cues, researchers have developed a wide range of microfabricated systems, such as microprinted lines and nanoridges, to mimic specific ECM structures[43]. Most of the work studying contact guidance has been performed using these *in vitro*, 2D models to create a highly controlled and structurally defined environment[44].

The concept of contact guidance was first proposed by Paul Weiss in 1941[45], and since then three primary theories have been postulated to explain contact guidance-mediated migration. First proposed by Dunn and Heath in 1976, the mechanical restriction theory proposed that the shape of the substrate imposes limits on the formation of the actin cytoskeleton[46]. They theorized that actin filaments are fairly inflexible, so curved substrates lead to shortened actin protrusions that have insufficient traction and thus inhibit cell polarity. Accordingly, it has been shown that filopodia, thin actin-rich protrusions, sense topographies through anisotropic force generation, and on nanoridges, filopodia prefer to align with the nanoridges[47–51].

While the mechanical restriction theory provided insight into how cells sense a single topographical feature, it does not explain how cells will react to continuous topographies such as aligned grooves. Therefore, Ohara and Buck proposed the focal adhesion restriction theory in 1979 using various cell types and grooved substrates. Focal adhesions are mechanosensitive, multiprotein complexes that connect the actin cytoskeleton to an extracellular substrate, and therefore, they are crucial for substrate sensing. Observing that cell-substrate interactions were confined to the surfaces of the ridges, they suggested that forming longer and larger focal adhesions allows for greater cell adhesion and thus, cells may favor developing focal adhesions

parallel to grooves[52]. In support of this hypothesis, recent work demonstrates that focal adhesions mature in an anisotropic fashion along aligned architectures causing a subsequent alignment of the actin cytoskeleton[53–55]. However, studies have observed the maturation of focal adhesions both parallel and perpendicular to substrate orientation[56,57], though perpendicular adhesions have been demonstrated to be less stable than parallel focal adhesions[58]. It is still to be determined whether these focal adhesion patterns promote contact guidance or are a result of contact guidance. Lastly, in 1990 Curtis and Clark built upon both of these theories by proposing the discontinuity theory[59]. They asserted that discontinuities, such as microgroove edges or steep curvatures, induce actin condensation leading to focal adhesion formation and cell polarization at these sites. This hypothesis has been supported by other work from the 1990s which observed rapid actin condensation at substrate edges[57,60]. The signaling pathways controlling contact guidance have yet to be fully elucidated, largely due to the variety of cell migration modes and diverse substratum conditions. Yet, generally focal adhesions, actin protrusions, and contractility all play crucial roles during contact guidance sensing.

1.3 Directed Cell Migration: Mechanisms and Modes

Directed cell migration is a complex cell behavior that is crucial for a variety of physiological processes such as embryonic development, angiogenesis, immune response, and wound healing. Additionally, cancer cells utilize these morphogenetic programs to migrate throughout the body during cancer invasion and metastasis[61,62]. Directed cell migration requires coordination between numerous signaling pathways to execute a dynamic reorganization of the cytoskeleton and the formation of cell-matrix adhesions[63–65]. Cells can sense a variety of cues within the ECM including chemical signals (such as chemokines and secreted proteins) as well as physical cues (such as stiffness, topology, and porosity) which all lead to directional

migration[65]. Generally, cells can either move individually (amoeboid or mescheymal migration) or collectively (in strands, sheets, or clusters); however, the exact mechanisms distinguishing these different modes are not fully understood[66].

During migration, all cells exhibit both adhesion and contractility, but the mechanisms regulating these steps are highly dependent on the type of migration mode. Single cell migration can be generally classified into two modes of migration, mesenchymal and amoeboid, though changes in the cell's environment can highly influence the migration phenotype[66,67]. Amoeboid migration generally refers to a type of rapid cell migration characterized by a rounded cell morphology, low traction force generation, and a lack of mature focal adhesions and stress fibers[68,69]. Amoeboid cells generate adhesions that are non-integrin or weak integrin mediated which facilitate faster migration[70]. Many immune cells and the social amoeba *Dictyostelium discoideum* use an amoeboid migration mode which allows for rapid cell shape changes and protease independent migration in 3D matrices. On the other hand, fibroblasts and many cancer cells migrate using a mescheymal migration mode which is characterized by stable integrin-based adhesions and higher traction force generation compared to amoeboid cells[71]. These cells adopt elongated, spindle-like morphology with well-defined front and back polarity[72]. The signaling pathways that regulate migration phenotypes vary between migration modes, but alterations in these signaling pathways allow cells to switch modes. For example, either the suppression of integrin signaling or confinement allows for a switch from a mesenchymal migration to amoeboid migration[73]. Conversely, inhibition of Rho/ROCK signaling can switch amoeboid-like melanoma cells toward a mesenchymal morphology[74].

Cell migration involves a series of coordinated events that can be generally categorized into four phases: polarization, protrusion, adhesion, and contractility. These cycles are

continuously repeated to allow for directional migration and occur simultaneously. To initiate directional migration, a cell must first establish polarity in response to an external stimulus, such as a mechanical or chemical cue. Polarization creates distinct leading and trailing edges and is mediated by a network of signaling molecules including small GTPases Rac1 and Cdc42[75,76]. After establishing polarity, Rac1 then stimulates WAVE and Arp2/3, central actin nucleators, to polymerize actin at the leading edge[77]. The branched polymerizing actin structures, termed lamellipodia, push against the cell membrane inducing membrane protrusions[78–80]. The protrusions are stabilized by binding to nascent adhesions which link the cell to the substrate. Cellular adhesion and traction primarily rely on integrins, which are transmembrane receptor molecules that form heterodimers and attach to ECM proteins[81]. Immature, nascent adhesions can mature into larger and more stable structures termed focal adhesion complexes, usually upon RhoA activation or due to external tension force[82–85]. Focal adhesions not only serve as cellular mechanosensors but also as traction sites where cells can generate the necessary tensional forces to propel the cell body forward[86]. Contraction forces are generated by myosin motors that bind and contract actin filaments leading to forward movement[87,88]. Myosin II activity is controlled by the activity of a number of kinases including Rho-associated protein kinase (ROCK) and myosin light-chain kinase (MLCK)[89]. Adhesions are dissembled at the leading edge and the rear of the cell through the activity of focal adhesion kinase (FAK) and Src[90]. Adhesion disassembly at the rear is necessary for the translocation of the cell and regulated by myosin II dependent actin contractility[91]. These repeated cycles of protrusions, formation of adhesion complexes, and retractions characterize cell migration.

1.4 Cancer Invasion and Collective Migration

It has been demonstrated that the majority of solid cancers, including breast cancers, use collective migration strategies during metastasis[92–94], which often make them more metastatic compared to single tumor cells[95,96]. During cancer invasion, the first step of metastasis, carcinoma cells acquire a migratory phenotype which allows them to cross the basement membrane and invade the surrounding tissue stroma (**Figure 1.3**)[97,98]. The term collective invasion encompasses numerous morphological phenotypes such as multicellular strands (with or without a lumen), small clusters, blunt protrusive strands with no discernable leader cells, and amoeboid-like multicellular streams with loose cell-cell adhesions[62]. The diversity of migration

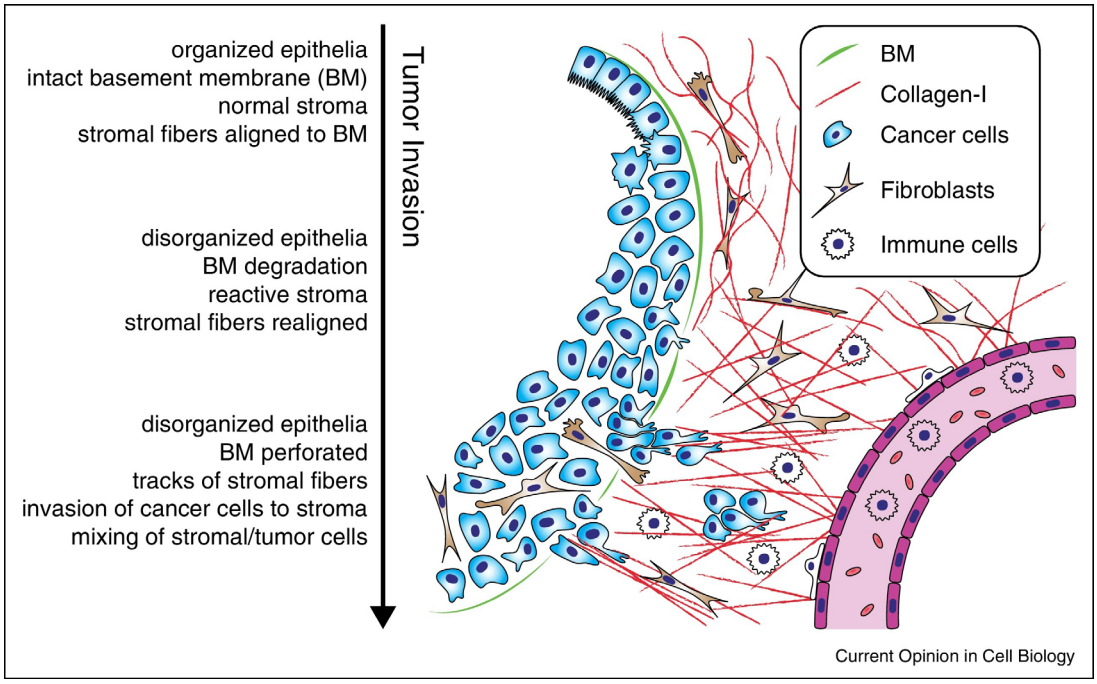

Figure 1.3 General steps of epithelial cancer cell invasion into stroma.

Schematic first illustrates carcinoma in situ, which is the first stage of cancer growth where tumor cells are proliferating but encapsulated by the basement membrane. During cancer progression, cancer cells become disorganized, often losing apical-basal polarity and gaining migratory abilities. At this stage, tumor cells can cross the basement membrane and migrate into the tumor stroma. Tumor stroma often displays greater numbers of immune cells and fibroblasts as well as changes to collagen networks that can facilitate the migration of cancer cells. (Modified from Clark et al. Curr. Opin. Cell Biol., 2015).

strategies highlights the fundamental ability of cancer cells to adapt to their environmental conditions.

Collective migration is the cohesive and coordinated movement of multicellular groups in response to local chemical and mechanical signals[99,100]. Collective migration is essential for many normal cellular processes including wound healing and embryonic development as well as pathological conditions such as cancer metastasis[94,101–103]. Compared to single cell migration, collectively migrating cells display more efficient directional migration due to soluble and contact-mediated interactions between cells within the tissue. Similar to front-rear polarity in single cell migration, migrating cell sheets often display a tissue-scale polarization with distinct populations of leader and follower cells[104–106]. Follower cells compose the major cell population within the sheet and migrate at low speeds behind leader cells[107]. At the leading edge, leader cells display polarized actin protrusions and sense changes within the ECM. Leader-follower kinetics rely on strong cell-cell adhesions to promote persistent directional migration[108–110]. In fact, collective migration involves a complex interplay between cell-matrix and cell-cell interactions, both of which are crucial for proper directional migration.

Throughout collective migration, cells maintain close contact with each other through intercellular junctions. Stable cell-cell junctions provide coordinated cytoskeletal activity between neighboring cells and therefore are crucial for cell sheet polarization[111]. There are four main types of intercellular junctions: adherens junctions, tight junctions, gap junctions, and desmosomes[112–114]. Tight junctions promote the maintenance of apical-basal polarity as well as regulating the paracellular transport of ions and solutes[115]. Gap junctions contain channels that allow for passive movement of molecules between neighboring cells[116]. Finally, adherens

junctions and desmosomes anchor neighboring cells to each other, linking the actin and intermediate filament cytoskeletons, respectively[117].

Adherens junctions are composed of classical cadherins, such as E-cadherin and N-cadherin, and cytoplasmic catenin family members, including p120-catenin, β-catenin, and α-catenin[118]. Cadherins link the plasma membranes of neighboring cells through homophilic interactions[119]. Their cytoplasmic domains bind catenins which in turn associate with a variety of other molecules including the actin cytoskeleton and cytoskeletal regulators[120]. E-cadherin, a member of the classical calcium-dependent cadherin family, mediates cell-cell adhesion in epithelial tissues and is the best characterized marker of epithelial tissues. E-cadherin not only plays a role in adhesion between adjacent cells, but it is also critical for the sensing of mechanical tension within an epithelial tissue[121,122]. In addition to serving as a critical regulator of tissue homeostasis and morphogenesis[123], E-cadherin has been implicated as a tumor suppressor for decades[124–126]. In fact, the progression of breast cancer is often correlated with the downregulation or loss of E-cadherin expression[126–130]. Additionally, E-cadherin expression is lost in over 85% of invasive lobular mammary carcinomas[131,132].

Desmosomes are calcium-dependent, intercellular junctional complexes which link the intermediate filament cytoskeleton between neighboring cells[133,134]. Desmosomes provide strong cell-cell adhesion and thus are essential in tissues which undergo large amounts of mechanical strain, such as the epidermis and heart[134,135]. In addition to providing adhesion, desmosomes are signaling scaffolds for proliferation and differentiation[136,137]. Desmosomes are composed of three major gene families: armadillo proteins (plakophilins and plakoglobin), desmosomal cadherins (desmogleins and desmocollins), and plakin proteins (desmoplakin, plectin, envoplakin, and periplakin)[138–140]. Desmoglein and desmocollin heterodimers create the fundamental adhesive

unit between neighboring cells. Plakoglobin or plakophilins bind to the cytosolic domains of desmosomal cadherins via their N terminus and to plakin family members at their C terminus[141]. Plakophilins and plakogoblin directly interact with plakins, notably desmoplakin, which mediate the binding of the junction to the intermediate filament cytoskeleton. Though dysregulation of desmosomes are often linked to heart and skin diseases, desmosome family members, including desmosomal cadherins and armadillo protein family members, have been shown to act as tumor suppressors or oncogenes in various cancer types[142].

1.5 Rho GTPase regulation and effectors

The Rho-family of GTPases, a member of the Ras superfamily of small GTPases, contributes to several important cellular processes including cell migration, actin dynamics, microtubule organization, cell polarity, and regulation of gene expression[143], and many of the Rho GTPases have been implicated in the regulation of cancer progression[144–146]. Rho-family GTPases are found in all eukaryotes and are highly conserved[147]. In humans, there are 20 Rho-family GTPase family members which can be divided into eight subfamilies and classified as either typical or atypical depending on their regulation[148]. Like Ras proteins, typical Rho-family members cycle between an inactive GDP-bound form and an active GTP-bound form and are regulated by GTPase activating proteins (GAPs) and guanine nucleotide exchange factors (GEFs) (**Figure 1.4**). Conversely, atypical Rho family members do not follow the classical GTPase cycling and have unique regulatory mechanisms[149]. Within the Rho family, three typical Rho GTPases, Rac1, Cdc42, and RhoA, have been best characterized due to their ubiquitously high expression and critical roles in the regulation of the actin cytoskeleton[150].

Rho family members share about 30% identity in amino acid sequence with Ras proteins and between 40-95% identity with other family members[151]. All Rho family members contain

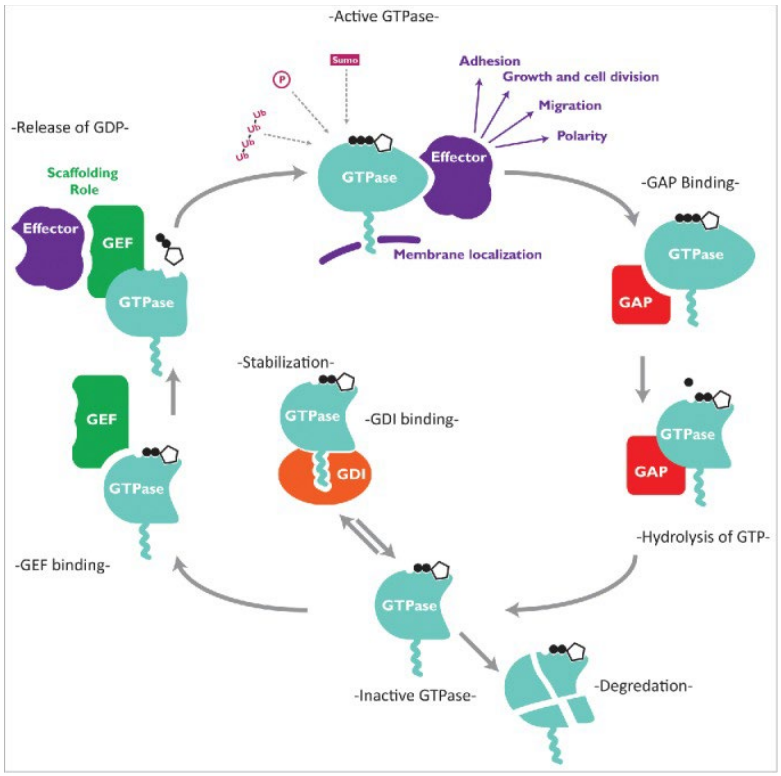

Figure 1.4 The typical Rho GTPase cycle is regulated by RhoGEFs, RhoGAPs, and RhoGDIs which alter protein localization and activity.

The binding of inactive Rho proteins to guanine nucleotide exchange factors (GEFs) results in the exchange of GDP for GTP. This exchange leads to protein activation and effector binding which mediates many cellular processes including adhesion, growth, and polarity. Binding with a GTPase activating protein (GAPs) increases the intrinsic hydrolytic GTPase activity of the protein thus promoting GDP-bound forms and ending signaling. Inactive GTPases can either be targeted for degradation or stabilized by binding to guanine disassociation inhibitors (GDIs). (Modified from Porter et al., *Small GTPases*, 2016.)

three amino acid sequence elements: a conserved G domain, a carboxyl-terminal hypervariable region, and core effector domain[143] (**Figure 1.5**). The highly conserved G-domain includes five consensus GDP/GTP binding motifs (G1 to G5) that are crucial for nucleotide binding and hydrolysis[152]. The second element, the core effector domain, corresponds to sequences that are involved in the interactions with downstream effector proteins. Lastly, all family members have a C-terminal hypervariable region which ends with a CAAX tetrapeptide motif (C: cysteine; A: an aliphatic amino acid; and X: a terminal amino acid)**.** The cysteine residue in the CAAX motif undergo a series of posttranslational modifications including prenylation (geranylgeranyl or farnesyl isoprenoid lipid), carboxyl methylation, and palmitoylation[153]. These modifications

enhance the association of Rho family members with the plasma membrane and/or endomembranes[154]. These lipid modifications allow typical Rho GTPases to bind to the appropriate lipid molecules on membranes which is required for their biological activity.

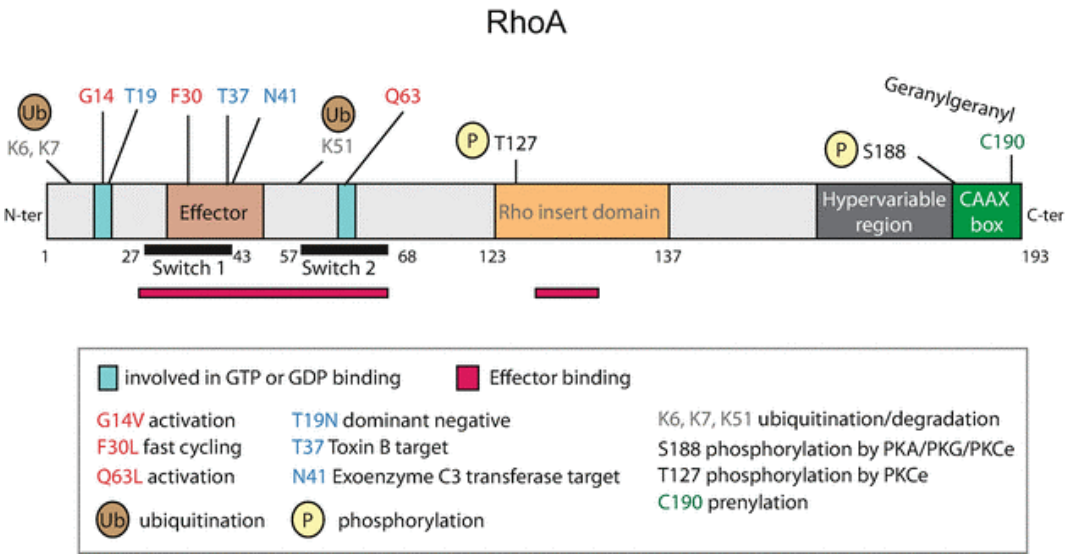

Figure 1.5 RhoA GTPase domains, important residues, and sites for posttranslational modifications.

Like other Rho family members, RhoA contains three main amino acid sequence elements: a conserved G domain, a carboxyl-terminal hypervariable region, and a core effector domain. RhoA mutations can result in the production of constitutively active proteins as well as dominant negative proteins depending on the residue. RhoA is regulated through phosphorylation, ubiquitination, and prenylation at multiple sites. (Modified from Orgaz et al., *Encyclopedia of Signaling Molecules*, 2018.)

Typical Rho GTPases are activated by GTP binding, causing a conformational change that enables their interaction with a wide range of downstream effector proteins[155]. Three unique types of regulatory proteins are responsible for controlling the GDP/GTP cycling of Rho family proteins: GTPase activating proteins (GAPs); guanine nucleotide exchange factors (GEFs); guanine nucleotide-disassociation inhibitors (GDIs)[156–158]. GEFs catalyze the exchange of bound GDP to GTP thereby activating the GTPase[159,160]. Conversely, GAPs stimulate the endogenous GTP hydrolysis activity of the GTPase promoting the formation of inactive, GDP-bound protein[161]. Rho GDIs regulate Rho GTPase activity by binding to the C-terminal prenyl group and sequestering them in the cytosol away from their sites of action at membranes[162,163]. Since free prenylated Rho GTPases are unstable in the cytosol, RhoGDI binding protects Rho GTPases

from degradation by the proteosome, therefore maintaining a stable pool of inactive Rho GTPases in the cytosol[164]. In mammals, there are over 80 RhoGEFs, 70 RhoGAPs, and 3 GDIs that have been identified, each with varying affinities for the unique Rho GTPases, thereby highlighting the complexities of Rho GTPase regulation[165]. Unlike Ras proteins, Rho GTPases are rarely mutated in cancer, instead their expression or activity are dysregulated[148,166]. In many cancers, the expression of GEFs, GAPs, and GDIs are altered leading to the dysregulation of Rho family members[159,167].

1.6 RhoA in healthy tissue and cancer

At this time, the Rho GTPase superfamily contains 20 family members which can be divided into eight subfamilies based on protein structure and function[168]. The Rho subfamily includes RhoA, RhoB, and RhoC which share about 85% identity in amino acid sequence with the majority of divergence in identity around the C-terminus[168]. All three subfamily members have been shown to regulate actin assembly[169,170], however recent studies have uncovered various functional differences as well as differences in cellular localization between subfamily members[171,172]. RhoA is the most well-characterized Rho subfamily member, and is known to directly bind 11 effector proteins including Rho-associated kinase (ROCK1/2), the myosin phosphatase-targeting subunit 1 of myosin light chain (MLC) phosphatase, mDia, Protein kinase N (PKN), Citron, Citron-kinase, Rhotekin, and Rhophilin[168].

RhoA is well known to induce cellular contractility through the activation of its major downstream effector ROCK1/2[173]. ROCKs are multifunctional serine/threonine kinases and the most well-characterized effectors of RhoA[174]. ROCKs enhance actin-myosin contractile force generation by phosphorylating a variety of downstream targets including myosin light chain 2 (MLC2)[175,176], LIM kinases[177,178], and the myosin binding subunit of myosin light chain

phosphatase 1 (MYPT1)[179], thereby regulating numerous cellular events including cell proliferation, cytokinesis, polarity, survival, and adhesion[180–182]. In addition, ROCKs are known to regulate microtubule and intermediate filament stability and formation[183–187]. ROCK has two isoforms, ROCK1 and ROCK2, which are encoded by two separate genes, *ROCK1* and *ROCK2*[188]. ROCK 1 and ROCK 2 share 92% amino acid identity in their kinase domain and 65% homology in their overall amino acid sequences[189–191], though they also have unique functions[192–194]. Both ROCK1 and ROCK2 have an N-terminal catalytic kinase domain, a central coiled-coil domain which contains a Rho binding domain (RBD) binding domain, and a C-terminal PH domain[195]. The RBD exclusively binds to GTP-bound RhoA, RhoB, and RhoC.

Rho GTPases play a critical role in the regulation of various signaling pathways that are critical for the maintenance of healthy tissues, but also fundamental for cancer development[196–198]. These pathways include cell proliferation, growth, migration, and survival[148]. Unlike Ras GTPases which are mutated in 15-30% of human tumors[199], Rho GTPases are generally not mutated in cancer, with the notable exception of activating Rac1 mutations[200,201]. Rho GTPase-dependent signaling pathways are more frequently dysregulated through overexpression or hyperactivation of various signaling components, including the overexpression of Rho GEFS or of the Rho GTPase itself[144,202–204]. Overexpression of RhoA has been shown in breast[205,206], colorectal[205,207], lung[205], cervical[208], bladder[209], head and neck[210], gastric[211], and testicular cancers[212]. Interestingly, recent advances in whole-genome sequencing have identified recurrent loss-of-function and gain-of-dominant-negative function mutations in *RHOA* in T-cell lymphomas[213–216], diffuse large B-cell lymphoma[217], and diffuse-type gastric cancer[218,219]. These more recent findings suggest that either wild-type RhoA functions as a tumor suppressor or that the loss of RhoA signaling somehow enhances oncogenic signaling. Although it seems that

RhoA can play an important role in cancer progression, it is still uncertain how the interplay with other Rho members affects cancer growth and whether there are different roles for RhoA throughout cancer progression.

1.7 Overview of dissertation

In this dissertation, I present an investigation into how contact guidance signals alter breast cancer cell collective migration. In Chapter 2, I describe how we investigated and quantified collective migration phenotypes in response to electrospun fibers. In Chapter 3, I detail the role of RhoA GTPase during collective contact guidance. In Chapter 4, I discuss the implications of this work in the field of contact guidance and collective migration.

Chapter 2 An Adaptive and Versatile Method to Quantitate and Characterize Collective Cell Migration Behaviors on Complex Surfaces

The work presented in this chapter has been previously published as follows: Loesel K.E., Hiraki, H.L., Baker, B.M., Parent, C.A. (2023). An adaptive and versatile method to quantitate and characterize collective cell migration behaviors on complex surfaces. Frontiers in Cell and Developmental Biology, 11. https://doi.org/10.3389/fcell.2023.1106653

2.1 Abstract

Collective cell migration is critical for proper embryonic development, wound healing, and cancer cell invasion. However, much of our knowledge of cell migration has been performed using flat surfaces that lack topographical features and do not recapitulate the complex fibrous architecture of the extracellular matrix (ECM). The recent availability of synthetic fibrous networks designed to mimic *in vivo* ECM has been key to identify the topological features that dictate cell migration patterns as well as to determine the underlying mechanisms that regulate topography-sensing. Recent studies have underscored the prevalence of collective cell migration during cancer invasion, and these observations present a compelling need to understand the mechanisms controlling contact guidance within migratory, multicellular groups. Therefore, we designed an integrated migration analysis platform combining tunable electrospun fibers that recapitulate aspects of the biophysical properties of the ECM, and computational approaches to investigate collective cell migration. To quantitatively assess migration as a function of matrix topography, we developed an automated MATLAB code that quantifies cell migration dynamics, including speed, directionality, and the number of detached cells. This platform enables live cell imaging while providing enough cells for biochemical, proteomic, and genomic analyses, making our system highly adaptable to multiple experimental investigations.

2.2 Introduction

The extracellular matrix (ECM), the non-cellular component of a tissue, acts not only as a supportive cellular scaffold but also provides biochemical and biophysical cues to cells[220]. ECM composition varies greatly between tissue types and even within the same tissue as a function of disease, where the presence of various chemical and physical cues is known to influence cell division, migration, polarity, and metabolism. In particular, gradients of physical and chemical cues promote directed cell migration, a process that is essential during development, wound healing, immune responses and tumor progression[39,65]. For instance, during breast cancer invasion, high intra-tumoral stiffness, often due to increased deposition and crosslinking of collagen fibers, induces cancer cell migration into healthy, peripheral mammary tissue[221]. Cells sense ECM architecture, such as aligned fibers, through a process termed contact guidance or topotaxis[222–224]. It is widely accepted that contact guidance provides a powerful cue to promote cancer invasion[43]. Aligned collagen fibers that radiate from the periphery of a primary tumor have been shown to promote directional migration in murine breast cancer models, and tumor ECM tension induces the alignment of random fibrillar matrices leading to greater directionality and invasive cell migration[24,34,225].

In recent years, it has been demonstrated that many solid cancer cells principally invade local tissues by retaining their cell-cell contacts and migrating as collective groups of cells[101,226]. Similarly, during wound healing, cell sheets polarize and migrate as a cohesive unit to close the wound[99,227]. These collectively migrating cells integrate signals arising from cell-ECM interactions as well as cell-cell contact as they navigate complex ECM architectures. It is therefore critical that we understand the role of contact guidance during collective cell migration.

To address these questions, we developed a method to investigate how multicellular groups undergo contact guidance using an adaptable *in vitro* system.

Wound healing assays, where a scratch "wound" is created in a confluent monolayer, are often used to study cell sheet migration but can create cell debris and be complicated by variations in "wound" size; in addition, this assay lacks physiologically relevant topology. As an alternative to wound healing assays, other groups have employed 2D spheroid migration assay[228–231]. Previous studies have applied spheroids onto 2D surfaces to study durotaxis[232] and chemotaxis[233], yet how spheroids interpret contact guidance signals remains unexplored. Therefore, we developed a method to study collective cell migration dynamics using live cell imaging of spheroids on complex, fibrous 2D surfaces. The method allows visualization in phase and fluorescent modes when using cells expressing fluorescent probes. Furthermore, collection of the cells migrating on the 2D surfaces allows for concomitant biochemical and transcriptional characterizations of signaling pathways. By tuning of electrospinning parameters, we can investigate the influence of fiber diameter, fiber mat density, fiber alignment, and ECM adhesive components on collective cell migration behavior. Through this systematic deconstruction of the complex ECM, a better understanding of the mechanisms by which multicellular groups sense the various fibrous architectures of the ECM can be achieved and provide parameters that can be applied to more complex 3D models. To demonstrate the utility of this innovative system, we characterized collective migration of the highly invasive and metastatic breast cancer cell line MDA-MB-231 on aligned and random fiber mats.

2.3 Methods

2.3.1 Synthesizing electrospun fiber mats

To create fibrous 2D surfaces for studying cancer cell migration, we utilized electrospinning, a highly tunable fiber production method. Electrospinning has been previously established to generate fibrous topography from a variety of natural and synthetic polymers. In this method, charged polymeric material is ejected from a spinneret under a high-voltage electric field onto a collection surface where the material solidifies to retain a fibrous structure[234]. Depending on the material type, the width of the fibers can range from nanometer to micrometer in scale and various crosslinking and functionalization methods can be sequentially employed to modulate the fiber mechanical properties or adhesive ligand presentation[235–237]. The generation of fibrous topographies has been widely employed to model cell migration on fibrous ECM mimetics where properties such as fiber orientation, density, and ligand presentation can be readily tuned. For our experiments, we used fibers with 1–2 μm diameters, which mimic collagen fibers observed in the murine mammary gland *in vivo*[34].

As originally published by Davidson et al.[236], the synthetic fibers we used are composed of dextran vinyl sulfone (DexVS). DexVS matrices are resistant to hydrolytic degradation thereby allowing for long term cell culture experiments. The percent of vinyl sulfone functionalization of the dextran backbone was confirmed by nuclear magnetic resonance (NMR) spectroscopy. To create DexVS, we dissolved 5.0 g of high molecular weight (86 kDa) dextran in 0.1 N NaOH solution in a 500 mL bulb flask. In a chemical safety hood, the solution is stirred at approximately 250 rpm for 5 min or until the dextran is completely dissolved. Then, 12.5 mL pure divinyl sulfone is added to the bulb flask, which should turn the solution red within 1 min. The reaction is terminated by adding 2.5 mL 12 M HCl solution. If the solution does not turn pale green, we iteratively add 0.5 mL 12 M HCl solution. After terminating the reaction, the solution is transferred to 12–14 kDa dialysis tubing and dialyzed against Milli-Q for 72 h,

changing the water every 12 h. After dialysis, 30 mL of purified DexVS solution is aliquoted into 50 mL conical tubes and frozen at −80°C for at least 1 h or until fully frozen. The frozen solution is lyophilized at −86°C and 0.040 mBar for 72 h. Finally, the 50 mL tubes are sealed with parafilm and the dry DexVS polymer is stored at −30°C until use.

To prepare the electrospinning solution, we thaw a 50 mL tube of dry DexVS at room temperature and weigh the dry polymer into a 20 mL scintillation vial. DexVS is dissolved at 0.6 g/mL in 1:1 dimethylformamide (DMF)/MQ with 10 mg/mL lithium phenyl-2,4,6-trimethylbenzoylphosphinate (LAP), 0.75 mM methacryloxyethyl thiocarbamoyl rhodamine B, and 5 vol% glycidyl methacrylate on a stir plate at ∼100 rpm for 2–4 h. The electrospinning solution can then be stored at 4°C for up to 1 month.

To create electrospun fibers mats, we draw DexVS electrospinning solution into a 1 mL syringe and attach a 305 mm 18G stainless steel (SS) needle. We seal the syringe-needle interface with electrical tape to prevent leakage and push out air bubbles through the needle before use. Next, we attach the syringe to an automated syringe pump at 0.2 mL/h flow rate and place it in a humidity-controlled glove box at 30%–35% relative humidity. To create random fiber mats, we place a round 12 mm2 glass coverslip on top of a grounded copper collection surface centered below the SS needle tip. Then we situate the tip of the SS needle 7 cm from the copper collection surface and connect the needle to the voltage source with an alligator clamp. We set the power source to −7.0 kV and turn on the automated syringe and voltage. As electrospinning solution begins to deposit, we adjust the copper stage to center the electrospinning cone above the glass coverslip. To create aligned fibers, we set the voltage source connected to the SS needle to +4.0 kV and balance the coverslip between two parallel electrodes set to −4.0 kV. We then deposit the electrospun fibers onto the coverslip for 30 s to 3

min depending on the desired thickness of the fiber mat. When the fiber mat reaches the desired thickness, we wet a cotton swab in water and run the swab tip around the edges of the coverslip to separate the fiber network on the coverslip from the surrounding copper collection surface. We then primary crosslink the fiber mats under 365 nm UV light at 100 mW/cm2 for 20 s to stabilize the fibers. The fiber-coated coverslips can be stored in a low humidity environment for up to 1 month.

The coverslips can be mounted on 24 well plates, thereby allowing the simultaneous recording of up to 24 different conditions. This is accomplished by drilling 10 mm2 holes in the bottom of a polystyrene 24 well plate using a Dremel 7,760 tool and a tungsten carbide, double-cut 25° pointed cone drill bit. After creating the well plate, we glue the coverslips on the plates using Dow SYLGARD™ 164 Silicone Elastomer kit, which is easily peeled off for further use after live cell imaging. After hydrating the fiber mat using heparin methacrylate (HepMA; see next section), we sterilize the coverslips with 70% ethanol for 10 min to prevent contamination. This setup can be easily scaled down to 12 or six well plate setups by spinning on larger coverslips.

2.3.2 Live cell imaging of cancer spheroids

To allow cells to adhere to the synthetic fibers, we incubate the fiber mats in 50 µL of 2.5 w/v% HepMA, a structural analog to heparan sulfate, diluted in LAP followed by exposure to UV light (100 mW cm−2) for 20 s. Heparan sulfate proteoglycans (HSPGs), which bind many ECM proteins, are distributed throughout the ECM and are present at the cell surface[238]. The reaction covalently binds vinyl sulfone groups to methacrylate and enables coating of the fibers with any HSPG-binding proteins, such as type I collagen, fibrinogen, and fibronectin (**Figure 2.1A**). For our experiments we coat the fiber mats with 100 µg/mL type 1 bovine collagen for 1

h at 37°C. We also coat glass with 100 µg/mL type 1 bovine collagen for 1 h at 37°C as a control for our experiments. Following collagen binding, fiber mats or glass are rinsed three times with DPBS before adding spheroids.

To study collective cell migration, we use a spheroid migration assay where spheroids generated from the MDA-MB-231 cell line are plated onto fiber-coated 2D coverslips and imaged in real time as they migrate on the surface while retaining cell-cell contacts (**Figure 2.1B**). We generate spheroids using low adhesion 96 well plates coated with 1.2% 2-hydroxyethylmethylmethacrylate (polyHEMA). To create polyHEMA coated plates, we prepare a stock concentration of (12% or 120 mg/mL) polyHEMA solution and then dilute the stock to 1.2% in 95% ethanol. The stock and the working Poly-HEMA solutions can be stored at room temperature for several months. We then add 100 µL/well of 1.2% poly-HEMA and let the plates dry at 37°C until the alcohol is evaporated (2–3 days). To create spheroids, 1,000 cells in 80 µL are seeded into each well of the low adhesion V-bottom 96 well plates. After 6 days, a time point determined to generate tight spheroids with no necrotic core, we collect the spheroids and stain them with 0.8 µg/mL Hoechst 333482, a cell permeable nuclear dye, for 10 min at 37°C and wash in full media. For a 24 well plate setup, we seed ~4 spheroids into each well in 500 µL of full media. The spheroids are allowed to settle and adhere to the fibers for 2 h at 37°C, 5% CO2 before live imaging. The spheroids and fiber mats are imaged using a Zeiss Axio Observer Z.1 LED epifluorescence microscope equipped with an environment chamber that maintains temperature (37°C) and CO2 (5%) levels. The spheroids are imaged using phase-contrast microscopy every 10 min and fluorescence microscopy to image the Hoechst label every 30 min for 24 h (**Figure 2.1C**; Supplementary Movies S1, S2[1]). In addition, an image of the fluorescent

[1]The supplementary movie files can be found at the following link:
https://www.frontiersin.org/articles/10.3389/fcell.2023.1106653/full#supplementary-material

fiber mats on the first timepoint is acquired for later quantification of fiber mat density and alignment. After the experiments, the coverslips can be easily peeled off, and the well plate can be reused after sterilization with 70% ethanol.

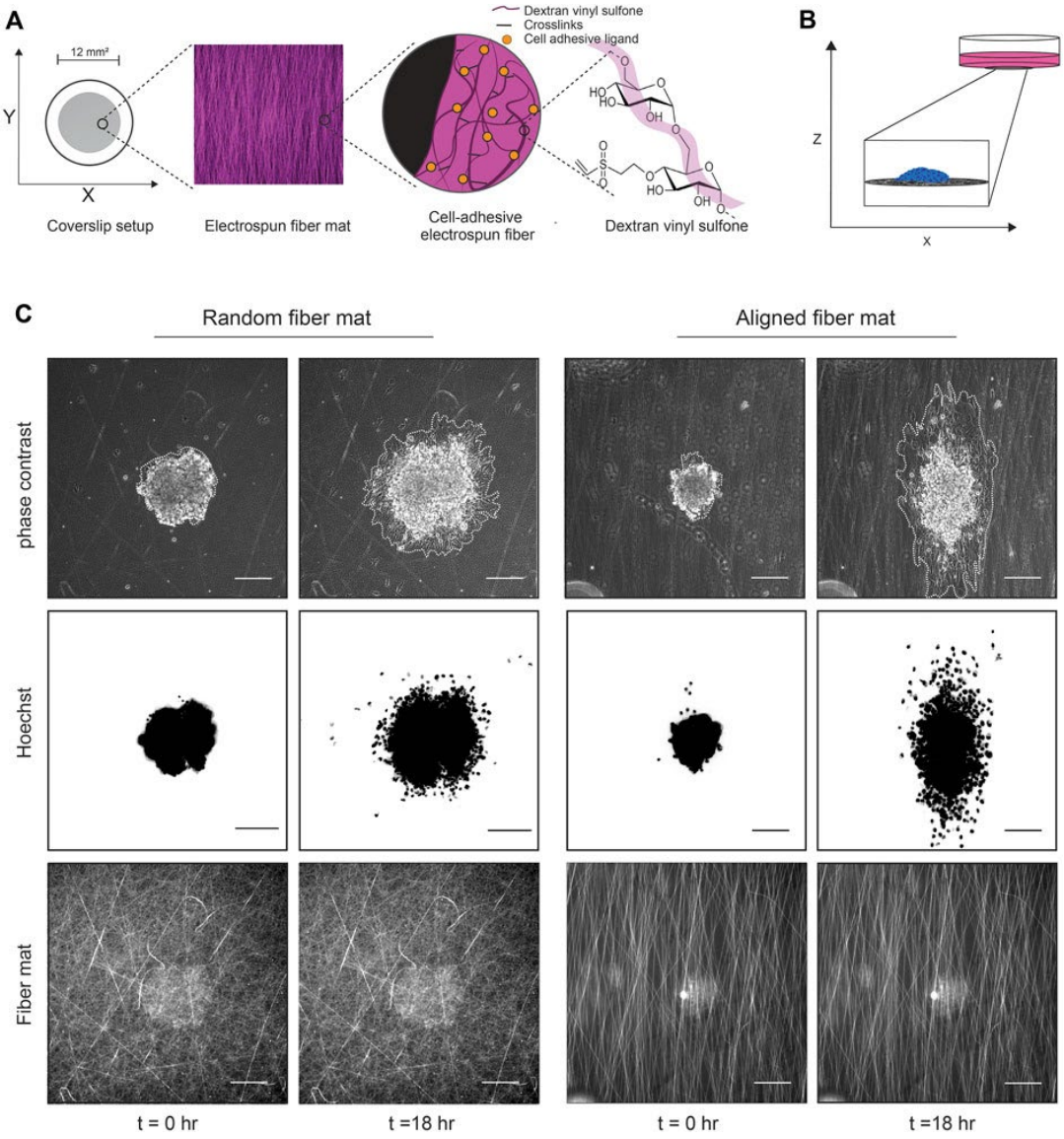

Figure 2.1 Experimental setup using DexVS fibers and cancer cell spheroids.

(A) Cartoon depicting the method used to generate the fibers. Dextran is reacted with vinyl sulfone to create DexVS, which then is mixed with LAP and electrospun to create fiber mats on coverslips. (B) Cartoon depicting the 2D spheroid migration assay. After functionalization with collagen, cancer cell spheroids are plated onto fiber mats of interest and imaged over time to assess migration. (C) Representative phase contrast images of a MDA-MB-231 spheroid migrating on random or aligned fiber mats taken at the times 0 and 18 h. Spheroids are outlined in white to delineate the extent of cell spreading.

2.4 Results

2.4.1 Utilizing TrackMate to generate cell tracks

To obtain migration metrics, we use the open-source ImageJ plugin, TrackMate 6.0.2, to detect the Hoechst-positive nuclei and output individual nuclear locations over time[239]. Before importing the live cell TIF file images into TrackMate, we remove non-migrating dead cells from the data set by selecting the nuclei with the polygon selection tool and clearing them using the clear function (Image → Clear). Next, we load the TIF files to track in TrackMate. For our analysis, we use a Laplacian of Gaussian (LoG) detector and a 12 μm diameter within TrackMate to detect nuclei. Next, we use the linear assignment problem tracker to link nuclei from frame to frame and create tracks. In the last prompt, the user can export the overlay of the tracks on the video and the spot statistics. The spot statistic data, which includes unique nuclei ID numbers, frame intervals, and the X and Y location of the nuclei, are then loaded into MATLAB for analysis. Using these values, we create an adaptable MATLAB script that calculates cell migration metrics, including Euclidean and accumulated distances, mean and median cell speed, instantaneous cell speed, mean cell directionality, and instantaneous cell directionality (**Figure 2.2A**). In addition, correlations between speed and directionality can be measured to further gain insight into migration phenotypes.

To demonstrate the capabilities of this platform, we measured the migration dynamics of the MDA- MB-231 breast cancer cell line on random and aligned electrospun fiber mats (**Figure 2.2B;** Supplementary Movie S3). Using the TrackMate plugin, we tracked 200–800 nuclei per frame (**Figure 2.2C**). We observed a gradual increase in the number of cells migrating over time due to persistent migration of the cells from the spheroid body (**Figure 2.2D**). Interestingly, we

tracked a higher number of cells from spheroids after migration on glass compared to fiber mats, which is likely due an increase in cell speed on glass (see below).

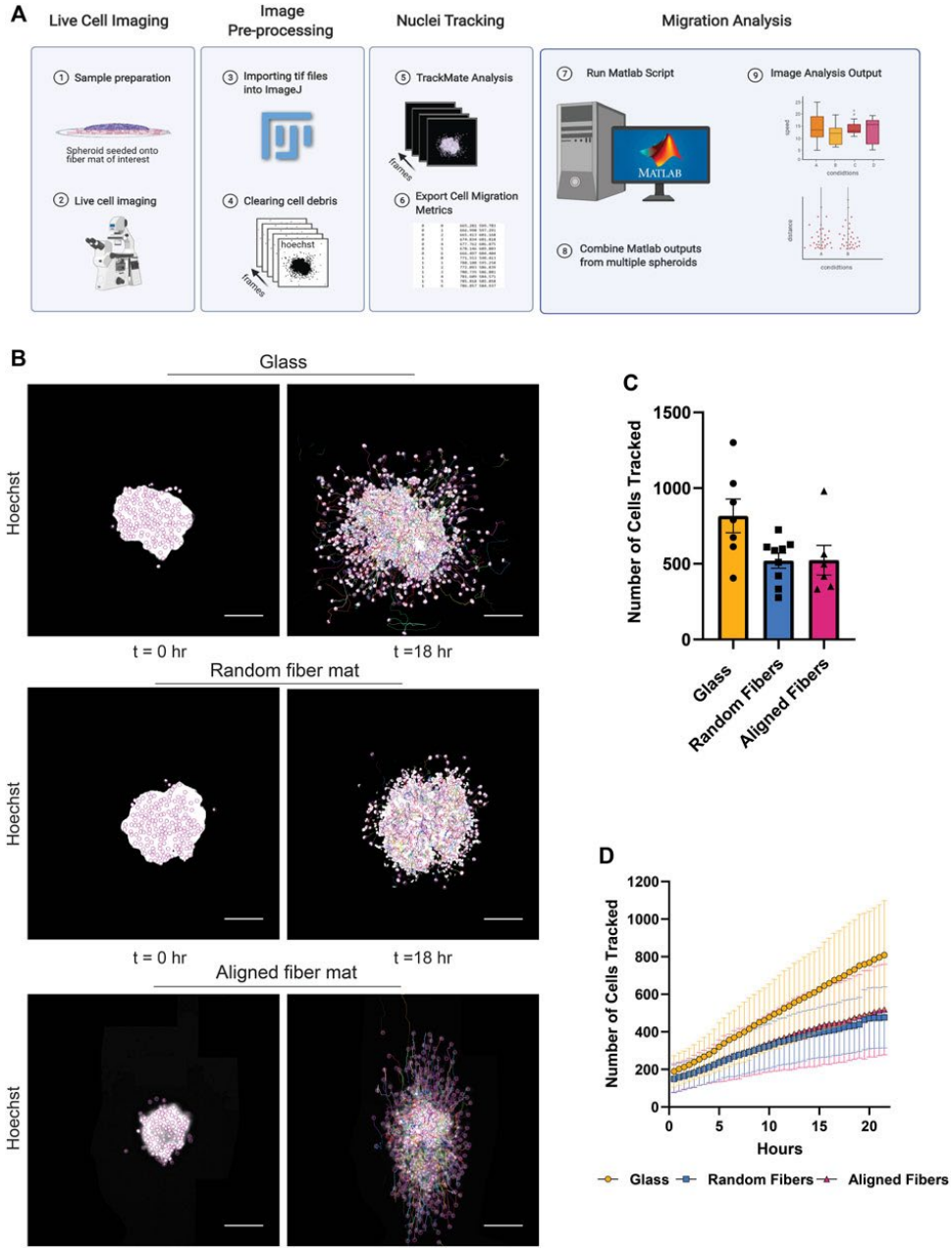

Figure 2.2 Methodology used to obtain cell migration metrics.

(A) Workflow for image processing to compute cell migration metrics after live cell imaging. (B) Representative fluorescent images of a MDA-MB-231 spheroid migrating on glass, random or aligned fiber mats taken at the times 0 and 18 h. (C) Graph depicting the number of nuclei tracked at 22 h for spheroids migrating on the different surfaces. Each point represents an independent experiment. (D) Graph depicting the number of cells tracked as a function of time. Data represented as a mean ± SEM for C and± SD for (D). Figure 2.2A created using BioRender.com.

2.4.2 Analyzing cell migration metrics using MATLAB

After analysis using our MATLAB script, we found that MDA-MB-231 spheroids show strong contact guidance when migrating on aligned fiber mats compared to isotropic surfaces such as glass and random fibers. The polar histograms illustrate the probability of migration direction with aligned fibers corresponding to the −90° and +90° directions (**Figure 2.3A**). We also found that cells migrate faster and farther on glass surfaces compared to fiber mats (**Figures 2.3B, C**). It has been reported that 3D collagen matrix alignment does not affect MDA-MB-231 cell speed[240], and similarly we found that in 2D the MDA-MB-231 cells migrate at comparable speeds on random and aligned fiber surfaces (**Figure 2.3C**). Additionally, we measured instantaneous metrics to assess migration changes over time. We found that speed decreased over time for all the conditions, but cells on glass showed a consistently higher cell speed at all time points (**Figure 2.3D**).

To dissect potential heterogeneity in migration within the group, we next determined whether cell speed correlated with cell directionality. To do so, we partitioned the cell speed data into four bins based on the individual mean cell speed of the cells and plotted the corresponding cell directionalities (**Figure 2.3E**). In the context of the contact guidance response observed on aligned fiber mats, we found no correlation between speed and directionality as cells in all bins exhibited strong directional migration on aligned fibers. In addition, we found that cells plated on surfaces without a directional cue–such as the random fiber mats or glass–migrated consistently

in all directions. Taken together, these findings suggest that MDA-MB-231 cells display a highly uniform directional response to fiber alignment.

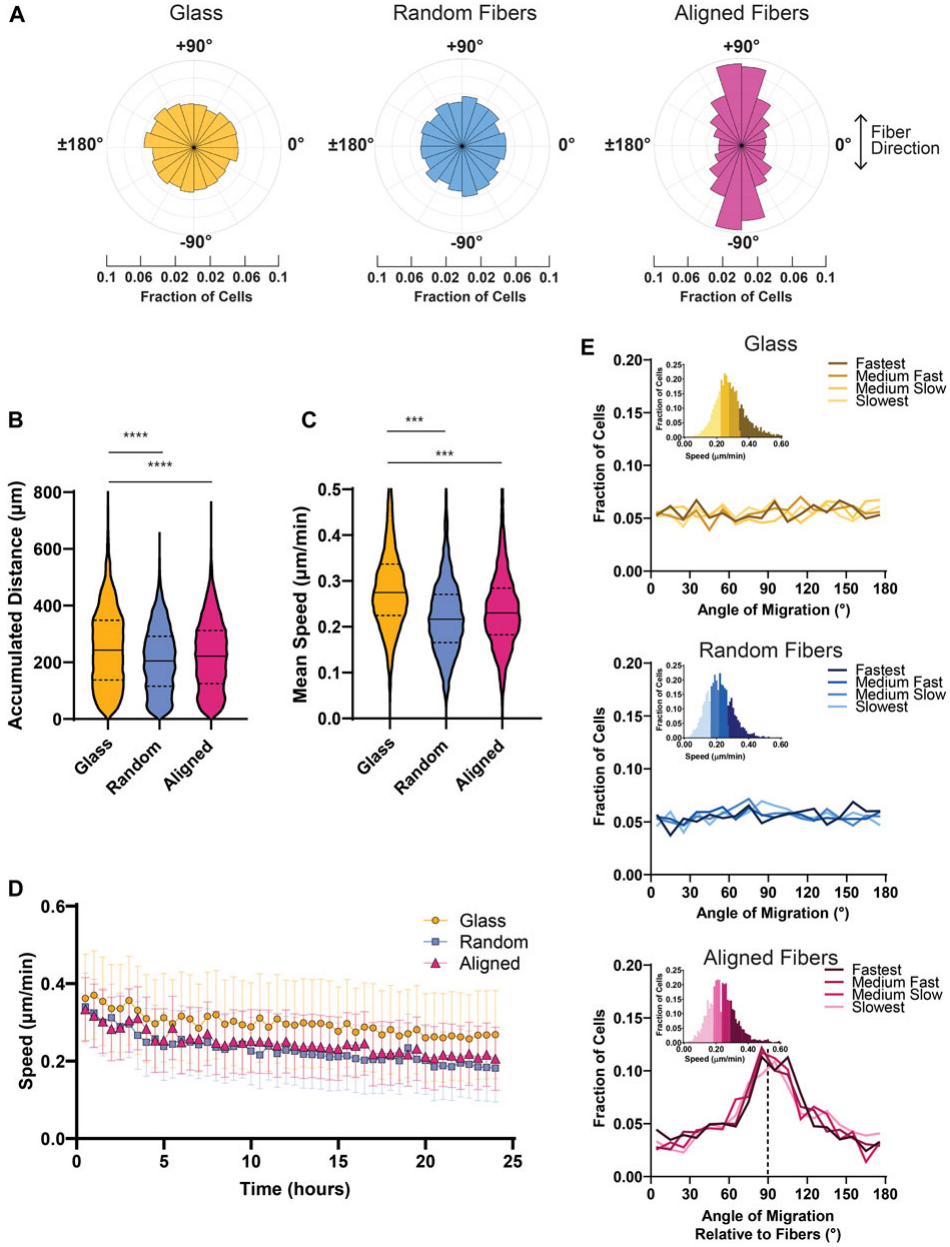

Figure 2.3 Bulk cell migration metrics of MDA-MB-231 spheroids migrating on glass and fiber surfaces.

(A) Probability distribution plots of cell motion direction for MDA-MB-231 cells migrating on glass or fiber mats. (B) Graph depicting the mean accumulated distance for MDA-MB- 231 cells migrating for 22 h on glass, random fiber mats, or aligned fiber mats. (C) Graph depicting the mean cell speed of MDA-MB-231 cells migrating on glass or fiber mats. (D) Instantaneous cell speed (mean +/- SEM) of MDA-MB-231 spheroids over 24 h. (E) Graphs depicting the frequency of directional migration on glass or fiber mats. The different colors represent cell speeds that were binned as depicted. Analyses were performed on seven spheroids on glass, 11 spheroids on random fibers, and 11 spheroids on aligned fibers (n ≥ 3 biological replicates). p values are determined using an unpaired t-test. *p < 0.05, **p < 0.01, ***p < 0.001.

2.4.3 Identification and quantification of single cell dispersion.

We next set out to measure the migration metrics of cells within the group and those which break away from the group (i.e., single cells). To accomplish this, we used the k-nearest neighbor (KNN) algorithm, which compares a point of interest to candidate points using Euclidean distance. Using the nearestneighbour function[241], we compared the distance between each nucleus to all other nuclei within a frame, and identified nuclei that did not have nearest neighbors, based on a user defined input distance. After identifying the total number of single cells and their corresponding cell IDs within each frame, the code then loops through every frame, so the user has the number and cell ID of single cells in each timepoint. More specifically, we first loop through each frame and calculate X and Y coordinates for all nuclei. Next, using a nested loop, we assigned each nucleus as the point of interest and use the KNN algorithm to determine if that nucleus has neighbors within a specified distance threshold. After indexing through each nucleus in frame 1, the script then proceeds to frame 2. In addition to outputting the number of single cells in each frame and their corresponding cell ID, we utilized the videowriter function to output an AVI video file that displays all the cells over time and denotes "single" cells in color and "group" cells in grey. Finally, after classifying cells into "single" or "group" cells, cell speed and directionality between these two groups can easily be measured.

To determine the optimal distance between nuclei for single cell designation in the MDA-MD-231 cells, we tested three KNN distance thresholds—30, 50, and 100 μm. As expected, we found that a higher threshold (100 μm) identified fewer single cells compared to a lower threshold of 50 or 30 μm (**Figures 2.4A, B**; Supplementary Movie S4). Using the AVI file exported from MATLAB and our original phase-contrast video, we then determined the best threshold for each cell line. By comparing the phase contrast video with the AVI file output from

MATLAB, we were able to determine which nuclei belongs to single cells. We determined that a 40 μm threshold most accurately represents our data, which show that MDA-MB-231 cells migrating on glass coverslips display a significantly greater increase in single cells dissemination compared to cells on fibers (**Figure 2.5A**). In addition, to account for any variation between the total number of migrating cells, we plotted the ratio of the number of single cells over the total number of cells as a function of time on all three surfaces and found that the proportion of single cell dispersion also increases over time, and that spheroids on glass show the greatest proportion of single cell dispersal (**Figure 2.5B**). This loss of group migration on glass, which also correlated with increased speeds, is likely due to the lack of topographical complexity.

In addition to identifying and quantifying the number of single versus groups of cells over time, we further investigated any changes in speed or directionality between these two groups. By comparing the mean cell speed over time of cells within groups versus single cells on fiber or glass surfaces, we found that single cells move faster than cells within the group at all time points on glass surfaces, while both single and group cells on fiber mats tend to move at the same speed over time (**Figure 2.5C**). Based on previous literature, we envision that the lack of substrate complexity and increased substrate stiffness of glass surfaces allow for more stable cell-substrate interactions leading to increased traction force and cell speed[242–245]. Finally, we also studied the directionality of single cells by plotting each cell's instantaneous directionality over time. Not surprisingly, we found that single cells migrating on aligned fiber mats exhibit strong contact guidance compared to single cells migrating on glass or random fibers surfaces (**Figure 2.5D**).

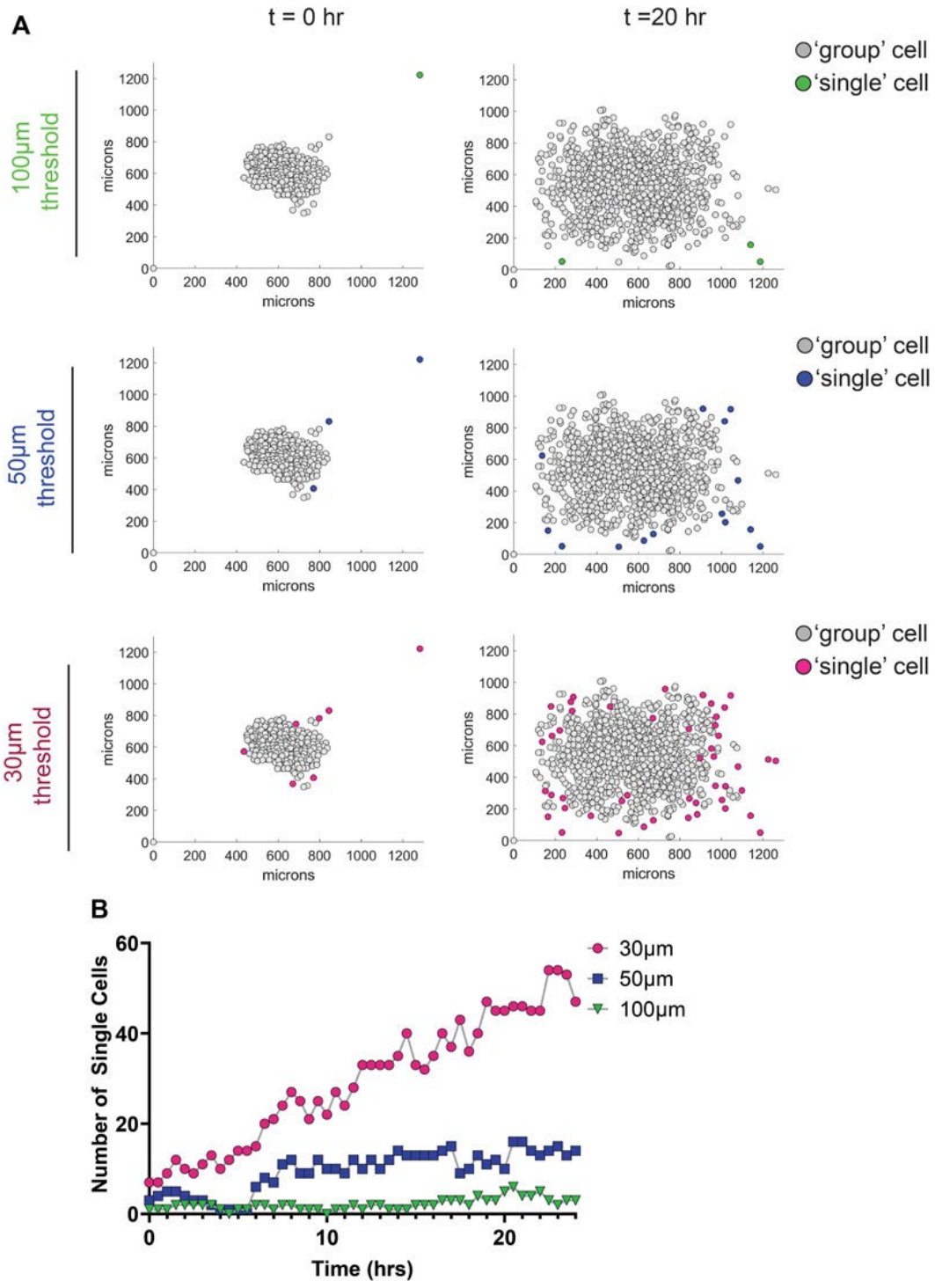

Figure 2.4 Effect of different nearest neighbor thresholds on single cell dispersion metrics of MDA-MB-231 spheroids migrating on glass.

(A) Graphs depicting the location of cells 0 and 20 h after the initiation of migration using different nearest neighbor thresholds. Group cells are displayed in grey and single cells are displayed in color. (B) Graph depicting the number of single cells as a function of time for the different threshold used.

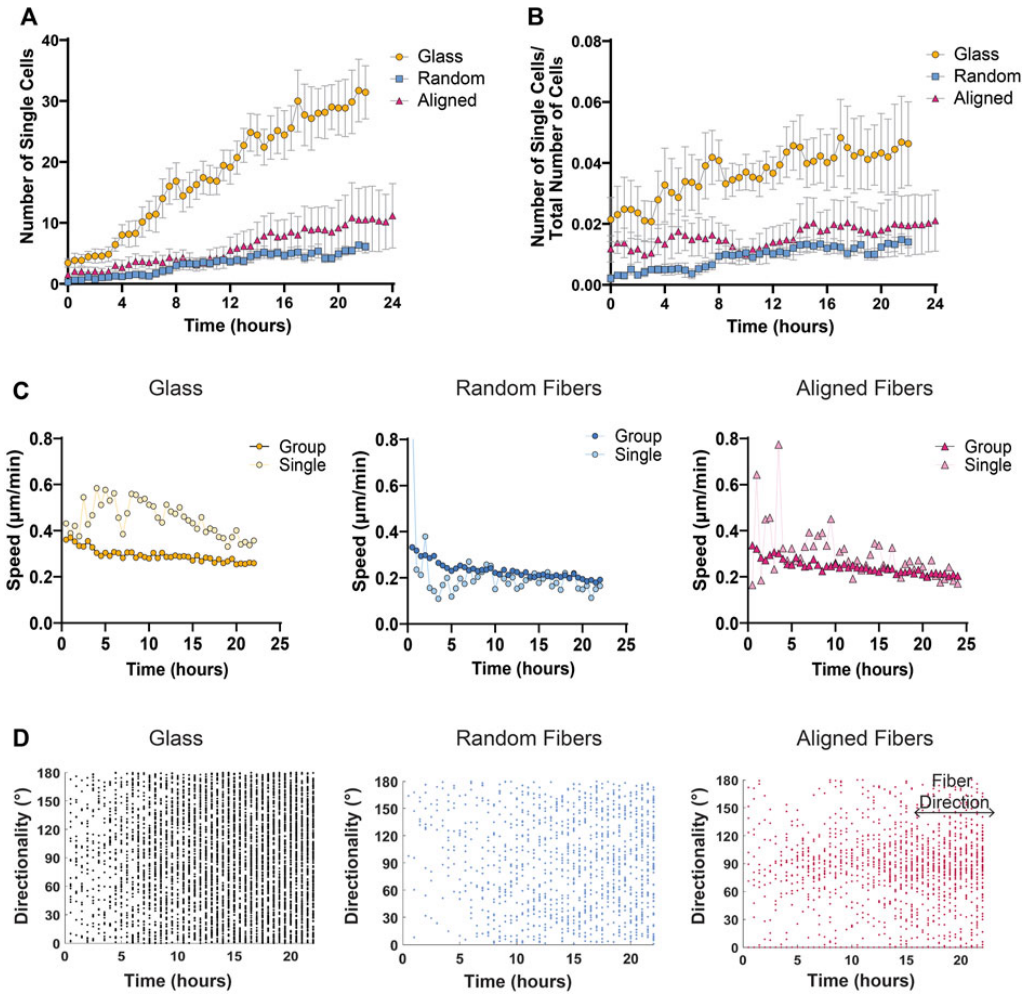

Figure 2.5 Single cell migration metrics of MDA-MB-231 spheroids migrating on glass and fiber surfaces.

(A) The number of single cells detached from the cell sheet over time. (B) Differences in the number of single cells over the number of total cells to account for differences in total number of cells detected. (C) Mean cell speed of collective cell groups or single cells on various fiber mats over time. (D) Directionality of single cells over time on glass, random fiber mats, and aligned fiber mats with fibers at 90° direction for aligned fiber mats. Each dot represents the instantaneous directionality of one single cell. Analyses were performed on seven spheroids on glass, 11 spheroids on random fibers, and 11 spheroids on aligned fibers ($n \geq 3$ biological replicates). All data presented as mean ± SEM.

2.4.4 Visualizing protein localization and protein expression changes during migration on fiber mats

The dynamic distribution of proteins of interest in cells migrating on the various substrate can readily be studied by constructing cells expressing fluorescently tagged proteins and capturing images at relevant time points during migration (see live cell imaging section above). In addition, immunofluorescence can be used to visualize static protein distribution in cells

migrating on the various surfaces. For both applications, the fluorescent fibers provide a mean to assess the distribution of protein of interests in relationship with the fibers (**Figure 2.6A**). Furthermore, the fixed samples can be complimentary to the live cell imaging analyses by using cells expressing fusions with fluorescent markers. As a proof of concept, we fixed cells that migrated on the surfaces for 24 h with 4% PFA for 10 min at 37°C followed by washing with PBS. Next, we permeabilized the cells in 0.1% Triton-X100, and blocked non-specific binding using 4% bovine serum albumin (BSA). We stained for β-tubulin at 4°C overnight in 1% BSA. After conjugation with a compatible fluorescent secondary antibody and incubation with phalloidin-488 and Hoechst, the cells were imaged using a Zeiss 880 confocal microscope. As expected, MDA-MB-231 cells showed a dramatic difference in cytoskeletal morphology on random, aligned or glass surfaces (**Figure 2.6A**). On glass surfaces, the cells commonly displayed stress fibers due to the rigidity of the glass, and β-tubulin fibers radiated from the center of the cell. On random fibers, the cytoskeleton formed strong interactions with the random matrix that seemed to direct F-actin and β-tubulin localization. Whereas MDA-MB-231 cells migrating on aligned fibers showed an elongated and aligned actin and microtubule cytoskeleton.

In addition to assessing migration dynamics using live cell imaging, the system we developed can readily be used to measure changes in protein expression and/or activation status after collective cell migration on the fibrous surfaces using western blot analysis. For these applications, we prepare cell lysates once all the cells have migrated out of the spheroids onto the 2D surfaces, which is 6 days for the MDA-MB-231 cells. To obtain enough material for these measurements, we plate approximately ten spheroids onto a 25 mm2 coverslip. To extract proteins of interest, we place the coverslips on ice and use 200 µL of 2X Laemmli lysis buffer per coverslip to initiate cell lysis. After 5 min on ice, the lysates are scraped, transferred in a

microcentrifuge tube and centrifuged at 10,000×g for 15 min at 4°C to remove fibers and clarify the cell lysate. At this point, the samples can be subjected to gel electrophoresis and changes in a protein of interest can be investigated using immunoblotting. As an example, we collected sufficient protein to compare differences between β-tubulin expression in MDA-MB-231 cell migration on random fibers or glass coverslips (**Figure 2.6B**).

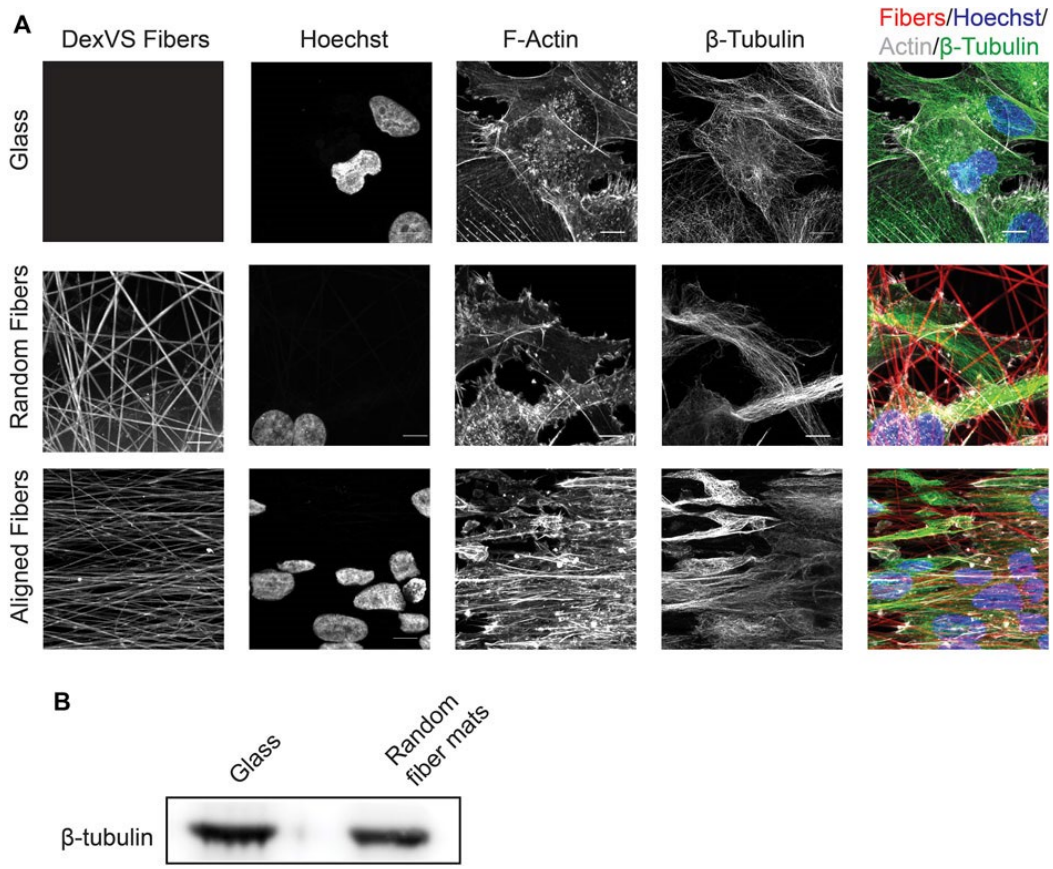

Figure 2.6 Expression and distribution of β-tubulin after cell migration on glass or fiber mats.

(A) Immunofluorescence localization of β-tubulin and F-actin after 24 h of cell migration on fiber mats or glass. Scale bar is 10 μm. (B) Immunoblot depicting β-tubulin expression after 6 days of cell migration on glass of random fiber mats.

2.5 Discussion

In summary, we present a highly adaptable method to investigate collective cell migration on complex surfaces using live cell imaging, in depth automated migration quantification, as well as biochemical analyses which can be performed following live cell

imaging. Building on previous systems investigating cell migration in response to chemical and stiffness cues, we developed a method to provide a holistic understanding of how different cell types migrate on fibrous surfaces of various topographies and allow the investigation of the molecular changes that occur as cells encounter and migrate on these surfaces. We demonstrate that by combining the use of cancer cell spheroids with electrospun fiber mats, it is possible to measure migration dynamics of collective groups as well as individual cells moving on physiologically relevant fiber topographies. As a proof of concept, we demonstrate the full capabilities of our method using the highly metastatic breast epithelial cell line, MDA-MB-231, on two distinct fiber topographies, using glass as a control.

In addition to optimizing the spheroid-fiber migration assay, we also successfully automated much of the cell migration analysis using the TrackMate plugin from ImageJ[239] and by developing a custom MATLAB script. Our MATLAB script can quickly process all datasets within a user-specified folder allowing for rapid migration analysis. In addition to calculating bulk migration data, we also utilize the k-nearest neighbor algorithm to distinguish single versus group migration, allowing us to analyze migration changes within these subsets. We showed that MDA-MB-231 cells show an increased mean cell speed and accumulated distance on glass surfaces compared to fiber mats. Additionally, we showed that speed and directionality are not correlated in MDA-MD-231 cell migration. We further investigated differences in migration between cells within the group and cells which break away from the group and found that while single cells migrating on fiber mats show similar speeds as their corresponding group cells, MDA-MB-231 single cells migrate much faster on glass than cells that are part of the group.

The assays can easily be modified according to the user's interests: changing cell matrix protein (i.e., fibronectin, collagen IV); including other cell types to produce a co-culture system;

genetic manipulations or inhibitor treatment; as well as changes in fiber size, density and organization or fiber mat size. In addition, developing methods to expand the capabilities of the cell tracking workflow to incorporate more intricate quantification such as changes in nuclear morphology over time can readily be done. Finally, in the future, we envision that this system could be scaled to 3D using a fiber-enforced hydrogel[246,247]. While image acquisition and quantification methods are more challenging in 3D environments, we recently published an automated image analysis framework that can be used in future 3D experiments[248]. Additionally, we are currently expanding our 2D aligned fiber mat system to a more complex 3D aligned fiber system through the use of superparamagnetic iron oxide nanoparticles (SPIONs) embedded in synthetic fiber segments[249].

Our approach has some limitations that leave room for future improvement. These include the lack of automation during the TrackMate analysis, which we plan to streamline by integrating TrackMate with MATLAB using the ImageJ-MATLAB extension. The addition of this automated step will greatly increase the efficiency and speed of the workflow. Also, while k-nearest neighbor identification of single cells allows for an equal classification based on a user-defined constant between experimental conditions, there are drawbacks to this method. For example, the user is required to define the distance threshold which subsequently determines the classification of a single or group cell. So, while this adds bias to the quantification, it also allows for analysis of cell types with different migration phenotypes and cytoskeletal morphologies. In the future, it may be useful to stain cells with a cytosolic fluorescent dye, so that this classification can be done without user bias.

2.6 Data availability statement

The raw data supporting the conclusions of this article will be made available by the authors, without undue reservation. The code developed for this work is available upon request.

2.7 Author contributions

KL and CP conceptualized and designed the experiments. KL and HH performed the experiments, analyzed, and interpreted the data. KL drafted the manuscript. KL, HH, BB, and CP critically revised the manuscript. CP and BB supervised the study. All authors reviewed the manuscript. All authors contributed to the work and approved the submitted version.

2.8 Funding

This work was supported by funding from the University of Michigan School of Medicine, the University of Michigan Rogel Cancer Center Nancy Newton Loeb Fund, and by NIH grant R01 EB030474.

2.9 Acknowledgments

We thank the members of the Parent and Baker laboratories for their insight and suggestions. In particular, we thank Lauren Hein for her advice and feedback on the development of the code.

2.10 Conflict of interest

The authors declare that the research was conducted in the absence of any commercial or financial relationships that could be construed as a potential conflict of interest.

Chapter 3 RhoA Controls Contact Guidance in Collectively Migrating Breast Cancer Cells by Regulating Cell-Cell Junctions and Focal Adhesions

3.1 Abstract

Collective cell migration is a fundamental process involved in a wide array of physiological and pathological responses and a hallmark of cancer invasion and metastasis. It has been demonstrated that physical features of the dysregulated tumor extracellular matrix (ECM), such as collagen fiber alignment, influence invasion phenotypes. Contact guidance is the process through which cells sense and respond to substrate anisotropies, such as aligned fibers, ultimately altering adhesion formation, directionality, and migration. The coordinated and directed movement of cells within a group is regulated by multiple extracellular signals and intracellular signaling pathways. Among these pathways, RhoA GTPase serves as a crucial regulator, orchestrating cytoskeletal dynamics, focal adhesion dynamics, and cell-cell adhesions which are all essential for proper collective cell migration. We sought to investigate the mechanisms by which multicellular groups sense aligned fibers by assessing whether RhoA facilitates contact guidance in migrating cell sheets. We found that loss of RhoA or inhibition of a major Rho effector, Rho-associated protein kinase (ROCK), led to a significant decrease in the contact guidance ability of collectively migrating breast epithelial cells. Based on these findings, we sought to determine if the loss of collective contact guidance was due to changes in focal adhesions or cell-cell junctions. We found that the loss of RhoA led to a decrease in focal adhesion lifetime. Also, the loss of RhoA led to dramatic changes in the distribution of cell-cell

adhesion proteins, with RhoA null cells exhibiting increased E-cadherin and decrease Desmoplakin localization at cell-cell junctions compared to scramble controls. Together, our study explores the intricate signaling networks controlling contact guidance, identifying a pivotal role of RhoA/ROCK signaling in mediating contact guidance during collective cell migration. Furthermore, our findings demonstrate that RhoA regulates the dynamics of focal adhesions and cell-cell adhesions, which are both crucial for effective collective contact guidance.

3.2 Introduction

Extracellular mechanical cues, such as stiffness and topography, are increasingly recognized as powerful signals that can drastically alter cell growth, differentiation, and migration[39]. The non-cellular component of a tissue, termed the extracellular matrix (ECM), is composed of a complex network of structural proteins, glycoproteins, growth factors, and enzymes[1,250]. The topology of fibrillar collagen, the main structural component of the ECM, dictates cell behavior and migration[34]. In fact, collagen alignment within the tumor ECM has been shown to drive the directed migration of cancer cells along fiber orientation in a process termed contact guidance[24,40,41,251–253]. Contact guidance refers to the ability of cells to polarize and migrate along aligned architectures, such as aligned collagen fibers[42]. Until recently, much of the work studying contact guidance has been performed using single cells, although collective cell migration has been shown to be the primary mode of invasive migration *in vivo*[101,105,254].

Collective cell migration is a highly coordinated process that requires the cohesive movement of cells in response to local chemical and mechanical signals[99,100]. Collective cell migration is essential for many normal cellular processes including wound healing and embryonic development. Additionally, during the initial steps of cancer metastasis, malignant epithelial cells collectively invade healthy tissue surrounding a tumor[94,102]. Collective cell

migration involves a complex interplay between cell-matrix and cell-cell interactions, both of which are crucial for proper directional migration. Throughout collective cell migration, cells maintain close contact with each other through intercellular junctions, such as adherens junctions (AJs) and desmosomes. Stable cell-cell junctions provide coordinated cytoskeletal activity between neighboring cells and therefore are crucial for cell sheet polarization. In addition, cells form integrin-based adhesions, termed focal adhesions, with ECM components, such as collagen and fibronectin[82,83]. Focal adhesions are mechanosensitive protein complexes that directly link the actin cytoskeleton to the ECM, thus allowing cells to sense and respond to changes within their environment[86]. Contact guidance has been proposed to be driven by constrained focal adhesion maturation along aligned architectures and subsequent alignment of the actin cytoskeleton[55].

The Rho family of GTPases control actin dynamics and therefore highly influence cell polarity and migration. They switch between an inactive GDP-bound form and an active GTP-bound form through the enzymatic activity of Rho GTPase activating proteins (GAPs) and guanine nucleotide exchange factors (GEFs) [156,157]. Additionally, guanine nucleotide dissociation inhibitors (GDIs) serve as negative regulators of Rho GTPases by controlling the localization and stability of GTPase activity[158]. While over 20 Rho GTPase family members have been identified, three family members—Rac1, Cdc42, and RhoA—have been studied extensively due to their critical roles in the regulation of the actin cytoskeleton. RhoA is known to induce cellular contractility and actin polymerization through the activation of its downstream effectors Rho-associated protein kinase (ROCK1/2) and the formin mDia, respectively. ROCK enhances actomyosin contractility by directly phosphorylating myosin light chain as well as indirectly through the inactivation of myosin phosphatase[176,255,256]. RhoA has crucial roles in the assembly

and stability of focal adhesions in single cells[257,258]. Additionally, RhoA is important for maintaining epithelial sheets through the stabilization of E-cadherin, an essential AJ protein[259–261]. RhoA may be critical for robust collective contact guidance due to its significant role in regulating the formation of cell-substrate and cell-cell contacts, however this has not been directly tested.

We hypothesize that RhoA plays an important role in contact guidance during collective cell migration through the regulation of actomyosin contractility, focal adhesions dynamics, and cell junction stability. In this study, we employed nanofabrication technology, live cell imaging, and robust quantitative analyses. We report a dramatic loss in contact guidance in the absence of RhoA during collective cell migration. We provide evidence that depleted RhoA/ROCK signaling results in faster focal adhesion disassembly. We also demonstrate that loss of RhoA causes a dramatic increase in E-cadherin membrane localization while drastically decreasing desmosome plaques at the cell junctions. Our findings suggest that RhoA coordinates collective contact guidance through the regulation of focal adhesion dynamics and cell-cell adhesions.

3.3 Results

3.3.1 Synthetic, aligned electrospun fibers provide a platform to study contact guidance during collective cell migration.

We generated synthetic, aligned electrospun fiber mats to study contact guidance as previously described (**Suppl. Figure S3.1A**)[236]. These fiber mats are composed of fibers with diameters of 1-2 μm which resemble murine collagen fibers observed *in vivo*[24]. To examine collective cell migration on fiber mats, we created spheroids from breast cancer cell lines with varying malignant potentials, plated them onto fiber mats coated with collagen I, and imaged every 10 min over 22 hrs (**Suppl. Figure S3.1B**). We quantified the migration of individual cells

within the spreading spheroid by tracking Hoechst-stained nuclei using TrackMate and a custom MATLAB script[262,263]. We first compared the migration phenotypes of four breast epithelial cell lines – pre-malignant MCF10AT (M2), poorly invasive BT-474, highly invasive MDA-MB-231, and highly invasive MCF10CA1a (M4) - on fiber mats composed of either aligned or randomly oriented fibers. We chose these cell lines based on their unique genetic backgrounds and their previously established differences in malignant potential[264–268]. The M2 and M4 cell lines are part of the well-established MCF10A (M1) cell series progression model[269]. The parental M1 cells were derived from a patient with fibrocystic breast disease and are nonmalignant. The M2 cells were created by transfection of the M1 cells with mutant H-ras and xenograft-passaging in nude mice; the M2 cells are considered premalignant, as they generate premalignant lesions that spontaneous progress to primary tumors in 25% of mice[265]. The highly invasive M4 cells were derived from xenografts after a series of implantations into nude mice. M4 cells readily produce tumors when subcutaneously injected into nude mice and form metastatic legions following tail vein injection[264]. In contrast, the estrogen-receptor positive BT-474 cell line rarely forms metastatic lesions when injected subcutaneously in mice[270,271]. Additionally, we used the MDA-MB-231 cells which were derived from a patient with metastatic ductal breast carcinoma[272]. When injected into the mammary fat pad of nude mice, MDA-MB-231 cells can spontaneously metastasize to lymph nodes and distant organs[271,273].

While we observed considerable variation between the four cell lines in the distance they migrated and their collectivity (**Figure 3.1A, see Chapter 3 appendix for further migration quantification**), all cell lines migrated directionally along the aligned fiber mats as represented

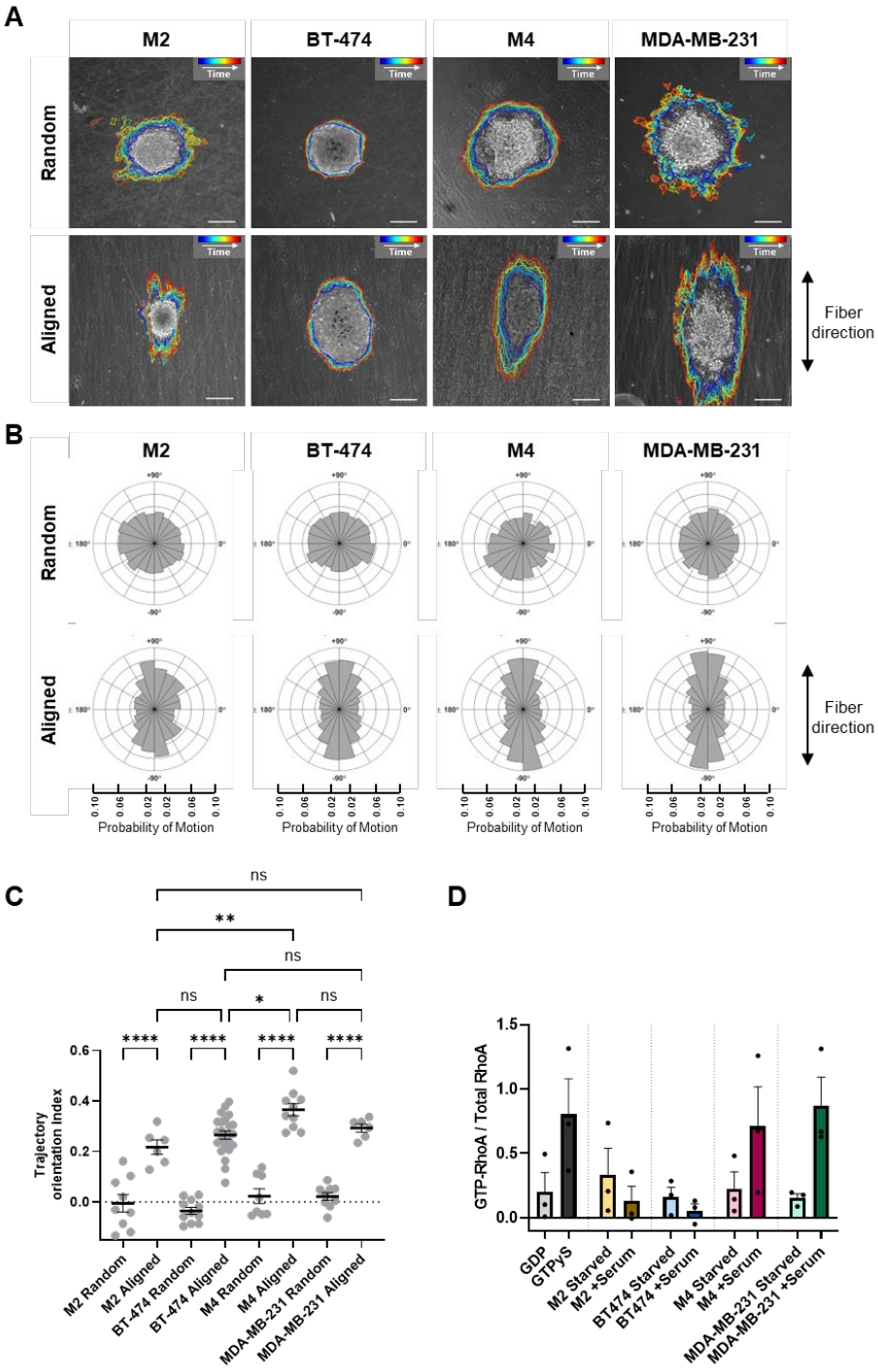

Figure 3.1 Highly invasive, breast epithelial M4 cells display strong RhoA activation and strong contact guidance response.

(A) Phase contrast images of migrating breast epithelial cell lines on aligned or randomly oriented fiber mats after 18 hours of migration. Colored outlines depict collective migration over time, which increases from blue to red. Scale bars are 200 μm. (B) Polar histograms demonstrating cell directionality on random or aligned fibers. Aligned fibers are oriented in +90° and -90° direction. (C) Trajectory orientation index of cells on random and aligned fiber mats. Each point represents the mean TOI of all the cells from one spheroid. Middle solid line is the mean value. (D) Serum-starved cells were stimulated with serum, lysed, and GTP-RhoA was pulled down using GST-Rhotekin-RBD beads. GTP-bound RhoA and whole cell lysates were subjected to gel electrophoresis and probed with anti-RhoA antibody. Data in C and D are mean +/- SEM. *P< 0.05, **P< 0.01, ****P<0.0001, ns = no significance (one-way ANOVA with Tukey's multiple comparisons test: C)

in the polar histograms (**Figure 3.1B**). As expected, cells that migrated on the fiber mat lacking alignment (random fibers) showed no preference in the direction of migration. (**Figure 3.1B**). To quantify the contact guidance response, we calculated a trajectory orientation index (TOI) of each migrating cell based on its initial and final location. The TOI has a maximum value of 1 for a cell migration track that travels perfectly aligned to the fibers and a minimum value of -1 for a track that travels perpendicular to the fiber (**Suppl. Figure S3.1C**)[55]. As expected, the TOI values for all four cell lines migrating on randomly oriented fibers were approximately 0, indicating random movement (**Figure 3.1C**). We found that M4 cells displayed the highest TOI among the four cell lines migrating aligned fiber mats, while the premalignant M2 cells exhibited the lowest TOI on aligned fibers (**Figure 3.1C**).

3.3.2 Highly invasive M4 cells display strong contact guidance and high RhoA activation

Since RhoA strongly influences actin dynamics and cell polarity, we hypothesized that the contact guidance response positively correlates with the extent of RhoA activation. We therefore assessed the levels of active GTP-bound RhoA using a rhotekin-RBD pulldown assay in the four breast epithelial cell lines in monocultures on collagen I-coated glass. Cells were serum-starved for 2 days to inactivate Rho, and GTP-RhoA levels were measured in response to serum stimulation. Serum, which contains lysophosphatidic acid (LPA), is a well-known activator of Rho[274,275] and provides a means to compare RhoA activation levels across cell lines. We found that the highly invasive breast epithelial cell lines, M4 and MDA-MB-231, showed the strongest activation of RhoA in response to serum addition (**Figure 3.1D**). Interestingly, the pre-malignant M2 and poorly invasive BT-474 cells displayed a mild decrease in RhoA activation following serum stimulation, indicating that these cells are not responsive to RhoA activating

stimuli. As M4 cells show a robust RhoA activation and a strong contact guidance response, we therefore used these cells to assess the role of RhoA during collective contact guidance.

3.3.3 Loss of RhoA leads to a decrease in contact guidance during collective cell migration

To study the role of RhoA during contact guidance, we used CRISPR/Cas9 RhoA knockout (KO) or scramble control (SCR) M4 cells previously generated in our lab[276] and monitored their migration as described above (see **Figure 3.1**). Additionally, we generated RhoA KO cells expressing eGFP alone or eGFP-RhoA as a rescue cell line. We found that SCR and eGFP-RhoA expressing cells migrated cohesively with tight cell-cell junctions, while RhoA KO and eGFP expressing cells displayed single cells breaking off the migrating sheet (**Figure 3.2A**). Additionally, while SCR and eGFP-RhoA expressing cells traveled directionally along the fiber orientation, RhoA KO and eGFP expressing cells showed frequent deviation from the fiber direction as demonstrated by representative cell tracks (**Figure 3.2B**). Contact guidance was considerably reduced in RhoA KO and eGFP expressing cells compared to SCR and eGFP-RhoA expressing cells (**Figure 3.2C**). We found that RhoA KO cells had an almost twofold reduction in TOI compared to the SCR (**Figure 3.2D**), indicating that RhoA is important for contact guidance during collective cell migration. Additionally, the RhoA KO cells migrated significantly faster than the SCR control cells (**Figure 3.2E**).

Upon further analysis of the cell sheet migration phenotypes, we observed signs of defective cell-cell adhesions within RhoA KO and eGFP expressing cell sheets compared to SCR and eGFP-RhoA expressing cell sheets. To visualize the cytoskeleton at the leading edge, we fixed the cells after 48 hours of migration on fibers and stained for F-actin. We observed that the leading edge of the RhoA KO cell sheet displayed gaps between neighboring cells, indicating junctional fracturing and defective cell sheet organization (**Figure 3.2F**). To quantify this

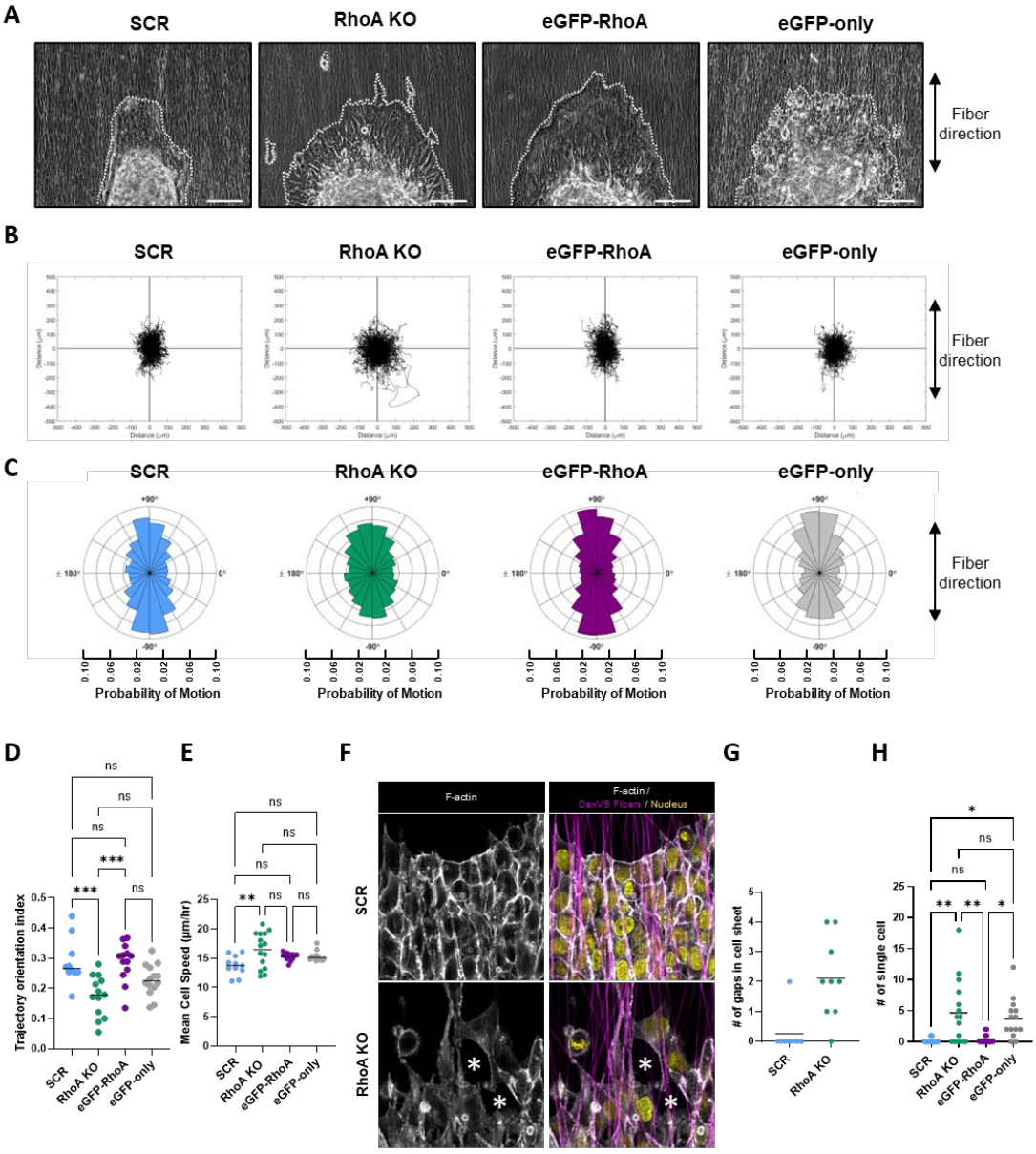

Figure 3.2 Loss of RhoA leads to a reduction in contact guidance.

(A) Phase contrast images of M4 SCR, RhoA KO, eGFP-RhoA rescue, and eGFP-only cells after 18 hours of migration on aligned fiber mats. Scale bars are 100 μm. (B) Representative tracks of cell migration over 22 hours on aligned fiber mats. Aligned fibers are oriented in +90° and -90° direction. (C) Polar histograms demonstrating cell directionality on aligned fibers. Aligned fibers are oriented in +90° and -90° direction. (D) Trajectory orientation index of cells on aligned fiber mats. Middle solid line is the mean value. Each point represents the mean TOI of all the cells from one spheroid. (E) Average speed of cells on aligned fiber mats. Each point represents one spheroid. Middle solid line is the mean value. (F) Representative immunofluorescence image of SCR and RhoA KO cell sheet at leading edge after migration on DexVS aligned fibers labeled with rhodamine methacrylate (magenta) and stained with phalloidin-647 (white) and Hoechst 33342 (yellow). Scale bar is 20 μm. Asterisk depicts gap in cell sheet. (G) Number of gaps between cells at the leading edge. Middle solid line is the mean value. N=2 biological replicates. (H) Number of single cells that have broken away from the migrating sheet. Middle solid line is the mean value. Each point represents one spheroid. *P<0.05, **P<0.01, ***P< 0.001, ns = no significance (one-way ANOVA with Tukey's multiple comparisons test: D, E, H).

behavior, we defined the leading edge of the cell sheet as the first 80-100 μm of the migrating front, quantified the number of gaps between cells in that region, and found that RhoA cell sheets contained more gaps within the leading edge (**Figure 3.2G**).

Additionally, RhoA KO and eGFP expressing cells often displayed single cells breaking away from the migrating sheet. Using an unbiased quantification based on the k-nearest neighbors (KNN) algorithm, we quantified the number of single cells breaking off the migrating sheet over 24 hours of migration. We observed a significant increase in the number of single cells breaking off in cells that lack RhoA (**Figure 3.2H**). Taken together, these data demonstrate that RhoA is crucial for collective contact guidance, possibly through the regulation of cell-cell adhesions.

3.3.4 Contact guidance during collective cell migration is dependent on Rho/ROCK signaling

Active RhoA promotes actomyosin contractility through its effector, ROCK[146]. Therefore, we next tested if inhibition of ROCK1/2 also disrupts contact guidance during collective cell migration. After allowing spheroids to attach to fiber mats, we treated M4 spheroids with the selective, ATP-competitive ROCK1/2 inhibitor Y-27632[277–279], and assessed changes in contact guidance during collective cell migration. After treatment with Y-27632, we observed individual cells breaking off the migrating sheet (**Figure 3.3A**). Consistent with our hypothesis, ROCK1/2 inhibition resulted in a decrease in directional migration along fiber orientation as demonstrated by representative cell tracks (**Figure 3.3B**). Polar histograms of cell directionalities show a decreased proportion of cells travelling along the orientation of fibers following ROCK1/2 inhibition (**Figure 3.3C**). Furthermore, after ROCK1/2 inhibition, we calculated a significant decrease in TOI (**Figure 3.3D**). Like RhoA KO cells, after ROCK1/2 inhibition, we observed an increase in single cells breaking off the migrating sheet compared

with vehicle control, though the phenotype was less dramatic (**Figure 3.3E**). Together these results show that ROCK1/2 activity is crucial for robust contact guidance during collective cell migration and suggest that cell sheet polarization and directional migration require myosin-dependent contractile forces.

3.3.5 Contact guidance during single cell migration is independent of RhoA signaling

We next investigated whether the decreased contact guidance ability of RhoA KO cells represents a cell-autonomous property. In contrast to collective migration, which depends on

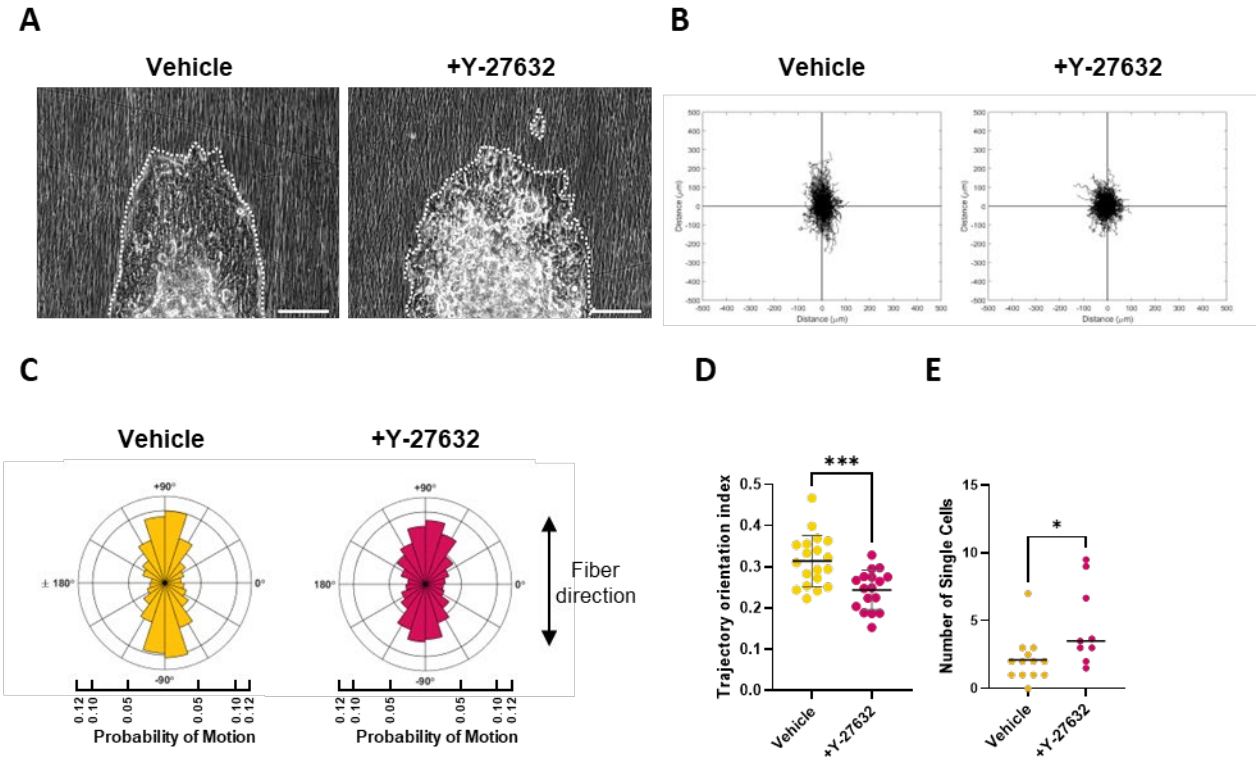

Figure 3.3 ROCK1/2 inhibition leads to a reduction in contact guidance.

(A) Phase contrast images of M4 WT spheroids treated with 10μM Y-27632 or vehicle control. Images taken after 18 hours of migration on aligned fiber mats. Scale bars are 100 μm. (B) Representative tracks from spheroids treated with either 10μM Y-27632 or vehicle after migration on aligned fiber mats. Aligned fibers are oriented in +90° and -90° direction. (C) Polar histograms demonstrating cell directionality on aligned fibers. Aligned fibers are oriented in +90° and -90° direction. (D) Trajectory orientation index of cells on aligned fiber mats. Each point represents the mean TOI of all the cells from one spheroid. (E) Number of single cells that have broken away from the migrating sheet. Middle solid line is the mean value. Each point represents one spheroid. (C: vehicle: n = 5354 cells, 19 spheroids; Y-27632: n = 3859 cells, 11 spheroids). Data in D are mean +/- SD. *P<0.05, ***P< 0.001 (unpaired t-test: D, E).

both cell-substrate and cell-cell interactions, single cell migration depends exclusively on cell-substrate interactions. To avoid the influence of cell-cell adhesions, we therefore focused on investigating individual cell migration by seeding individual cells on fiber mats at a low plating density. We tracked the migration properties of SCR or RhoA KO single cells plated on aligned fiber mats. Using live cell imaging, we observed strong directional migration along fibers for both SCR and RhoA KO single cells (**Figure 3.4A**). Indeed, both SCR and RhoA KO single cells traveled almost exclusively along the fiber orientation as demonstrated by polar histograms of cell directionalities and the similar high trajectory orientation index (**Figure 3.4B&C**). We also found that RhoA KO single cells traveled significantly faster and almost twice as far as SCR single cells (**Figure 3.4D&E**).

Additionally, we observed significant changes to cell morphology after the loss of RhoA, consistent with previous reports[280–282]. SCR cells had a flattened and elongated cell shape along the fiber orientation, while RhoA KO cells had a rounded cell morphology with reduced cell spread area and protrusions (**Figure 3.4F&G**). To quantify changes to cell shape, we calculated the ratio between the major and minor axis of the cell as well as the height of each cell based on F-actin staining (1 = rounded, >1 = elongated). SCR single cells were significantly more elongated along fiber orientation and flatter than the RhoA KO single cells (**Figure 3.4H&I**). Together, these findings show that although the loss of RhoA alters cell shape, it does not impact contact guidance responses during single cell migration thereby suggesting that the decrease contact guidance observed during collective migration is not a cell-autonomous trait.

3.3.6 RhoA depletion leads to changes in focal adhesion elongation and size during individual and collective contact guidance

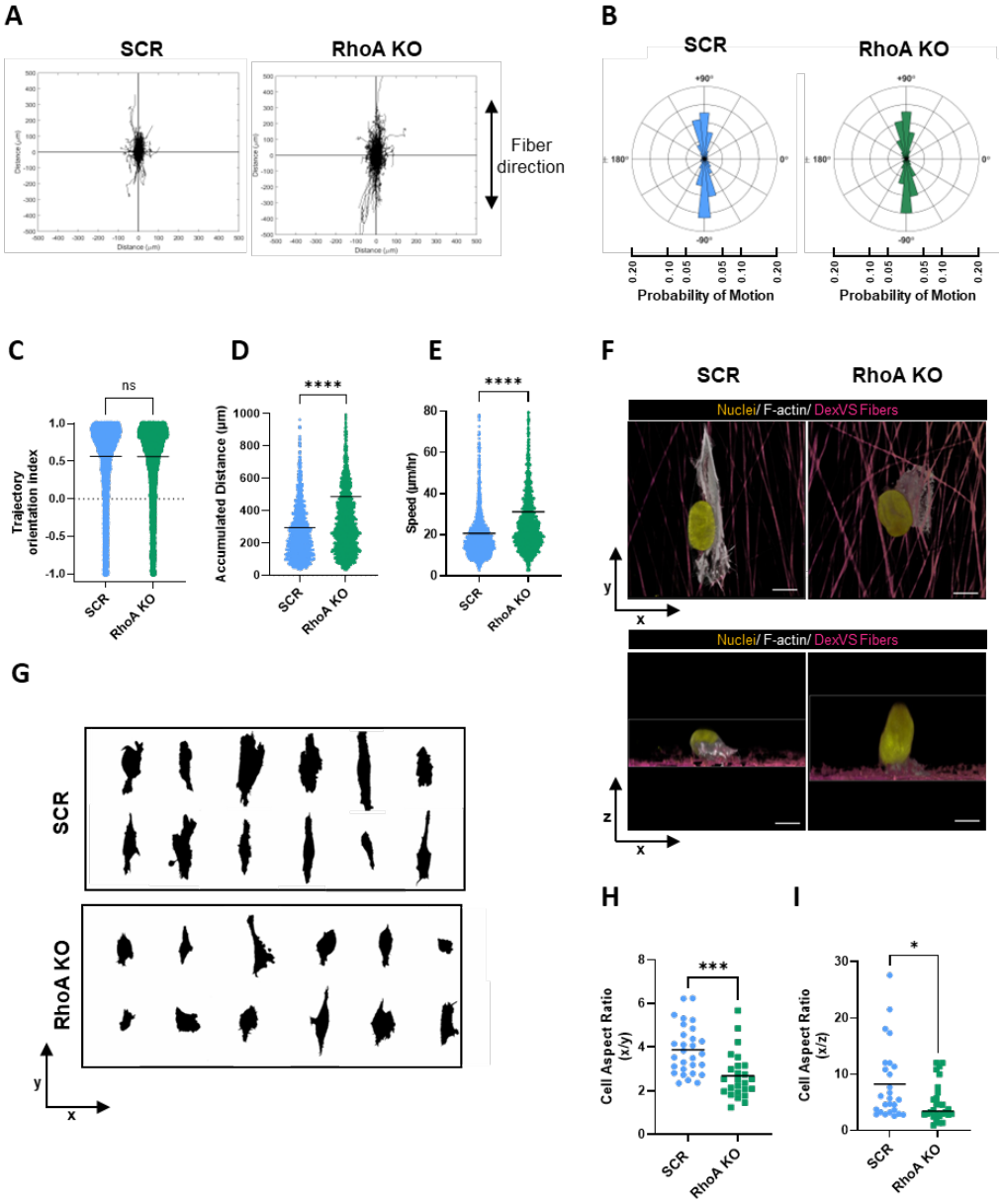

Figure 3.4 Loss of RhoA does not affect contact guidance ability but alters single cell morphology.

(A) Representative tracks from SCR or RhoA KO single cells after migration on aligned fiber mats. Aligned fibers are oriented in +90° and -90° direction. (B) Polar histograms demonstrating cell directionality on aligned fibers. Aligned fibers are oriented in +90° and -90° direction. (C) Trajectory orientation index of cells on aligned fiber mats. Each point represents the TOI of a single cell. Middle solid line is the mean value. (D) Average accumulated distance of single cells after migration on aligned fiber mats. Each point represents the average accumulated distance of a single cell. Middle solid line is the mean value. (E) Average mean speed of single cells after migration on aligned fiber mats. Each point represents the average accumulated distance of a single cell. Middle solid line is the mean value. (F) Representative immunofluorescence image of SCR and RhoA KO single cells migrating on DexVS aligned fibers labeled with rhodamine methacrylate (magenta) and stained with phalloidin-647 (white) and Hoechst 33342 (yellow). Scale bar is 10 µm. (G) Cell outlines of 12 representative single cells in X/Y direction. Aligned fibers are oriented in +90° and -90° direction. (H) Individual cell aspect ratios in X/Y direction. Each point is a cell. Middle solid line is the mean value. (I) Individual cell aspect ratios in X/Z direction. Each point is a cell. Middle solid line is the mean value. (A-E: SCR: n = 1,545 cells; RhoA KO: n = 2,033 cells). ****P< 0.0001, ***P< 0.001, *P<0.05, ns =not significant (unpaired t-test: C-E, H-I).

Aligned architectures spatially constrain focal adhesion formation leading to polarized actin formation and subsequent directional migration[55,283]. As Rho activation is known to play a key role in the formation of focal adhesions[257], we next investigated how the loss of RhoA alters focal adhesions during either individual or collective migration on aligned fiber mats. After integrin-mediated adhesion, paxillin, a focal adhesion adaptor protein[82,284], is recruited to nascent focal adhesions where it serves as a scaffold signaling protein and is crucial for focal adhesion growth[285,286]. Paxillin activation is regulated by numerous phosphorylation events, including phosphorylation at tyrosine residues 118 and 31 by focal adhesion kinase and Src[287–289]. Therefore, we analyzed the morphology and distribution of Y118 phosphorylated paxillin (p-paxillin) after in SCR and RhoA KO cells after 24 hours of migration on aligned fiber mats. We first investigated changes to focal adhesions in individually plated cells. While both SCR and RhoA KO single cells displayed highly aligned focal adhesions along fibers, we observed a decrease in the number of focal adhesions in cells lacking RhoA (**Suppl. Figure S3.2A**). For high-throughput, unbiased quantification of focal adhesions, we utilized the versatile ImageJ plugin TrackMate v7 with integrated Weka Trainable Segmentation detector[262,290] and found that RhoA KO cells displayed approximately half the number of focal adhesions per individual cell compared to SCR cells (**Suppl. Figure S3.2B**). To compensate for the dramatic cell shape changes we observed in RhoA KO cells (see **Figure 3.4F-I**), we quantified the number of focal adhesions per cell area. While the difference did not reach statistical significance, we observed a trend towards a reduction in the number of focal adhesions over cell area in the RhoA KO cells, compared to the SCR (**Suppl. Figure S3.2C**). These findings suggest that since RhoA KO cells exhibit a rounded cell shape, they have less area in contact with the fibers thus leading to a decrease in focal adhesions.

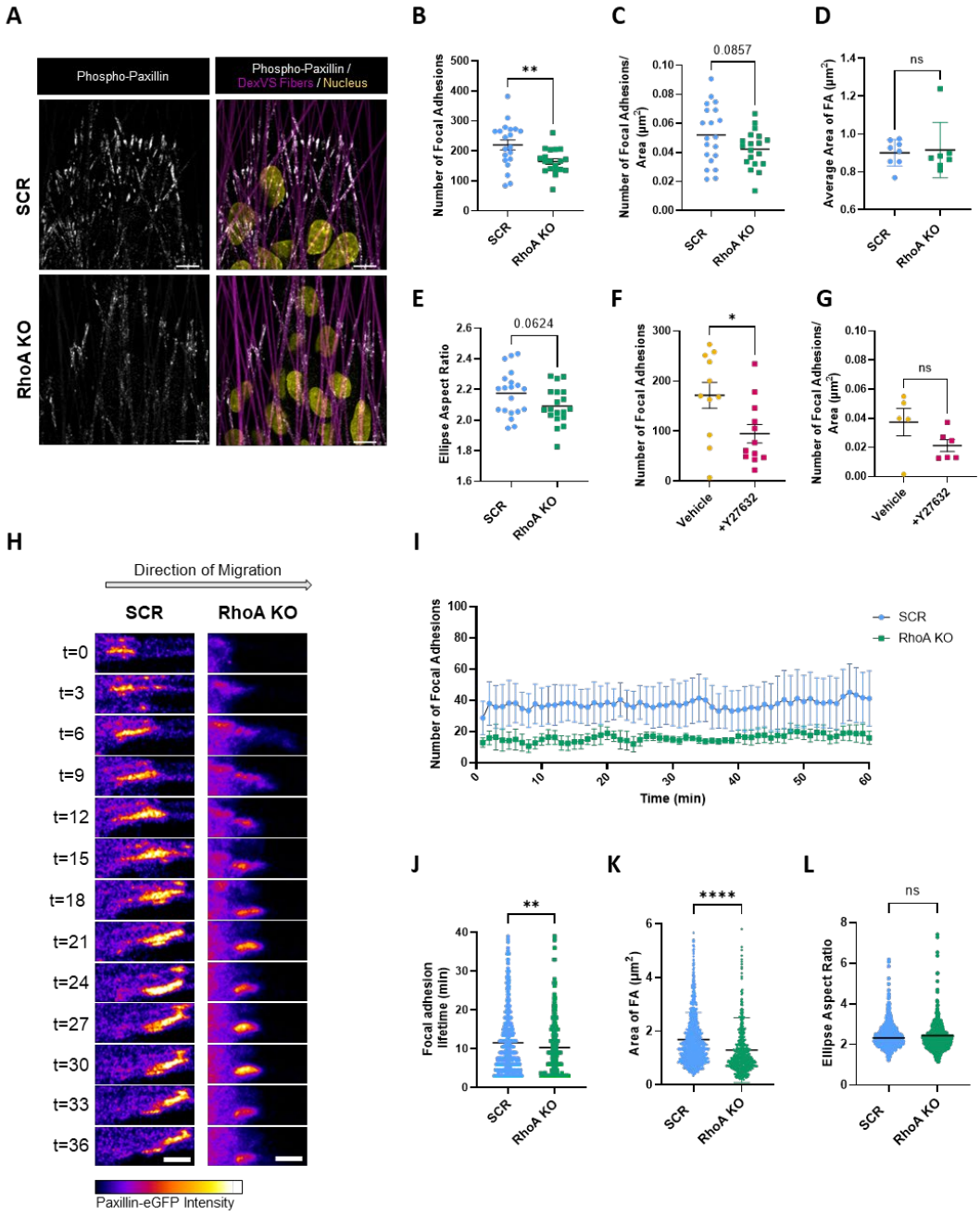

Figure 3.5 RhoA depletion leads to changes in focal adhesion elongation, size, and lifetime during individual and collective contact guidance.

(A) Representative immunofluorescence image of SCR and RhoA KO cells migrating on DexVS aligned fibers labeled with rhodamine methacrylate (magenta) and stained with phospho-Paxillin-Tyr118 (white) and Hoechst 33342 (yellow). Scale bar is 10 μm. (B) Average number of focal adhesions at leading edge after migration on fiber mats. (C) Average number of focal adhesions over cell area after migration on fiber mats. (D) Ellipse aspect ratio of focal adhesions. Each point represents one image. (E) Average area of focal adhesions. Each point represents one image. (F) Average number of focal adhesions after treatment with 10 μm Y-27632 or vehicle control at leading edge after migration on fiber mats. (G) Average number of focal adhesions over cell area after treatment with 10 μm Y-27632 or vehicle control after migration on fiber mats. (H) Montage of a focal adhesion from the leading edge of a SCR or RhoA KO spheroid during migration on aligned fibers. Scale bar is 4 μm. (I) Number of focal adhesions over 1 hour of migration on fiber mats. (J) Average focal adhesion lifetime for SCR and RhoA KO cells. (K) Area of focal adhesions. (L) Ellipse aspect ratio of focal adhesions. (B-E: SCR: n = 4418 focal adhesions, n = 20 spheroids; RhoA KO: n = 3155 focal adhesions, n= 19 spheroids). ****P< 0.0001, **P< 0.01, ns =not significant (unpaired t-test: B-G, J-L). Data in I are mean +/- SEM.

We also measured the average focal adhesion area per cell and focal adhesion ellipse aspect ratio. We found that RhoA KO single cells had larger and more elongated focal adhesions, compared to SCR cells (**Suppl. Figure S3.2D&E**). Thus, in cell migrating individually, while the loss of RhoA did not result in a change in the number of focal adhesions per cell area, the focal adhesions were larger and more elongated.

Next, we investigated focal adhesions at the leading edge of cells migrating collectively on aligned fibers. Similar to observations in single cells, we found that loss of RhoA resulted in a significant decrease in the number of focal adhesions at the leading edge (**Figure 3.5A&B**). After compensating for changes in cell area, we also measured a trend towards a reduction in the number of focal adhesions at the leading edge in RhoA KO cell sheets compared to SCR cells (**Figure 3.5C**). While the loss of RhoA did not affect the area of the focal adhesions (**Figure 3.5D**), we did find that focal adhesions at the leading edge of the collectively migrating cells were almost half the size of the focal adhesions in single cells (compare **Figure 3.5D** with **Suppl. Figure S3.2D**). Furthermore, in contrast to what we observed in single cells, the loss of RhoA did not produce more elongated focal adhesions in collectively migrating cells, if anything, we observed a trend towards reduced focal adhesion elongation in the RhoA KO cell sheets compared to SCR cells (**Figure 3.5E**). Of note, inhibition of ROCK activity using Y-27632, gave rise to similar findings regarding the number of focal adhesions/cell area (**Figure 3.5F&G**). Together, our findings suggest that the way focal adhesions form along aligned structures differs depending on whether cells are migrating individually or collectively.

3.3.7 Focal adhesion lifetime decreases after loss of RhoA during collective contact guidance

As focal adhesions are dynamic protein assemblies, we set out to investigate how the loss of RhoA affects focal adhesion lifetime. It has been reported that early adhesions, which are

generally defined to last 1-3 min in epithelial cells when migrating on flat surfaces [291,292], are more dependent on Rac1, another small Rho GTPase and critical regulator of cytoskeletal dynamics, while mature focal adhesion formation requires high RhoA activation and lower Rac1 activity[293]. To monitor focal adhesion assembly over time, we expressed paxillin-eGFP, which has been reported to faithfully localize to focal adhesions[294], into SCR and RhoA KO cells and imaged the leading edge for one hour as the cells migrated on aligned fiber mats. We tracked focal adhesion localization and dynamics over time using the Weka detector within TrackMate, as previously described[262]. We observed that the collectively migrating SCR cells displayed stable focal adhesion structures that did not appear to retrograde over time (**Figure 3.5H**). We also found that the loss of RhoA resulted in fewer focal adhesions at the leading edge compared to SCR cells over one hour; however, due to experimental conditions, we were not able to calculate the number of adhesions compared to cell area (**Figure 3.5I**). Furthermore, loss of RhoA resulted in shorter focal adhesion lifetime compared to SCR cells (**Figure 3.5J**). We also found that, compared to SCR cells, RhoA KO cells had smaller focal adhesions (**Figure 3.5K**), although the ellipse aspect ratio remained unchanged (**Figure 3.5L**). Together, we show that, similar to other reports[257,258], RhoA is necessary for proper focal adhesion maturation.

3.3.8 Collectively migrating RhoA KO cells display altered adherens junctions and desmosomes

RhoA is well-known to influence cell-cell junction formation and stability in epithelial cells[295,296]. We therefore hypothesized that the diminished contact guidance response of RhoA KO cells is partially due to defective cell-cell adhesions. AJs are mechanosensitive multi-protein complexes that link the actin cytoskeleton between neighboring epithelial cells and are important in collective epithelial migration[118,297]. Therefore, we first examined changes to E-cadherin, a

well-characterized AJ protein, in cells that migrated for 48 hours on fibers. It has been previously shown that loss of RhoA results in a decrease in E-cadherin membrane localization[259,298], likely because active RhoA is known to stabilize E-cadherin at AJs and thus promote coordinated collective cell migration[260,261,299]. Indeed, we observed frequent gaps between cells within the RhoA KO migrating sheet, indicating defects in cell-cell adhesion and sheet formation (**Figure 3.2F-H**). Surprisingly, however, using immunostaining, we observed that the loss of RhoA results in a dramatic increase in E-cadherin localization to cell-cell junctions at the leading edge (**Figure 3.6Ai&Aii**).

The unexpected increase in E-cadherin localization in RhoA KO cells migrating on aligned fiber mats led us to ask whether other cell-cell junctions were affected. Therefore, we next investigated changes in desmosomes, a type of cell-cell adhesion that connects the intermediate filament cytoskeleton of neighboring cells. It has been demonstrated that AJs and desmosomes interact to maintain epithelial integrity[114]. In fact, E-cadherin has been shown to localize to desmosomes and promote desmosome assembly[300–302]. Thus, we assessed changes in desmosome formation by immunostaining for Desmoplakin, a component of desmosomes[140]. As expected for epithelial cells, we found that Desmoplakin localized to cell-cell junctions in distinct punctate in migrating SCR cells. However, we observed that RhoA KO cells displayed a dramatic decrease in the intensity of Desmoplakin punctate at cell-cell adhesions (**Figure 3.6Bi&Bii**). Furthermore, inhibition of ROCK activity using Y-27632 gave rise to similar findings, although the decrease in Desmoplakin punctate staining was less dramatic than what we

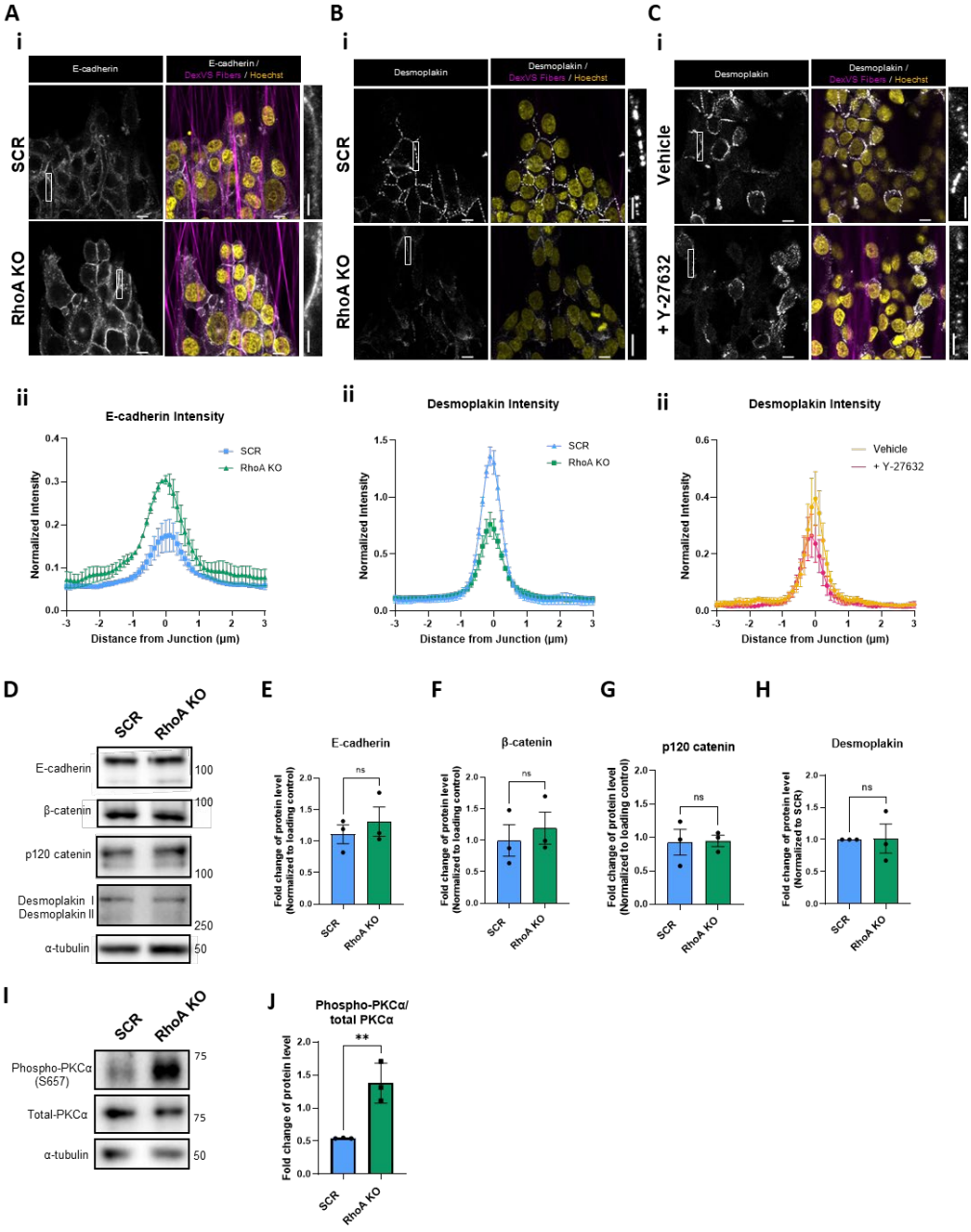

Figure 3.6 Migrating RhoA KO cells display altered adherens junctions and desmosomes.

(Ai) Representative immunofluorescence image of SCR and RhoA KO cells migrating on DexVS aligned fibers labeled with rhodamine methacrylate (magenta) and stained with E-cadherin (white) and Hoechst 33342 (yellow). Aligned fibers are oriented in +90° and -90° direction. Scale bar is 10µm. Insert scale bar is 5µm. (Aii) Quantification of the relative intensity of E-cadherin immunofluorescence across a 6 µm line scan. (Bi) Representative immunofluorescence image of SCR and RhoA KO cells migrating on DexVS aligned fibers labeled with rhodamine methacrylate (magenta) and stained with Desmoplakin (white) and Hoechst 33342 (yellow). Scale bar is 10µm. Insert scale bar is 5µm. (Bii) Quantification of the relative intensity of Desmoplakin immunofluorescence across a 6 µm line scan. (Ci) Representative immunofluorescence image of M4 WT cells treated with 10µM Y-27632 or vehicle control migrating on DexVS aligned fibers labeled with rhodamine methacrylate (magenta) and stained with Desmoplakin (white) and Hoechst 33342 (yellow). Scale bar is 10µm. Insert scale bar is 5µm. (Cii) Quantification of the relative intensity of Desmoplakin immunofluorescence across a 6 µm line scan. (D, I) Western blot analysis of whole-cell lysates harvested from SCR and RhoA KO cells. (E-H, J) Quantification of western blot results of three biological replicates. **P< 0.01, ns =not significant (unpaired t-test: E-H, J).

observed in the RhoA KO cells (**Figure 3.6Ci&6Cii**). These findings provide evidence that changes in desmosomes in RhoA KO cells are dependent on ROCK activity.

To determine if changes in protein localization were due to alterations in total protein levels, we performed western blot analysis of E-cadherin, β-catenin, and Desmoplakin. We additionally probed for p120 catenin, a central player in AJ stability, which has a well-established relationship with RhoA at AJs[303–305]. We measured no significant changes in steady-state protein levels for E-cadherin, β-catenin, p120 catenin, and Desmoplakin (**Figure 3.6D-H**), indicating that loss of RhoA is altering E-cadherin and Desmoplakin localization to cell-cell adhesion, and not altering global protein expression.

It has been demonstrated that protein kinase C α (PKC-α) regulates both desmosome formation[306,307] and disassembly[308,309] through phosphorylation of desmosomal components. In fact, it has been shown that PKC-α phosphorylates the C-terminal tail of Desmoplakin leading to destabilization of desmosomes[310]. Therefore, we next investigated whether total and active phosphorylated PKC-α levels change in RhoA KO cells. We found that, while total levels of PKC-α protein are identical in SCR and RhoA KO cells, the levels of phospho- PKC-α increase in RhoA KO cells compared to SCR cells (**Figure 3.6I&IJ**). These findings suggest that the loss of Rho/ROCK signaling leads to increased PKC-α activity which could in turn destabilize desmosomes. Together, our findings demonstrate that RhoA is crucial for the proper formation of both AJs and desmosomes in migrating epithelial cells.

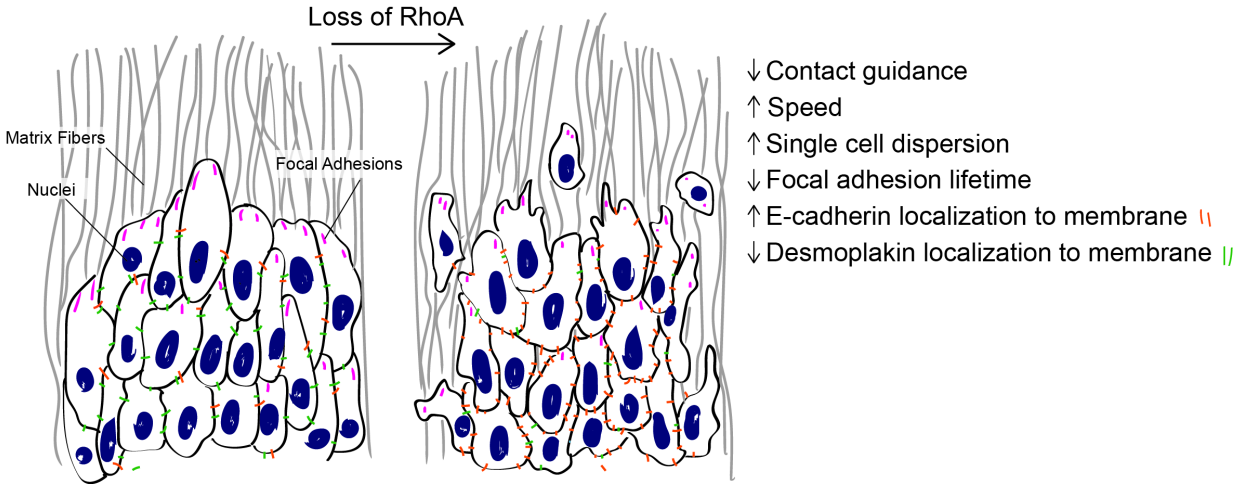

Figure 3.7 Schematic representation of how the genetic loss of RhoA affects contact guidance during collective cell migration.

3.4 Discussion

The purpose of this study was to determine whether RhoA signaling controls contact guidance during collective cell migration in breast cancer cells. It has been demonstrated that RhoA plays a critical role in directed cell migration, largely due to its regulation of actomyosin contractility which is necessary for proper force generation[79]. While several studies have suggested that inhibition of RhoA reduces directional migration[311,312], other studies reported that loss of RhoA results in greater directional persistence[313,314] or has no effect[315,316]. Further, it has been demonstrated that focal adhesions are critical for proper directed cell migration[63] and contact guidance fidelity[53–55], and RhoA activity has been shown to be critical for focal adhesion stability[257,258,317]. Using aligned electrospun fibers as a contact guidance cue, we studied the role of RhoA in contact guidance in collective and single cell migration. We showed that RhoA/ROCK signaling is involved in mediating contact guidance during collective cell migration, though RhoA is dispensable for contact guidance in single cells. Moreover, we

discovered that disruption of both cell-matrix and cell-cell interactions are involved in the loss of contact guidance (**Figure 3.7**).

Much of the work studying contact guidance has been done using single cells, though collective cell migration is a primary mode of invasion *in vivo*[101,105,254]. In our study, we investigated the role of RhoA in contact guidance during both collective and single cell migration. Interestingly, we found that RhoA is crucial for collective contact guidance, while it is dispensable for contact guidance in single cells. Interestingly, we discovered that focal adhesions in RhoA KO single cells were larger and more elongated than SCR single cells, while focal adhesions in RhoA KO collectively migrating cells did not show any change in size or elongation compared to SCR cells. The differences we observed in focal adhesions between single and collectively migrating cells is likely due to crosstalk between AJs and focal adhesions[318–320]. In fact, classical cadherins, found at AJs, have been shown to be crucial for focal adhesion positioning and cell polarization ultimately directing directional migration[321–323]. Therefore, the influence of intercellular junctions may influence focal adhesion elongation and size, thereby leading to different focal adhesion patterns in single and collectively migrating cells.

We found that loss of RhoA results in shorter focal adhesion lifetimes in collectively migrating cells, which is consistent with previous findings during single cell migration[257,258]. It has been demonstrated that early adhesions are more dependent on Rac1 activity than RhoA[324,325], while mature focal adhesion formation requires high RhoA and lower Rac1 activity[85,312,326–328]. Also, it has been shown that diminished RhoA signaling causes a decrease in the number of focal adhesions[329–333], while elevated levels of RhoA can lead to greater focal adhesion size and stability[334]. The shorter focal adhesion lifetimes we observe may be due to

reduced activity of mDia, a downstream effector of RhoA, since it has been reported that loss of mDia impairs directed single and collective migration through the inhibition of adhesion turnover and polarization[84,335,336]. Alternatively, it has been proposed that ROCK-induced myosin activity is critical for adhesion maturation[258,336]. The loss of RhoA, and the subsequent decrease in cellular contractility, may result in insufficient tension generation required for mature focal adhesion formation and stability. Future studies are necessary to determine whether mDia or ROCK signaling is responsible for the changes in focal adhesion lifetime we observe in our system.

Collective cell migration also depends on cell-cell cooperation which is primarily achieved through cell junctions such as AJs[337]. Active RhoA has been shown to be localize AJs during epithelial migration where it promotes the formation of AJs[298,338] and increases E-cadherin stability[261,299,339,340]. In fact, RhoA at AJs has been shown to promote orderly migration[261] and be crucial for the preservation of epithelial integrity during migration[341]. We found that the loss of RhoA increases the localization of the AJ protein E-cadherin to cell junctions which is counter to what has been shown, though we observed that RhoA KO results in fractures at cell junctions and disordered migration which aligns with previous literature. Interestingly, inhibition of ROCK1/2 has been shown to both promote AJ stability[342] as well as disrupt AJ assembly[304,343,344]. Additionally, mDia activation by Rho is known to be important for AJ integrity[345,346] and epithelial polarity[347]. Therefore, future studies will investigate which downstream effectors of Rho are responsible for these changes in AJs.

Crosstalk between AJs and desmosomes has long been established as E-cadherin is well-known to localize to desmosomal plaques[300,348–350]. In fact, E-cadherin-mediated adhesion regulates the organization of desmosomal adhesions[351]. We found that the increase in E-cadherin

localization to the membrane following RhoA ablation occurred concomitantly with a decrease in desmosomal plaques at cell junctions. Additionally, we found that inhibition of ROCK1/2 activity resulted in a decrease in desmosomal plaques, though the decrease was not as dramatic as that resulting from the genetic deletion of RhoA. Not much is known about the relationship between RhoA and desmosomes. It has been reported that depletion of plakophilin 2, a desmosomal protein, results in a failure of activated RhoA to localize to cell-cell junctions[352]. Additionally, it has been demonstrated that Desmoplakin is required for tension-activated RhoA signaling at AJs[353]. Based on our findings, we hypothesize that junctional tension within the migrating cell sheet is not properly sensed due to the loss of RhoA, thus leading to the fracturing of epithelial junctions. In an effort to restore epithelial integrity, more E-cadherin is then recruited to the junctions which ultimately leads to a disruption in desmosome formation. It remains to be determined how the loss of RhoA affects other intercellular junctions in our system and whether this response is dependent on migration-induced tension.

Much remains to be determined about the mechanisms by which RhoA regulates contact guidance during collective cell migration. Others have shown that loss of RhoA activity results in drastic changes to other Rho GTPases, notably Rac1[354], RhoB[311,355,356], and RhoC[355,357]. Despite their high homology, Rho family GTPases often have unique cellular functions and intricate temporal and spatial coordination during cell migration on flat surfaces[164,168,358]. Notably, it has been demonstrated that the depletion of RhoB, a Rho isoform, results in decreased directional persistence and focal adhesion lifetime on flat surfaces[359], and drives E-cadherin internalization from cell-cell junctions[360]. These studies highlight the potential overlapping roles of RhoA and RhoB isoforms in regulating contact guidance. Future studies will determine whether other Rho GTPases are essential for contact guidance, and how the genetic

knockout of RhoA affects the balance of Rho signaling in our system. Additionally, while we demonstrate that RhoA/ROCK signaling is crucial for proper collective contact guidance, we have yet to dissect the other key players responsible for this phenotype. While the genetic loss of RhoA resulted in much greater junctional fracturing compared to inhibition of ROCK1/2, both strategies decreased contact guidance in collective cell migration. Therefore, it is likely that another downstream effector, such as mDia, is acting to preserve epithelial integrity through the regulation of cell junctions.

In conclusion, our findings complement the previously established role of RhoA in cell migration, while establishing that RhoA/ROCK signaling directs contact guidance during collective migration through the dual regulation of focal adhesions as well as cell-cell adhesions. Future studies will aim to understand the role of other Rho GTPases in collective contact guidance as well as establishing the role of other Rho-activated kinases in this process. Taken together, our study furthers the understanding of how Rho GTPase-mediated signaling pathways contribute to directed collective cell migration.

3.5 Supplementary Materials

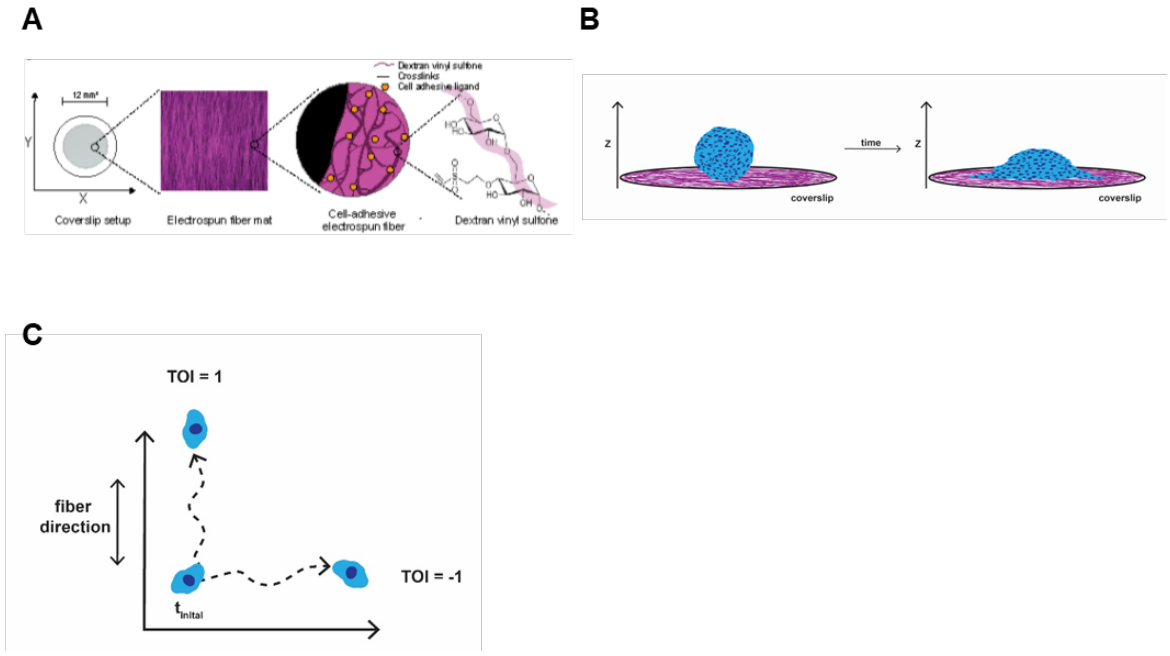

Figure S3.1 Graphic explanation of methods used in this chapter.

(A) Cartoon depicting the method used to generate fibers. Dextran is reacted with vinyl sulfone to create DexVS, which then is mixed with LAP and electrospun to create fiber mats on coverslips. (B) Graphic explanation of spheroid migration assay setup on DexVS fiber mats. (C) Cartoon of trajectory orientation index (TOI) calculation based on fiber direction.

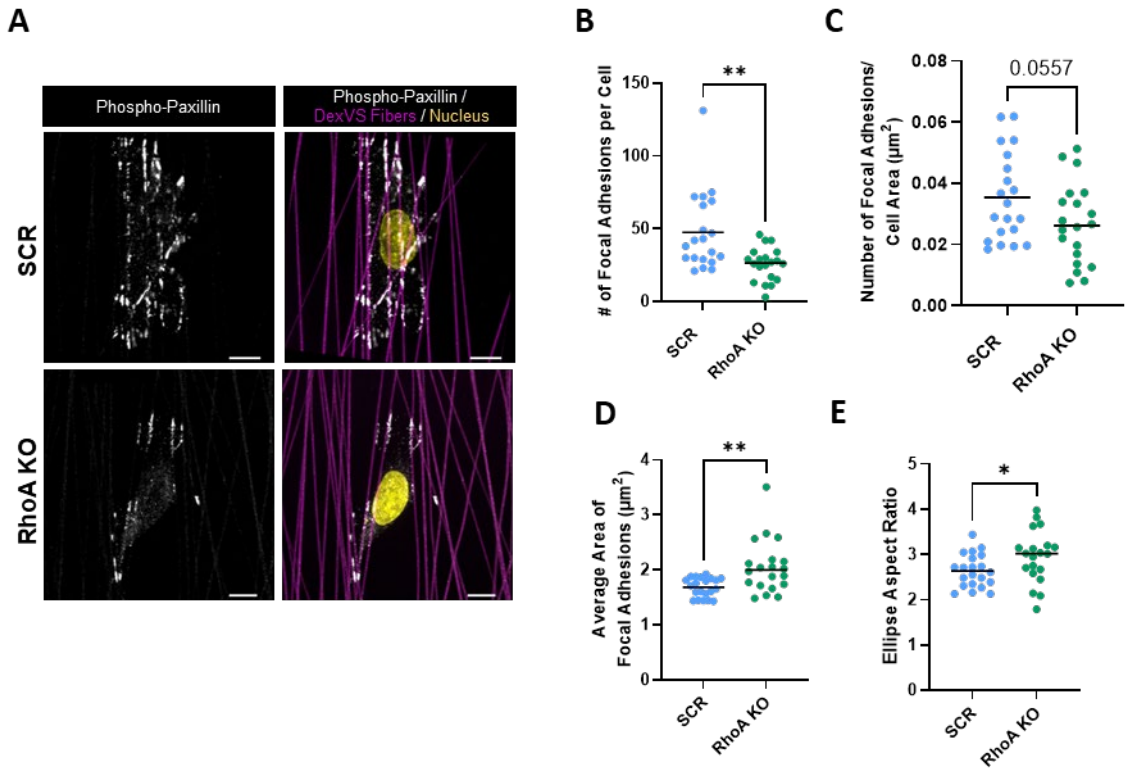

Figure S3.2 RhoA depletion leads to reduced number of focal adhesions per cell during individual contact guidance.

(A) Representative immunofluorescence image of SCR and RhoA KO single cells migrating on DexVS aligned fibers labeled with rhodamine methacrylate (magenta) and stained with phospho-Paxillin-Tyr118 (white) and Hoechst 33342 (yellow). Scale bar is 10 μm. (B) Average number of focal adhesions per cell after migration on fiber mats. (C) Average number of focal adhesions over cell area after migration on fiber mats. (D) Average area of focal adhesions. Each point represents one cell. (E) Ellipse aspect ratio of focal adhesions. Each point represents one cell. **P< 0.01, *P< 0.05, ns =not significant (unpaired t-test: B-E).

3.6 Methods

3.6.1 Dextran Vinyl Sulfone (DexVS) Synthesis

As previously published[236], 5 g of high molecular weight (86 kDa) dextran (Sigma) was dissolved into 250 ml of 100 mM sodium hydroxide and the solution was stirred at 250 RPM for 10 min. Stir plate was increased to 500 RPM, and 12.5 mL of divinyl sulfone was added to the reaction for 3.5 min. The reaction was terminated by adding 2.5 mL of 12M hydrogen chloride

slowly to the solution. The solution was dialyzed against Milli-Q water for 3 days and water was changed every 12 h. DexVS was aliquoted into 50 ml conical tubes and frozen for 1 h at -80°C. The aliquots were lyophilized at -86°C and 0.040 mBar for 72 h and stored at -30°C until use.

3.6.2 DexVS Fiber Fabrication

Lyophilized DexVS was dissolved at 0.6 g/mL in 1:1 dimethylformamide (DMF)/MQ with 10 mg/mL lithium phenyl-2,4,6- trimethylbenzoylphosphinate (LAP, Colorado Photopolymer Solutions), 0.75 mM methacryloxyethyl thiocarbamoyl rhodamine B (Polysciences, Inc.), and 5% glycidyl methacrylate on a stir plate at ~100 rpm for 4 h. DexVS spinning solution was drawn into a 1mL syringe attached to a bent 305 mm 18G stainless steel needle. The syringe was attached to a syringe pump (KD Scientific) set at 0.2 mL/h and placed into a humidity-controlled glove box (30-35% relative humidity). To create random fiber mats, a coverslip was set on a grounded copper collective surface centered 7 cm from the tip of the needle. The needle was connected to a high-voltage source (Gamma High Voltage Research) set at -7 kV. For aligned fiber mats, the coverslip was balanced between two copper plates set at +4 kV while the needle was set to -4 kV. Fibers were spun for 3 min per coverslip. Fiber-coated coverslips were primary crosslinked for 20 s under UV light at 100mW/cm^2. Coverslips were glued into a cut 12 well plate. Coverslips were then hydrated by the addition 80 µL of 2.5 w/v% heparin methacrylate diluted in 1 mg/mL LAP and exposed to 100mW/cm^2 UV light for 20 s. Coverslips were stored in DPBS for up to 3 days at room temperature (RT) before use.

3.6.3 Cell Culture

Epithelial cell lines MCF10AT (M2) and MCF10CA1a (M4) from the MCF10A cell series (Barbara Ann Karmanos Cancer Institute, Detroit, MI) were cultured in DMEM/F12

(Gibco) supplemented with 5% heat-inactivated horse serum (Gibco). Cells were cultured at 5% CO_2 and 37°C in humidified incubators. The media for M2 cells was also supplemented with 10 μg/mL insulin (Invitrogen), 10 ng/mL EGF (Peprotech), 0.5 μg/mL hydrocortisone (Sigma Aldrich), and 100 ng/mL cholera toxin (Sigma Aldrich). MDA-MB-231 cells were cultured in DMEM/high glucose (Gibco) supplemented with 10% fetal bovine serum (Gibco). BT-474 cells were cultured in RPMI (Gibco) supplemented with 10% fetal bovine serum. All cell lines were tested for mycoplasma contamination using the Mycoalert detection kit (Lonza).

RhoA KO was performed using CRISPR/Cas9 as previously described[276]. Briefly, the target sequence 5′-GAACTATGTGGCAGATA TCG-3′ was cloned into LentiCRISPRv2. Lentiviral particles were produced using HEK293T cells and a pPACKH1 kit (System Biosciences) per the manufacturer's instructions. After infection, M4 cells were selected using 2.5 μg/mL puromycin, cloned, and confirmed using western blot. Stably infected cells were maintained in puromycin (2.5 μg/mL).

Paxillin-pEGFP was a gift from Rick Horwitz (Addgene plasmid #15233). pcDNA3-EGFP-RhoA-wt was a gift from Gary Bokoch (Addgene plasmid # 12965). Paxillin-pEGFP and EGFP-RhoA sequences were subcloned into pBABE hygromycin backbone. pBABE-hygro was a gift from Hartmut Land & Jay Morgenstern & Bob Weinberg (Addgene plasmid # 1765). To generate M4 CRISPR SCR and M4 RhoA KO cells stably expressing paxillin-eGFP and M4 RhoA KO cells expressing eGFP-RhoA, Phoenix (human kidney epithelial) cells were transfected with the plasmid with Lipofectamine™ 3000 Reagent (Fisher Scientific) according to manufacturer's protocol. 48 h after transfection, cell culture media containing retroviral particles was collected, filtered through a 0.45 μm polyethersulfone (PES) membrane filter, and concentrated overnight. Cells were then infected with concentrated virus for 48 h. Cells were

selected and maintained using 200 μg/mL hygromycin. eGFP-RhoA rescue was confirmed using western blot.

Spheroids were formed by culturing cells in a low-adhesion plate. Briefly, 96 well v-bottom plates were coated with 100 μl of 1.2% 2-hydroxyethylmethylmethacrylate (polyHEMA, Sigma) diluted in 95% ethanol. Ethanol was allowed to evaporate for 3 days in a 37°C oven. Before plating cells, wells were washed twice with 200 μl of DPBS. Cells were diluted to 12,500 cells/mL and 80 μl of cell suspension was seeded into each well of a 96 well plate. Spheroids were grown for 6 days at 37°C and 5% CO_2. Spheroids were then collected and plated onto fiber mats as described below.

3.6.4 Migration Assays and Time-Lapse Imaging

Prior to seeding, fiber mats were sterilized with 70% ethanol for 10 min at RT. Fibers were then coated with 100 μg/mL bovine collagen I (Advanced BioMatrix #5005) diluted in water for 1 h at 37°C. For the spheroid migration assay, spheroids were collected and stained with 0.8 μg/mL Hoechst 333482 (Invitrogen #H21492) for 10 min at 37°C. Roughly 4-6 spheroids were plated into each well and allowed to adhere for 2 h at 37°C. For single cell migration assays, cells were grown to 70% confluency, trypsinized, and resuspended at 12,000 cells/mL in full media. 1mL of cells were plated per well and allowed to adhere for 3 h. For pharmacological studies, 10 μM Y-27632 (Tocris) was supplemented to media 2 h after spheroid seeding and refreshed after 24 h.

Cells were imaged using a Zeiss Axio Observer Z.1 LED epifluorescence microscope equipped with an automated stage and environmental chamber that maintains temperature (37°C) and CO_2 (5%) levels. Phase-contrast images were taken every 10 min and fluorescence images were acquired every 30 min for 20 h. Fluorescent fiber mats were imaged at the first timepoint.

For live cell paxillin-eGFP imaging, spheroids were seeded onto fiber mats as described above. Spheroids were allowed to adhere and migrate overnight at 37°C and 5% CO_2. Cells were then imaged with a Zeiss LSM 880 laser-scanning confocal microscope equipped with an environment chamber that maintains temperature (37°C) and CO_2 (5%) levels. Fluorescent images of the rhodamine fibers and paxillin-eGFP were acquired every 3 min using an oil-immersion, 63X objective.

3.6.5 Quantitative Analysis of Cell Migration

Time-lapse images were post-processed in ImageJ, and nuclei were tracked using the TrackMate plugin in ImageJ[239]. Tracking data was then imported into MATLAB for further analysis. Cells that traveled less than 5 frames or less than 20 μm from starting position to final position were filtered out. Accumulated distance was determined by calculating the nuclear displacement between two frames

$$\boldsymbol{d} = \sqrt{(\boldsymbol{x_2} - \boldsymbol{x_1})^2 + (\boldsymbol{y_2} - \boldsymbol{y_1})^2}$$

Cell speed was then determined by dividing accumulated distance over total time traveled. The direction of motion (θ) for each cell was determined by calculating the angle between the initial and final location of the cell. Trajectory orientation index was calculated to quantify cell trajectories along fiber alignment[55] as defined by

$$\boldsymbol{TOI} = \frac{\theta \text{ [in degrees]}}{45} - 1$$

where a value of 0 denotes a randomly migrating cell trajectory and 1 denotes a perfectly linear cell trajectory along the fiber orientation.

To quantify the number of single cells which broke off from the migrating sheet, the k-nearest neighbors algorithm[241] was utilized which identifies a single cell based on its distance to any

other cell within the frame. A cell was classified as a single cell if it was at least 50 μm away from any other cell within the frame.

3.6.6 Western Blotting Analysis

Western blotting was used to assess E-cadherin, β-catenin, p120-catenin (catenin δ-1), and Desmoplakin protein levels. To prepare samples, cells were plated into 6 well glass bottom plates coated with 100 μg/mL collagen I and grown for 48 h to 80% confluence. Cells were placed on ice and washed once with ice-cold DPBS. Cells were then lysed in RIPA buffer (G Biosciences) containing 1X phosSTOP phosphatase inhibitors (Roche) and cOmplete protease inhibitor cocktail (Roche) for 10 min on ice with gently agitation. Cells were spun at 13,200 RPM for 15 min at 4°C, supernatant was collected, and stored at -80°C until use. Lysates were diluted in 1X Laemmeli sample buffer (Bio-Rad) and boiled at 95°C for 10 min. 10 μg of protein was loaded per lane and resolved by 4-20% SDS-PAGE. Samples were transferred onto PDVF membranes (Millipore) and blocked with 5% bovine serum albumin (BSA, Sigma-Aldrich A9576) for 1 h at RT. Membranes were probed overnight with primary antibodies against: E-cadherin (Cell Signaling Technology, #3195, dilution 1:1,000), β-catenin (Cell Signaling Technology #9582, 1:1000), catenin δ-1 (Cell Signaling Technology, #4989, dilution 1:1000), Desmoplakin 1&2 (Sigma-Aldrich, #CBL173, dilution: 1:1000), and α-tubulin-HRP (Proteintech, HRP-66031, dilution: 1:10,000). Primary antibodies were diluted in blocking buffer. Bands were visualized using HRP-conjugated secondary antibodies (Jackson ImmunoResearch, dilution 1:10,000), SuperSignal™ West Pico PLUS Chemiluminescent Substrate (Thermo Fisher Scientific), and a C600 digital imaging system (Azure). Band integrated density was measured using ImageJ.

3.6.7 RhoA GTPase activation assay

RhoA activation was accessed using the Rho Activation Assay Biochem Kit (Cytoskeleton #BK036) according to manufacturer's instructions. Briefly, 12mL of M2, M4, BT-474, or MDA-MDA-231 cells were plated into 15 cm^2 dishes at 1.5 x 10^4, 1.0 x 10^4, 12.0 x 10^4, and 3.5 x 10^4 cells/mL, respectively. Seeding densities were determined based on growth rate. Cells were grown in full serum media for 48 h, and then serum starved for 48 h. For serum starvation, M2, M4, and MDA-MDA-231 cells were cultured without serum (0%), while BT-474 cells were cultured in reduced serum media (1% FBS) to prevent cell death. Our lab previously optimized serum starvation conditions for each cell line[267]. On day 4, all cell lines were at 20-30% confluence to increase RhoA activation response. Serum is a potent RhoA activator and was used to activate RhoA in our system[257,361]. Cells were treated with full serum for 12 min, washed once with ice-cold DPBS, and lysed on ice using cell lysis buffer (Cytoskeleton, #CLB01) with 1X protease inhibitor cocktail (Cytoskeleton, #PIC02). Lysates were scrapped, spun at 10,000 g for 1 min at 4°C and snap frozen in liquid nitrogen. As controls, 0.8 μg/μL M2 unstimulated lysates were loaded with either GDP or GTPγS (non-hydrolysable GTP analog) for 15 min rotating at RT before pulldown. 700 μg of cell lysate were mixed with 50 μg of Rhotekin-RBD beads (Cytoskeleton, #RT02) and rotated at 4°C for 1 h. Lysates were spun at 4°C for 1 min at 5,000 RCF and washed with Wash Buffer. Then, lysates were spun again at 5,000 RCF for 3 min at 4°C and supernatant was removed and discarded. 20 μl of Laemelli buffer (Fisher Scientific #AAJ61337AD) was added to bead pellet and samples were boiled for 2 min at 95°C. Pulldown and whole-cell lysates were resolved using 4-12% SDS-PAGE. Samples were transferred onto a 0.2 μm PDVF membrane (Millipore) and let dry for 20 min at RT. Membranes were rehydrated in methanol and blocked using 5% non-fat dry milk for 30 min. Membranes were probed overnight at 4°C with anti-RhoA antibody (Cytoskeleton #ARH05, dilution: 1:500). Bands were

visualized using HRP-conjugated secondary antibodies (dilution 1:10,000, Jackson ImmunoResearch), SuperSignal™ West Pico PLUS Chemiluminescent Substrate (Thermo Fisher Scientific), and a C600 digital imaging system (Azure). Band integrated density was measured using ImageJ.

3.6.8 Immunofluorescence staining

For analysis of protein localization and actin morphology, spheroids were fixed after 48 h of migration on fiber mats. Cells were washed with DPBS twice and fixed with 4% paraformaldehyde (Electron Microscopy Sciences) for 10 min at 37°C. Once fixed, cells were washed three times with DPBS and permeabilized with 0.1% Triton X-100 (Fisher Scientific) for 15 min at RT. Cells were blocked in 4% BSA diluted in PBSt (DPBS + 0.1% Tween-20) for 1 h at RT. Cells were probed overnight at 4°C with primary antibodies against: E-cadherin (Cell Signaling Technology #3195, dilution 1:500), β-catenin (Cell Signaling Technology #9582, dilution: 1:400), Desmoplakin 1&2 (Sigma-Aldrich #CBL173, dilution: 1:200), phospho-Paxillin [Y118] (Cell Signaling Technology #2541, dilution: 1:250). Primary antibodies were diluted in 1% BSA:PBSt. Cells were stained with fluorescent secondary antibody (Invitrogen #A-21240, dilution: 1:1,000) diluted in 0.1% BSA:PBSt for 45 min at RT. For F-actin staining, cells were labeled with phalloidin-647 (Invitrogen #A22287, dilution: 1:200) for 45 min at RT. Cells were imaged using either a 40X water or 63X oil objective lens on a Zeiss LSM880 confocal microscope in Airyscan mode.

To quantify the number of gaps between cells at the leading edge, we manually counted the number of gaps for each field of view that had a diameter greater than 5 μm. Analysis of cell aspect ratio was done in ImageJ based on phalloidin and nuclear staining. To measure focal

adhesions based on phospho-paxillin immunofluorescence images, we used the TrackMate-Weka ImageJ plugin[262].

A line-scan analysis was performed in ImageJ to measure the relative intensity of E-cadherin and Desmoplakin immunofluorescence stains across cell-cell junctions.

3.6.9 Statistical Analysis

GraphPad Prism and MATLAB were used for data visualization, and Graphpad Prism was used to conduct statistical analysis. Statistical significance was determined using one-way analysis of variance (ANOVA) with Dunnett's multiple comparisons test or unpaired t-test where appropriate. The tests and size of samples are described in the respective figure legends. Significance is indicated by $p < 0.05$.

3.7 Appendix for Chapter 3

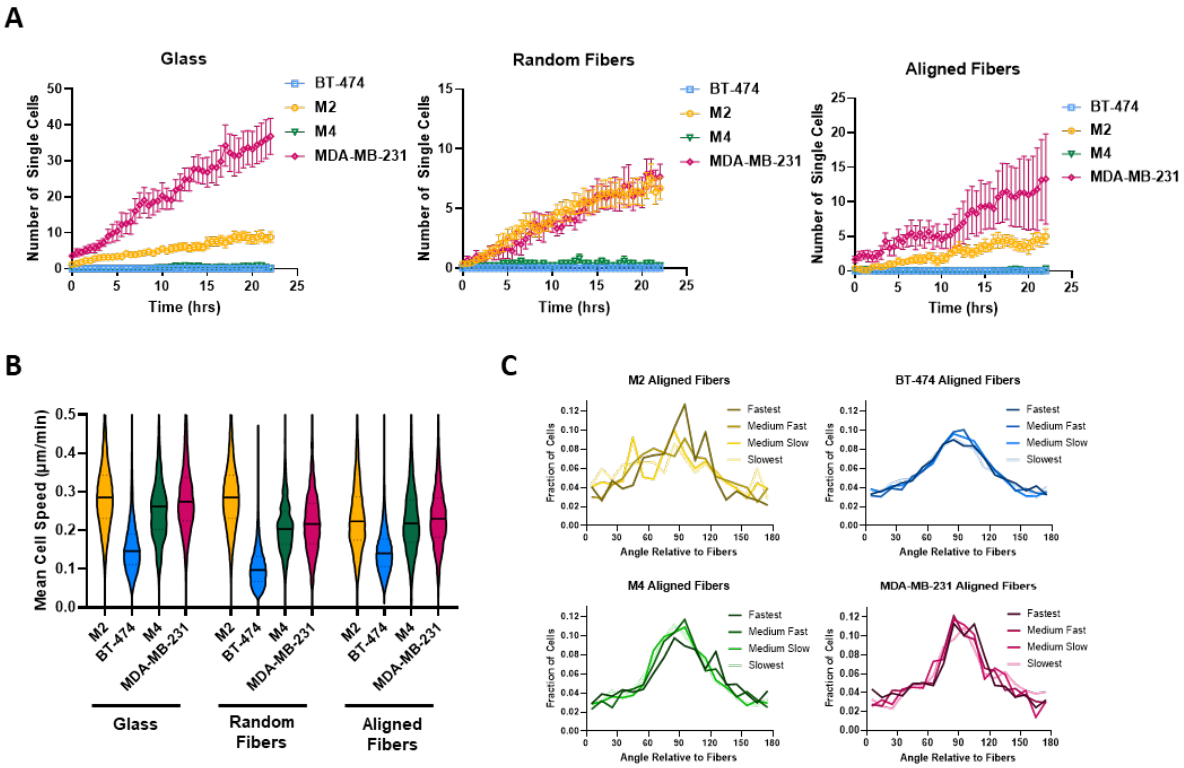

Figure S3.3 Migration metrics for collectively migrating breast epithelial cell lines on glass, random fiber mats, or aligned fiber mats.

(A) The number of single cells detached from the cell sheet over 22 hours on glass (left), random fiber mats (center), and aligned fibers (right). (B) Average speed of cells on glass, random fiber mats, and aligned fiber mats. Each point represents one cell. Middle solid line is the median value. (C) Graphs depicting the frequency of directional migration on aligned fiber mats. The different colors represent cell speeds that were binned as depicted.

Chapter 4 Conclusions and Future Directions

4.1 Summary

4.1.1 Quantification of collective cell migration on complex surfaces

Collective cell migration occurs during many essential physiological processes, such as embryogenesis, wound healing, and cancer invasion [99,101,103]. In the second chapter of this dissertation, we developed a versatile approach for studying the dynamics of collective cell migration by quantifying spheroid migration on electrospun, fibrous 2D surfaces[263]. We first described how to create electrospun fibers made of dextran vinyl sulfone (DexVS), which was originally published in Davidson et al[236]. We detailed how we create spheroids for the collective cell migration assay and how we coat fibers with collagen I to facilitate cell adhesion. To quantify migration behavior, we established an automated method for tracking nuclear location over time using fluorescent live cell imaging, an ImageJ plugin TrackMate[239], and a custom MATLAB code. Then, by manipulating electrospinning parameters to adjust fiber alignment, we examined how different fiber networks influence collective cell migration behaviors. To demonstrate the capabilities of our system, we quantified the migration dynamics of MDA-MB-231 spheroids on either glass coverslips or fiber mats composed of aligned or random synthetic fibers functionalized for cell adhesion. Our system allows for quantification of migration angle, accumulated distance, Euclidean distance, mean speed, instantaneous speed, and frequency of directional migration based on speed. Additionally, we showed how to measure the dispersal of single cells from the collectively migrating cell sheet based on distance between nuclei using the

k-nearest neighbor (KNN) algorithm. We not only identified the number of single cells that broke off the cell sheet over time, but we also demonstrated how to calculate the speed and directionality between single cells and cells migrating collectively. Finally, we showed how to observe protein localization and expression changes that occur after cells migrate on the fiber mats. This method expands upon previous systems for studying cell migration, enabling users to gain a comprehensive understanding of how cells migrate on fibrous topographies as well as allowing for the investigation of molecular changes that occur as cells encounter and migrate on these surfaces. Ongoing investigations aim to determine the feasibility of using this method to study the migration behavior in 3D hydrogels[248,249].

4.1.2 The role of RhoA during collective contact guidance

In the third chapter of this dissertation, I examined the role of RhoA GTPase during collective contact guidance since it is known to regulate cell-cell and cell-substrate interactions[257–261]. First, we characterized the collective cell migration phenotypes of four malignant breast epithelial cell lines on aligned and random fiber mats using the methods established in Chapter 2 of this thesis. We found that the genetic ablation of RhoA resulted in a significant decrease in the contact guidance ability of collectively migrating cells. Additionally, cells lacking RhoA displayed fractured junctions and broke off from the cell sheet more frequently. Since active RhoA signals to a variety of downstream effectors, we then investigated whether the inhibition of ROCK, a well-known RhoA effector, disrupts collective contact guidance. We found that inhibition of ROCK also resulted in a decrease in contact guidance, demonstrating that collective contact guidance is dependent on Rho/ROCK signaling. Interestingly, ROCK inhibition did not lead to as many individual cells breaking off the cell sheet, suggesting that other Rho effectors are promoting collectivity. Next, we sought to

determine whether the loss of contact guidance after RhoA KO was a cell-autonomous trait and found that in the context of single cell migration, contact guidance was independent of RhoA signaling. We then investigated whether the loss of collective contact guidance after RhoA KO was due to altered cell-substrate or cell-cell adhesions. In collectively migrating cells, the loss of RhoA resulted in a decrease in focal adhesion lifetime. Additionally, we showed that RhoA is crucial for proper AJs and desmosome formation. Specifically, we found that the loss of RhoA resulted in a dramatic increase in the localization of E-cadherin and a decrease in desmosomal plaques at cell membranes. Together, our findings not only support the previously established role of RhoA in cell migration but demonstrate that RhoA/ROCK signaling regulates collective contact guidance by controlling focal adhesions as well as cell-cell adhesions. Future studies aim to assess the role of mDia, another Rho effector, as well as determining whether migration-induced tension causes junctional fractures in RhoA KO cells.

4.2 Future Directions

4.2.1 Strategies for improvements to spheroid migration assay

In Chapter 2, we demonstrated a new method to assess collective cell migration on complex, fibrous surfaces which mimic collagen fibers observed *in vivo*[24]. While we were able to quantify several migration metrics for both collective and single cells, additional advances to the system would allow for more in depth quantification of migration behaviors.

There are several ways we can improve our system to reduce user time and increase the number of measurable parameters without considerably altering the experimental setup. In our current workflow, we track nuclear movement over time using TrackMate, a plugin within ImageJ. We then export the raw migration data to calculate bulk migration metrics in MATLAB. To streamline this process, we could utilize the ImageJ-MATLAB extension which allows

ImageJ to be run within MATLAB. We could also add quantifications for cell trajectory, sample variance, and migration persistence to further describe migration phenotypes. Additionally, machine learning is increasingly becoming an important component of image analysis in order to quantify changes in cell structures and behaviors more effectively and with less user bias[290,362–364]. Using Hoechst staining of nuclei, we could utilize segmentation tools, such as Weka segmentation[290], to identify nuclear morphology over time. These parameters could further be correlated to the location within the cell sheet thereby providing valuable information on changes to nuclear morphology, count and size in leader and follower cells. With the addition of a cell-membrane dye, we could also utilize machine learning techniques to quantify cell sheet dynamics such as the number of neighbors each cell has, cell area, and junction edge length. Additionally, the same membrane dye could be used to identify single cell dispersion more accurately from the migrating sheet. In our current system, we use distance between nuclei and the k-nearest neighbor algorithm to identify cells that break away from the group, but detection of single cells would be more accurate with a cell membrane marker. Together, the addition of machine learning techniques would allow us to characterize the migration dynamics of migrating cell groups more thoroughly.

4.2.2 Further studies on the role of RhoA during contact guidance

In Chapter 3 we found that the loss of RhoA resulted in fractured cell junctions and altered localization of several key cell-cell adhesion proteins. While we demonstrated that RhoA KO alters both AJs and desmosomes, it would be valuable to dissect the mechanism of how this occurs. I hypothesized that the loss of RhoA results in an insufficient detection of junctional tension within the cell sheet, ultimately leading to breaks within the epithelial junctions. To restore epithelial integrity, E-cadherin is then recruited to cell-cell adhesions leading to disrupted

desmosome formation. To test whether tension generated during migration leads to fracturing of cell junctions, I could grow RhoA KO and SCR cells as confluent monolayers to negate tension caused by migration. I could then assess changes to E-cadherin and Desmoplakin localization using immunofluorescence and determine the role of tension generation in our system. Additionally, it would be valuable to determine if the disruption of AJs cause changes in desmosomal formation or if altered desmosomes are a direct result of the genetic loss of RhoA. I hypothesize that the loss of RhoA is leading to disrupted AJ stability or formation which results in changes in desmosomal formation. To answer this question, I could attempt to rescue the phenotype by knocking down E-cadherin in RhoA KO cells to assess if decreased expression of E-cadherin reestablishes cell adhesion homeostasis. Using cells with E-cadherin knockdown in the RhoA KO background, I could then use our spheroid migration assay to assess contact guidance ability as well as changes to cell adhesions. These experiments would provide a greater understanding of the crosstalk between AJs and desmosomes and elucidate how tension during migration affects cell junction dynamics.

While we showed that RhoA/ROCK activity is important for collective contact guidance, it would be valuable to investigate whether other RhoA effectors are important for contact guidance. We found that ROCK inhibition resulted in decrease desmosomal plaques compared to vehicle control cells, though the response was not as dramatic as the genetic knockout of RhoA. It would be interesting to investigate the contribution of mDia, a well-established RhoA effector, in mediating the effect of RhoA. mDia is a member of the formin protein family which regulate the formation and elongation of actin filaments[365]. In fact, Rho/mDia activation has been shown to be crucial for the integrity of AJs[345,346] and epithelial polarity[347]. SMIFH2, a small molecule inhibitor of mDia 1 and mDia 2, was identified in 2009[366], though recent studies provide

evidence that it may inhibit all 15 formin-family proteins A and have off-target effects[367,368]. The redundancy of formin homology domains makes it difficult to targeting a specific formin protein, therefore mDia knockout would allow us to specifically study the role of mDia in our system. Since ROCK inhibition only partially mimicked the phenotype observed in RhoA KO cells, I hypothesize that mDia knockout would also result in decreased desmosomal plaques due to its known roles in cell junction integrity[345,346]. Based on our data, it seems likely that multiple RhoA effectors are crucial for epithelial integrity and subsequent collective contact guidance. To perform these experiments, I would use our spheroid migration assay on aligned fiber mats to quantify contact guidance followed by immunofluorescence staining to look at changes to E-cadherin and Desmoplakin. These experiments would establish which downstream effectors of RhoA are responsible for controlling contact guidance during collective cell migration, therefore providing a greater understanding of the mechanisms controlling invasive collective migration.

It has been demonstrated that RhoA localizes to intercellular junctions during collective epithelial migration on flat substrates[261,299,369], though the spatiotemporal dynamics of active Rho during contact guidance in single or collectively migrating cells have not been studied. To gain a more holistic understanding of how RhoA regulates contact guidance during collective cell migration, it would be valuable to identify the spatiotemporal dynamics of Rho signaling during migration on complex fiber mats. To identify sites of Rho activity on 2D fiber mats, I would express a Rho location biosensor which identifies active, endogenous Rho[370,371] into the wild type M4 cell line. Using the assay described in Chapter 2, I would generate spheroids with these cells and plate them onto aligned fiber mats. Then, I would perform confocal time lapse microscopy to visualize the spatiotemporal dynamics of active Rho. I would predict that in addition to localizing to cell junctions, Rho would also localize to points of contact with the

fibers. These studies would be beneficial by providing a deeper understanding of the dynamics of Rho activity during contact guidance.

Additionally, in Chapter 3 we found that the loss of RhoA resulted in individual cells breaking away from the migrating collective cell sheet. In future experiments, it would be beneficial to investigate whether these individually migrating cells possess an intrinsic characteristic that enables them to break away from the cell sheet. These studies would complement the recent work on leader-follower dynamics during collective migration[106,372].

4.3 Concluding Remarks

In this dissertation, I investigated how contact guidance cues are sensed by breast epithelial cells during collective cell migration. To quantify collective contact guidance, we developed an adaptable spheroid migration assay on electrospun fiber mats. Using this system, we then studied the role of RhoA /ROCK signaling during contact guidance. Future studies will focus on dissecting the role of RhoA signaling in epithelial junction assembly and stability and whether other RhoA effectors are important for collective contact guidance.

It has been demonstrated that the migration patterns of cancer cells *in vivo* are highly influenced by topographical features of the fibrous ECM[24,25]. Using a bioengineered, reductionist approach, this work demonstrates that Rho GTPase signaling controls contact guidance during collective breast cancer cell migration. By further elucidating the mechanisms controlling contact guidance during invasive migration, we envision that our studies will aid in the development of strategies to prevent cancer dissemination.

Appendix: Effects of Serum Starvation and Collagen IV Coating on Collective Cell Migration Behaviors

In preliminary studies, we investigated how serum starvation or migration on different collagen-coated surfaces affect collective migration behaviors of two invasive breast cancer cell lines, M4 and MDA-MB-231 cells. We employed either the spheroid migration assay on aligned fiber mats (as discussed in Chapters 2 and 3 of this dissertation) or a dot drop collective migration assay as previously described[373].

Cancer cells within solid tumors often experience severe nutrient deprivation due to hyperproliferation and poor blood supply[374–376]. These conditions can lead to oxidative stress which is known to influence cell division, differentiation, and migration[377]. Therefore, we investigated how serum deprivation affects contact guidance and collective cell migration of two breast cancer cell lines, MDA-MB-231 and M4 (as described in Chapter 3). For these experiments we utilized the spheroid migration assay on aligned, DexVS fiber mats as discussed extensively in Chapter 2 of this thesis. Spheroids were plated in full serum media, and after two hours serum was reduced (1% HS for M4 cells and 1% FBS for MDA-MB-231 cells). We observed that serum starvation did not influence the contact guidance ability of either cell line (**Figure A.1A&B**). Further, we did not observe any apparent differences in the collectivity of the cell sheets following serum deprivation. It should be noted that while we reduced the serum concentration from the cell culture medias, we did not completely remove serum since complete depletion of serum can result in cell death. Therefore, it is possible that the reduction in serum concentration was not low enough to elicit any migration phenotype. Together, these preliminary

studies suggest that serum deprivation does not influence the ability of invasive breast cancer cells lines to sense and respond to contact guidance cues, though more extensive studies are needed to validate these findings.

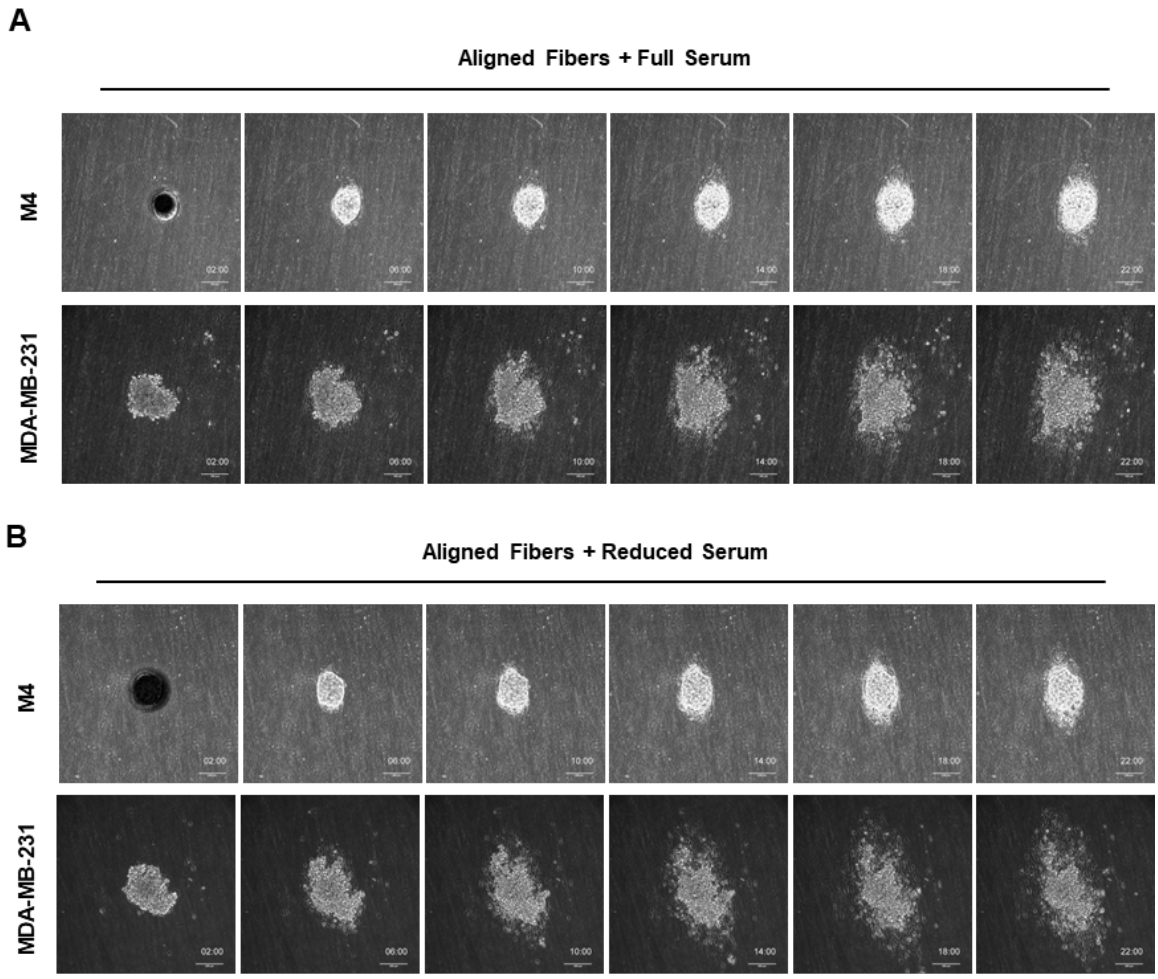

Figure A.1 Effects of serum starvation on contact guidance during collective migration of M4 and MDA-MB-231 cells.

(A) Phase contrast images of migrating breast epithelial cell lines cultured in full serum (5% HS) on aligned fiber mats over 20 hours of migration. Scale bars are 200 μm. (B) Phase contrast images of migrating breast epithelial cell lines on aligned fiber mats over 20 hours of migration after serum starvation (1% serum). Scale bars are 200 μm.

Throughout our studies we have investigated the migration of breast cancer cells on collagen I coated surfaces, because collagen I is the most prevalent collagen found within mammary tissue[7]. *In vivo*, epithelial cells encounter a diverse range of cell-adhesive ligands including collagen IV, a crucial component of the basement membrane[1]. Therefore, in

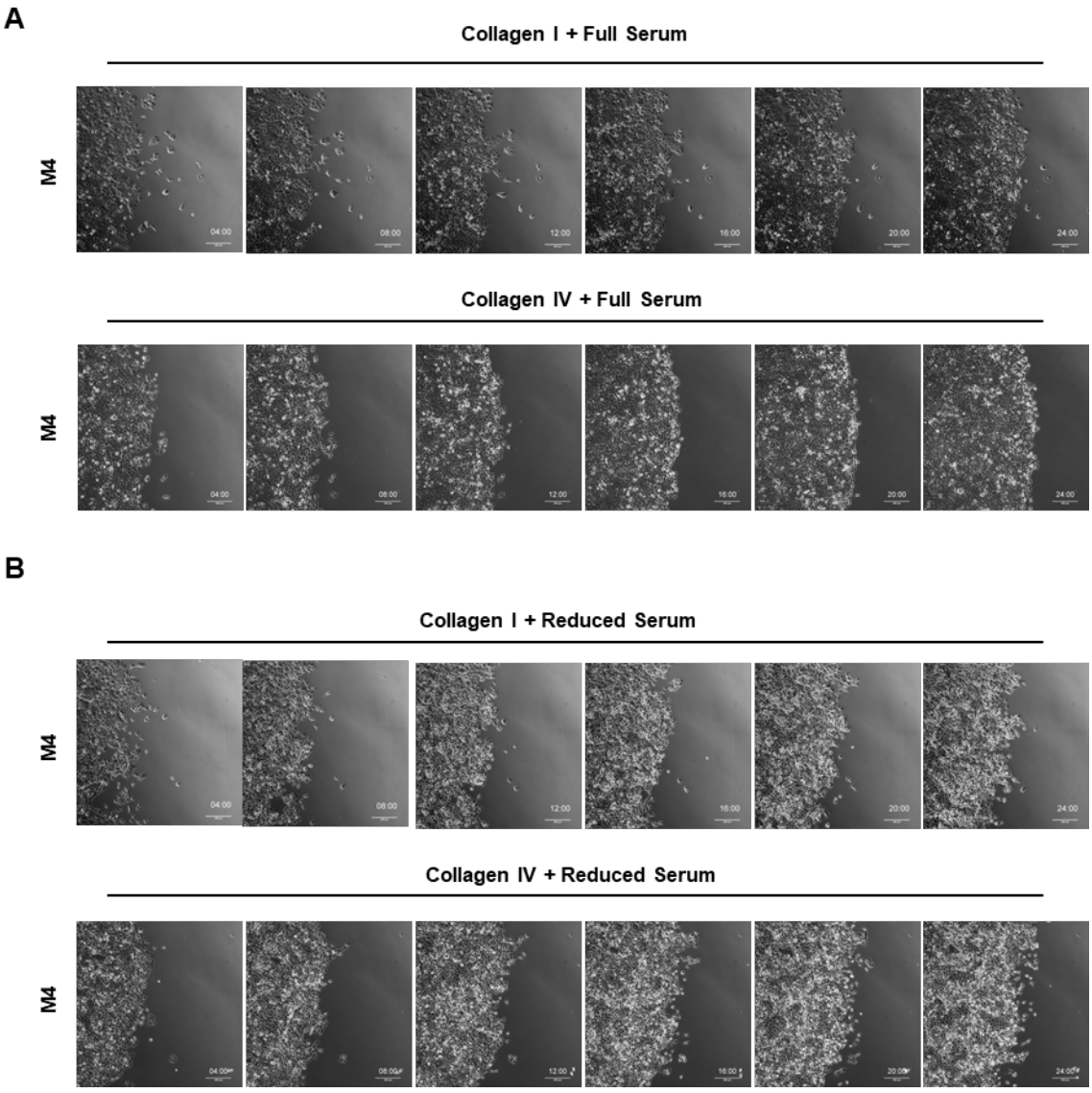

Figure A.2 Effects of collagen IV and serum starvation on the collective migration of M4 cells.

(A) Phase contrast images of migrating breast epithelial cell lines cultured in full serum (5% HS) on collagen I coated glass (100 μg/ml) or collagen IV coated glass (10 μg/ml) over 20 hours of migration. Scale bars are 200 μm. (B) Phase contrast images of migrating breast epithelial cell lines cultured in reduced serum (0.1% HS) on collagen I coated glass (100 μg/ml) or collagen IV coated glass (10 μg/ml) over 20 hours of migration. Scale bars are 200 μm.

preliminary studies we investigated how interactions with collagen IV affect collective epithelial cell migration. Additionally, we examined whether stress induced by serum starvation influenced migration phenotypes on collagen I or IV coated glass. For these experiments, we utilized the dot drop migration assay and visualized migration over 20 hours using phase-contrast imaging. We found that M4 cells cultured in full serum media showed cohesive collective cell migration over

22 hours when migrating on either collagen I or collagen IV (**Figure A.2A**). We also observed that migration on collagen IV resulted in greater single cell dispersal from the collectively migrating sheet. Additionally, we observed that stress induced by reduced serum resulted in more chaotic migration on either collagen I or collagen IV coated surfaces (**Figure A.2B**). These results suggest that stress induced by serum starvation promotes less cohesive collective migration phenotypes. Further studies will need to be conducted to validate these findings as well as quantification of migration behaviors using cell tracking.

Bibliography

1. Frantz, C., Stewart, K.M., and Weaver, V.M. (2010). The extracellular matrix at a glance. J. Cell Sci. *123*, 4195–4200. 10.1242/jcs.023820.
2. Bosman, F.T., and Stamenkovic, I. (2003). Functional structure and composition of the extracellular matrix. J. Pathol. *200*, 423–428. 10.1002/path.1437.
3. Rozario, T., and Desimone, D.W. (2010). The extracellular matrix in development and morphogenesis : A dynamic view. Dev. Biol. *341*, 126–140. 10.1016/j.ydbio.2009.10.026.
4. Yamada, K.M., Collins, J.W., Lu, J., Wang, S., and Doyle, A.D. (2019). Extracellular matrix dynamics in cell migration, invasion and tissue morphogenesis. Int. J. Exp. Pathol. *100*, 144–152. 10.1111/iep.12329.
5. Hynes, R.O., and Naba, A. (2012). Overview of the matrisome-An inventory of extracellular matrix constituents and functions. Cold Spring Harb. Perspect. Biol. *4*. 10.1101/cshperspect.a004903.
6. Schwarzbauer, J. (1999). Basement membrane: Putting up the barriers. Curr. Biol. *9*, 242–244. 10.1016/S0960-9822(99)80153-5.
7. Bonnans, C., Chou, J., and Werb, Z. (2014). Remodelling the extracellular matrix in development and disease. Nat. Publ. Gr. *15*, 786–801. 10.1038/nrm3904.
8. Holmes, D.F., Lu, Y., Starborg, T., and Kadler, K.E. Collagen Fibril Assembly and Function. 10.1016/bs.ctdb.2018.02.004.
9. Ricard-Blum, S., and Ruggiero, F. (2005). The collagen superfamily: from the extracellular matrix to the cell membrane. Pathol. Biol. *53*, 430–442. 10.1016/J.PATBIO.2004.12.024.
10. Mienaltowski, M., Birk, D., Mienaltowski, M.J., and Birk, D.E. (2014). Structure, Physiology, and Biochemistry of Collagens. Adv. Exp. Med. Biol. *802*, 5–29. 10.1007/978-94-007-7893-1_2.
11. Huxley -Jones, J., Robertson, D.L., and Boot-Handford, R.P. (2007). On the origins of the extracellular matrix in vertebrates. Matrix Biol. *26*, 2–11. 10.1016/j.matbio.2006.09.008.
12. Bella, J., and Hulmes, D.J.S. (2017). Fibrillar Collagens. In Fibrous Proteins: Structures and Mechanisms. Subcellular Biochemistry, D. Parry and J. Squire, eds. (Springer, Cham.), pp. 457–490.
13. Insua-Rodríguez, J., and Oskarsson, T. (2016). The extracellular matrix in breast cancer. Adv. Drug Deliv. Rev. *97*, 41–55. 10.1016/j.addr.2015.12.017.
14. Winkler, J., Abisoye-Ogunniyan, A., Metcalf, K.J., and Werb, Z. (2020). Concepts of extracellular matrix remodelling in tumour progression and metastasis. Nat. Commun. *11*. 10.1038/s41467-020-18794-x.
15. Lu, P., Takai, K., Weaver, V.M., and Werb, Z. (2011). Extracellular Matrix Degradation and Remodeling in Development and Disease. Cold Spring Harb. Perspect. Biol. *3*.
16. Cannon, A., Thompson, C., Hall, B.R., Jain, M., Kumar, S., and Batra, S.K. (2018). Desmoplasia in pancreatic ductal adenocarcinoma: Insight into pathological function and therapeutic potential. Genes and Cancer *9*, 78–86. 10.18632/genesandcancer.171.

17. Walker, R.A. (2001). The complexities of breast cancer desmoplasia. Breast Cancer Res. *3*, 143–145.
18. Whatcott, C., Posner, R., and Von Hoff, D. (2012). Desmoplasia and chemoresistance in pancreatic cancer. In Pancreatic Cancer and Tumor Microenvironment, P. Grippo and H. Munshi, eds. (Trivandrum (India): Transworld Research Network).
19. Jacobetz, M.A., Chan, D.S., Neesse, A., Bapiro, T.E., Cook, N., Frese, K.K., Feig, C., Nakagawa, T., Caldwell, M.E., Zecchini, H.I., et al. (2013). Hyaluronan impairs vascular function and drug delivery in a mouse model of pancreatic cancer. Gut *62*, 112–120. 10.1136/gutjnl-2012-302529.
20. Egeblad, M., Rasch, M.G., Weaver, V.M., Friedl, P., and Zallen, J. (2010). Dynamic interplay between the collagen scaffold and tumor evolution. Curr. Opin. Cell Biol. *22*, 697–706. 10.1016/j.ceb.2010.08.015.
21. Levental, K.R., Yu, H., Kass, L., Lakins, J.N., Egeblad, M., Erler, J.T., Fong, S.F.T., Csiszar, K., Giaccia, A., Weninger, W., et al. (2009). Matrix Crosslinking Forces Tumor Progression by Enhancing Integrin Signaling. Cell *139*, 891–906. 10.1016/j.cell.2009.10.027.
22. Tenti, P., and Vannucci, L. (2020). Lysyl oxidases: linking structures and immunity in the tumor microenvironment. Cancer Immunol. Immunother. *69*, 223–235. 10.1007/s00262-019-02404-x.
23. Paszek, M.J., Zahir, N., Johnson, K.R., Lakins, J.N., Rozenberg, G.I., Gefen, A., Reinhart-King, C.A., Margulies, S.S., Dembo, M., Boettiger, D., et al. (2005). Tensional homeostasis and the malignant phenotype. Cancer Cell *8*, 241–254. 10.1016/j.ccr.2005.08.010.
24. Provenzano, P.P., Eliceiri, K.W., Campbell, J.M., Inman, D.R., White, J.G., and Keely, P.J. (2006). Collagen reorganization at the tumor-stromal interface facilitates local invasion. BMC Med. *4*, 1–15. 10.1186/1741-7015-4-38.
25. Brett, E.A., Sauter, M.A., Machens, H.-G., and Duscher, D. (2020). Tumor-associated collagen signatures: pushing tumor boundaries. Cancer Metab. *8*, 1–5. 10.1186/s40170-020-00221-w.
26. Dickinson, R.B., Guido, S., and Tranquillo, R.T. (1994). Biased cell migration of fibroblasts exhibiting contact guidance in oriented collagen gels. Ann. Biomed. Eng. *22*, 342–356. 10.1007/BF02368241.
27. Tatti, O., Gucciardo, E., Pekkonen, P., Holopainen, T., Louhimo, R., Repo, P., Maliniemi, P., Lohi, J., Rantanen, V., Hautaniemi, S., et al. (2015). MMP16 mediates a proteolytic switch to promote cell-cell adhesion, collagen alignment, and lymphatic invasion in melanoma. Cancer Res. *75*, 2083–2094. 10.1158/0008-5472.CAN-14-1923.
28. Peng, D.H., Ungewiss, C., Tong, P., Byers, L.A., Wang, J., Canales, J.R., Villalobos, P.A., Uraoka, N., Mino, B., Behrens, C., et al. (2017). ZEB1 induces LOXL2-mediated collagen stabilization and deposition in the extracellular matrix to drive lung cancer invasion and metastasis. Oncogene *36*, 1925–1938. 10.1038/onc.2016.358.
29. Hartmann, N., Giese, N.A., Giese, T., Poschke, I., Offringa, R., Werner, J., and Ryschich, E. (2014). Prevailing role of contact guidance in intrastromal T-cell trapping in human pancreatic cancer. Clin. Cancer Res. *20*, 3422–3433. 10.1158/1078-0432.CCR-13-2972.
30. Ray, A., Callaway, M.K., Rodríguez-Merced, N.J., Crampton, A.L., Carlson, M., Emme, K.B., Ensminger, E.A., Kinne, A.A., Schrope, J.H., Rasmussen, H.R., et al. (2022). Stromal architecture directs early dissemination in pancreatic ductal adenocarcinoma. JCI

Insight *7*, 1–17. 10.1172/jci.insight.150330.
31. Drifka, C.R., Tod, J., Loeffler, A.G., Liu, Y., Thomas, G.J., Eliceiri, K.W., and Kao, W.J. (2015). Periductal stromal collagen topology of pancreatic ductal adenocarcinoma differs from that of normal and chronic pancreatitis. Mod. Pathol. *28*, 1470–1480. 10.1038/modpathol.2015.97.
32. Garcia, A.M., Magalhes, F.L., Soares, J.S., Junior, E.P., Lima, M.F.R.D., Mamede, M., and Paula, A.M.D. (2018). Second harmonic generation imaging of the collagen architecture in prostate cancer tissue. Biomed. Phys. Eng. Express *4*, 025026. 10.1088/2057-1976/AAA379.
33. Campbell, K.R., Chaudhary, R., Montano, M., Iozzo, R. V., Bushman, W.A., and Campagnola, P.J. (2019). Second-harmonic generation microscopy analysis reveals proteoglycan decorin is necessary for proper collagen organization in prostate. J. Biomed. Opt. *24*. 10.1117/1.JBO.24.6.066501.
34. Conklin, M.W., Eickhoff, J.C., Riching, K.M., Pehlke, C.A., Eliceiri, K.W., Provenzano, P.P., Friedl, A., and Keely, P.J. (2011). Aligned collagen is a prognostic signature for survival in human breast carcinoma. Am. J. Pathol. *178*, 1221–1232. 10.1016/j.ajpath.2010.11.076.
35. Xi, G., Guo, W., Kang, D., Ma, J., Fu, F., Qiu, L., Zheng, L., He, J., Fang, N., Chen, J., et al. (2021). Large-scale tumor-associated collagen signatures identify high-risk breast cancer patients. Theranostics *11*, 3229–3243. 10.7150/THNO.55921.
36. Conklin, M.W., Gangnon, R.E., Sprague, B.L., Van Gemert, L., Hampton, J.M., Eliceiri, K.W., Bredfeldt, J.S., Liu, Y., Surachaicharn, N., Newcomb, P.A., et al. (2018). Collagen alignment as a predictor of recurrence after ductal carcinoma in situ. Cancer Epidemiol. Biomarkers Prev. *27*, 138–145. 10.1158/1055-9965.EPI-17-0720.
37. Adur, J., Pelegati, V.B., de Thomaz, A.A., Baratti, M.O., Andrade, L.A.L.A., Carvalho, H.F., Bottcher-Luiz, F., and Cesar, C.L. (2014). Second harmonic generation microscopy as a powerful diagnostic imaging modality for human ovarian cancer. J. Biophotonics *7*, 37–48. 10.1002/jbio.201200108.
38. Esbona, K., Yi, Y., Sandeep Saha, zx, Yu, M., Van Doorn, R.R., Conklin, M.W., Graham, D.S., Wisinski, K.B., Ponik, S.M., Eliceiri, K.W., et al. (2018). The Presence of Cyclooxygenase 2, Tumor-Associated Macrophages, and Collagen Alignment as Prognostic Markers for Invasive Breast Carcinoma Patients. Am. J. Pathol. *188*. 10.1016/j.ajpath.2017.10.025.
39. Jansen, K.A., Donato, D.M., Balcioglu, H.E., Schmidt, T., Danen, E.H.J., and Koenderink, G.H. (2015). A guide to mechanobiology: Where biology and physics meet. Biochim. Biophys. Acta - Mol. Cell Res. *1853*, 3043–3052. 10.1016/j.bbamcr.2015.05.007.
40. Ilina, O., Gritsenko, P.G., Syga, S., Lippoldt, J., La Porta, C.A.M., Chepizhko, O., Grosser, S., Vullings, M., Bakker, G.J., Starruß, J., et al. (2020). Cell–cell adhesion and 3D matrix confinement determine jamming transitions in breast cancer invasion. Nat. Cell Biol. *22*, 1103–1115. 10.1038/s41556-020-0552-6.
41. Goetz, J.G., Minguet, S., Navarro-Lérida, I., Lazcano, J.J., Samaniego, R., Calvo, E., Tello, M., Osteso-Ibáñez, T., Pellinen, T., Echarri, A., et al. (2011). Biomechanical Remodeling of the Microenvironment by Stromal Caveolin-1 Favors Tumor Invasion and Metastasis. Cell *146*, 148–163. 10.1016/J.CELL.2011.05.040.
42. Ray, A., and Provenzano, P.P. (2021). Aligned forces: Origins and mechanisms of cancer dissemination guided by extracellular matrix architecture. Curr. Opin. Cell Biol. *72*, 63–

71. 10.1016/J.CEB.2021.05.004.
43. Leclech, C., and Villard, C. (2020). Cellular and Subcellular Contact Guidance on Microfabricated Substrates. Front. Bioeng. Biotechnol. *8*, 1–30. 10.3389/fbioe.2020.551505.
44. Nikkhah, M., Edalat, F., Manoucheri, S., and Khademhosseini, A. (2012). Engineering microscale topographies to control the cell-substrate interface. Biomaterials *33*, 5230–5246. 10.1016/j.biomaterials.2012.03.079.
45. Paul Weiss (1941). Nerve patterns: the mechanisms of nerve growth. Third Growth Symp. Growth *5*, 163– 203.
46. Dunn, G.A., and Heath, J.P. (1976). A new hypothesis of contact guidance in tissue cells. Exp. Cell Res. *101*, 1–14.
47. Faix, J., and Rottner, K. (2006). The making of filopodia. Curr. Opin. Cell Biol. *18*, 18–25. 10.1016/j.ceb.2005.11.002.
48. Teixeira, A., Abrams, G.A., Bertics, P.J., Murphy, C.J., and Nealey, P.F. (2003). Epithelial contact guidance on well-defined micro- and nanostructured substrates. J Cell Sci *116*, 1881–1892. 10.1038/jid.2014.371.
49. Ramirez-San Juan, G.R., Oakes, P.W., and Gardel, M.L. (2017). Contact guidance requires spatial control of leading-edge protrusion. Mol. Biol. Cell *28*, 1043–1053. 10.1091/mbc.E16-11-0769.
50. Kubow, K.E., Shuklis, V.D., Sales, D.J., and Horwitz, A.R. (2017). Contact guidance persists under myosin inhibition due to the local alignment of adhesions and individual protrusions. Sci. Rep. *7*, 1–15. 10.1038/s41598-017-14745-7.
51. Albuschies, J., and Vogel, V. (2013). The role of filopodia in the recognition of nanotopographies. Sci. Rep. *3*. 10.1038/srep01658.
52. Ohara, P.T., and Buck, R.C. (1979). Contact guidance in vitro. A light, transmission, and scanning electron microscopic study. Exp. Cell Res. *121*, 235–249. 10.1016/0014-4827(79)90002-8.
53. Kubow, K.E., Conrad, S.K., and Horwitz, A.R. (2013). Matrix microarchitecture and myosin II determine adhesion in 3D matrices. Curr. Biol. *23*, 1607–1619. 10.1016/j.cub.2013.06.053.
54. Saito, A.C., Matsui, T.S., Ohishi, T., Sato, M., and Deguchi, S. (2014). Contact guidance of smooth muscle cells is associated with tension-mediated adhesion maturation. Exp. Cell Res. *327*, 1–11. 10.1016/j.yexcr.2014.05.002.
55. Ray, A., Lee, O., Win, Z., Edwards, R.M., Alford, P.W., Kim, D.H., and Provenzano, P.P. (2017). Anisotropic forces from spatially constrained focal adhesions mediate contact guidance directed cell migration. Nat. Commun. *8*, 1–17. 10.1038/ncomms14923.
56. Zimerman, B., Arnold, M., Ulmer, J., Blümmel, J., Besser, A., Spatz, J.P., and Geiger, B. (2004). Formation of focal adhesion-stress fibre complexes coordinated by adhesive and non-adhesive surface domains. IEE Proc. Nanobiotechnology *151*, 62–66. 10.1049/IP-NBT:20040474.
57. Oakley, C., and Brunette, D.M. (1993). The sequence of alignment of microtubules, focal contacts and actin filaments in fibroblasts spreading on smooth and grooved titanium substrata. J. Cell Sci. *106*, 343–354. 10.1242/JCS.106.1.343.
58. Ventre, M., Natale, C.F., Rianna, C., and Netti, P.A. (2014). Topographic cell instructive patterns to control cell adhesion, polarization and migration. J. R. Soc. Interface *11*. 10.1098/RSIF.2014.0687.

59. Curtis, A.S.G., and Clark, P. (1990). The effects of topographic and mechanical properties of materials on cell behavior. Crit. Rev. Biocompat. *5*, 343–362.
60. Wójciak-Stothard, B., Curtis, A.S.G., McGrath, M., Sommer, I., Wilkinson, C.D.W., and Monaghan, W. (1995). Role of the cytoskeleton in the reaction of fibroblasts to multiple grooved substrata. Cell Motil. Cytoskeleton *31*, 147–158. 10.1002/cm.970310207.
61. Kai, F.B., Drain, A.P., and Weaver, V.M. (2019). The Extracellular Matrix Modulates the Metastatic Journey. Dev. Cell *49*, 332–346. 10.1016/j.devcel.2019.03.026.
62. Yamaguchi, H., Wyckoff, J., and Condeelis, J. (2005). Cell migration in tumors. Curr. Opin. Cell Biol. *17*, 559–564. 10.1016/j.ceb.2005.08.002.
63. Ridley, A.J., Schwartz, M.A., Burridge, K., Firtel, R.A., Ginsberg, M.H., Borisy, G., Parsons, J.T., and Horwitz, A.R. (2003). Cell Migration: Integrating Signals from Front to Back. Science *302*, 1704–1709. 10.1126/science.1092053.
64. Devreotes, P., and Horwitz, A.R. (2015). Signaling networks that regulate cell migration. Cold Spring Harb. Perspect. Biol. *7*. 10.1101/cshperspect.a005959.
65. SenGupta, S., Parent, C.A., and Bear, J.E. (2021). The principles of directed cell migration. Nat. Rev. Mol. Cell Biol. 10.1038/s41580-021-00366-6.
66. Friedl, P., and Wolf, K. (2010). Plasticity of cell migration: A multiscale tuning model. J. Cell Biol. *188*, 11–19. 10.1083/jcb.200909003.
67. Shellard, A., and Mayor, R. (2020). All Roads Lead to Directional Cell Migration. Trends Cell Biol. *30*, 852–868. 10.1016/j.tcb.2020.08.002.
68. Lämmermann, T., and Sixt, M. (2009). Mechanical modes of 'amoeboid' cell migration. Curr. Opin. Cell Biol. *21*, 636–644. 10.1016/J.CEB.2009.05.003.
69. Álvarez-González, B., Meili, R., Bastounis, E., Firtel, R.A., Lasheras, J.C., and Del Álamo, J.C. (2015). Three-Dimensional Balance of Cortical Tension and Axial Contractility Enables Fast Amoeboid Migration. Biophys. J. *108*, 821–832. 10.1016/J.BPJ.2014.11.3478.
70. Lämmermann, T., Bader, B.L., Monkley, S.J., Worbs, T., Wedlich-Söldner, R., Hirsch, K., Keller, M., Förster, R., Critchley, D.R., Fässler, R., et al. (2008). Rapid leukocyte migration by integrin-independent flowing and squeezing. Nature *453*, 51–55. 10.1038/nature06887.
71. Elosegui-Artola, A., Oria, R., Chen, Y., Kosmalska, A., Pérez-González, C., Castro, N., Zhu, C., Trepat, X., and Roca-Cusachs, P. (2016). Mechanical regulation of a molecular clutch defines force transmission and transduction in response to matrix rigidity. Nat. Cell Biol. *18*, 540–548. 10.1038/ncb3336.
72. Bear, J.E., and Haugh, J.M. (2014). Directed migration of mesenchymal cells: where signaling and the cytoskeleton meet. Curr. Opin. Cell Biol. *30*, 74–82. 10.1016/J.CEB.2014.06.005.
73. Liu, Y.J., Le Berre, M., Lautenschlaeger, F., Maiuri, P., Callan-Jones, A., Heuzé, M., Takaki, T., Voituriez, R., and Piel, M. (2015). Confinement and Low Adhesion Induce Fast Amoeboid Migration of Slow Mesenchymal Cells. Cell *160*, 659–672. 10.1016/J.CELL.2015.01.007.
74. Sahai, E., and Marshall, C.J. (2003). Differing modes of tumour cell invasion have distinct requirements for Rho/ROCK signalling and extracellular proteolysis. Nat. Cell Biol. *5*, 711–719. 10.1038/NCB1019.
75. Campanale, J.P., Sun, T.Y., and Montell, D.J. (2017). Development and dynamics of cell polarity at a glance. J. Cell Sci. *130*, 1201. 10.1242/JCS.188599.

76. Johnson, D.I. (1999). Cdc42: An Essential Rho-Type GTPase Controlling Eukaryotic Cell Polarity. Microbiol. Mol. Biol. Rev. *63*, 54. 10.1128/MMBR.63.1.54-105.1999.
77. Pollard, T.D., and Borisy, G.G. (2003). Cellular Motility Driven by Assembly and Disassembly of Actin Filaments. Cell *112*, 453–465. 10.1016/S0092-8674(03)00120-X.
78. Svitkina, T.M., and Borisy, G.G. (1999). Arp2/3 complex and actin depolymerizing factor/cofilin in dendritic organization and treadmilling of actin filament array in lamellipodia. J. Cell Biol. *145*, 1009–1026. 10.1083/jcb.145.5.1009.
79. Ridley, A.J. (2006). Rho GTPases and actin dynamics in membrane protrusions and vesicle trafficking. Trends Cell Biol. *16*, 522–529. 10.1016/J.TCB.2006.08.006.
80. Houk, A.R., Jilkine, A., Mejean, C.O., Boltyanskiy, R., Dufresne, E.R., Angenent, S.B., Altschuler, S.J., Wu, L.F., and Weiner, O.D. (2012). Membrane Tension Maintains Cell Polarity by Confining Signals to the Leading Edge during Neutrophil Migration. Cell *148*, 175–188. 10.1016/J.CELL.2011.10.050.
81. Sun, Z., Guo, S.S., and Fässler, R. (2016). Integrin-mediated mechanotransduction. J. Cell Biol. *215*, 445–456. 10.1083/JCB.201609037.
82. Legerstee, K., and Houtsmuller, A.B. (2021). A Layered View on Focal Adhesions. Biology (Basel). *10*. 10.3390/BIOLOGY10111189.
83. Burridge, K., and Burridge, C.K. (2017). Focal adhesions: a personal perspective on a half century of progress. FEBS J. *284*, 3355–3361. 10.1111/FEBS.14195.
84. Riveline, D., Zamir, E., Balaban, N.Q., Schwarz, U.S., Ishizaki, T., Narumiya, S., Kam, Z., Geiger, B., and Bershadsky, A.D. (2001). Focal contacts as mechanosensors: Externally applied local mechanical force induces growth of focal contacts by an mDia1-dependent and ROCK-independent mechanism. J. Cell Biol. *153*, 1175–1185. 10.1083/jcb.153.6.1175.
85. Rottner, K., Hall, A., and Small, J. V. (1999). Interplay between Rac and Rho in the control of substrate contact dynamics. Curr. Biol. *9*, 640–648. 10.1016/S0960-9822(99)80286-3.
86. Martino, F., Perestrelo, A.R., Vinarský, V., Pagliari, S., and Forte, G. (2018). Cellular mechanotransduction: From tension to function. Front. Physiol. *9*, 1–21. 10.3389/fphys.2018.00824.
87. Bugyi, B., and Carlier, M.F. (2010). Control of actin filament treadmilling in cell motility. Annu. Rev. Biophys. *39*, 449–470. 10.1146/annurev-biophys-051309-103849.
88. Zhovmer, A.S., Tabdanov, E.D., Miao, H., Wen, H., Chen, J., Luo, X., Ma, X., Provenzano, P.P., and Adelstein, R.S. (2019). The role of nonmuscle myosin 2A and 2B in the regulation of mesenchymal cell contact guidance. Mol. Biol. Cell *30*, 1961–1973. 10.1091/mbc.e19-01-0071.
89. Vicente-Manzanares, M., Ma, X., Adelstein, R.S., and Horwitz, A.R. (2009). Non-muscle myosin II takes centre stage in cell adhesion and migration. Nat. Rev. Mol. Cell Biol. *10*, 778–790. 10.1038/nrm2786.
90. Hamadi, A., Bouali, M., Dontenwill, M., Stoeckel, H., Takeda, K., and Rondé, P. (2005). Regulation of focal adhesion dynamics and disassembly by phosphorylation of FAK at tyrosine 397. J. Cell Sci. *118*, 4415–4425. 10.1242/JCS.02565.
91. Wolfenson, H., Bershadsky, A., Henis, Y.I., and Geiger, B. (2011). Actomyosin-generated tension controls the molecular kinetics of focal adhesions. J. Cell Sci. *124*, 1425–1432. 10.1242/JCS.077388.
92. Clark, A.G., and Vignjevic, D.M. (2015). Modes of cancer cell invasion and the role of

the microenvironment. Curr. Opin. Cell Biol. *36*, 13–22. 10.1016/j.ceb.2015.06.004.
93. Cheung, K.J., and Ewald, A.J. (2016). A collective route to metastasis: Seeding by tumor cell clusters. Science *352*, 167–169. 10.1126/science.aaf6546.
94. Ilina, O., Campanello, L., Gritsenko, P.G., Vullings, M., Wang, C., Bult, P., Losert, W., and Friedl, P. (2018). Intravital microscopy of collective invasion plasticity in breast cancer. Dis. Model. Mech. *11*. 10.1242/dmm.034330.
95. Duda, D.G., Duyverman, A.M.M.J., Kohno, M., Snuderl, M., Steller, E.J.A., Fukumura, D., and Jain, R.K. (2010). Malignant cells facilitate lung metastasis by bringing their own soil. PNAS *107*, 21677–21682. 10.1073/pnas.1016234107.
96. Aceto, N., Bardia, A., Miyamoto, D.T., Donaldson, M.C., Wittner, B.S., Spencer, J.A., Yu, M., Pely, A., Engstrom, A., Zhu, H., et al. (2014). Circulating Tumor Cell Clusters Are Oligoclonal Precursors of Breast Cancer Metastasis. Cell *158*, 1110–1122. 10.1016/J.CELL.2014.07.013.
97. Glentis, A., Gurchenkov, V., and Vignjevic, D.M. (2014). Assembly, heterogeneity, and breaching of the basement membranes. Cell Adhes. Migr. *8*, 236–245. 10.4161/cam.28733.
98. Wang, W., Goswami, S., Lapidus, K., Wells, A.L., Wyckoff, J.B., Sahai, E., Singer, R.H., Segall, J.E., and Condeelis, J.S. (2004). Identification and testing of a gene expression signature of invasive carcinoma cells within primary mammary tumors. Cancer Res. *64*, 8585–8594. 10.1158/0008-5472.CAN-04-1136.
99. Mayor, R., and Etienne-Manneville, S. (2016). The front and rear of collective cell migration. Nat. Rev. Mol. Cell Biol. *17*, 97–109. 10.1038/nrm.2015.14.
100. Haeger, A., Wolf, K., Zegers, M.M., and Friedl, P. (2015). Collective cell migration: Guidance principles and hierarchies. Trends Cell Biol. *25*, 556–566. 10.1016/j.tcb.2015.06.003.
101. Friedl, P., and Gilmour, D. (2009). Collective cell migration in morphogenesis, regeneration and cancer. Nat. Rev. Mol. Cell Biol. *10*, 445–457. 10.1038/nrm2720.
102. Alexander, S., Koehl, G.E., Hirschberg, M., Geissler, E.K., and Friedl, P. (2008). Dynamic imaging of cancer growth and invasion: A modified skin-fold chamber model. Histochem. Cell Biol. *130*, 1147–1154. 10.1007/s00418-008-0529-1.
103. Barriga, E.H., Franze, K., Charras, G., and Mayor, R. (2018). Tissue stiffening coordinates morphogenesis by triggering collective cell migration in vivo. Nature *554*, 523–527. 10.1038/nature25742.
104. Omelchenko, T., Vasiliev, J.M., Gelfand, I.M., Feder, H.H., and Bonder, E.M. (2003). Rho-dependent formation of epithelial “leader” cells during wound healing. Proc. Natl. Acad. Sci. U. S. A. *100*, 10788–10793. 10.1073/pnas.1834401100.
105. Poujade, M., Grasland-Mongrain, E., Hertzog, A., Jouanneau, J., Chavrier, P., Ladoux, B., Buguin, A., and Silberzan, P. (2007). Collective migration of an epithelial monolayer in response to a model wound. Proc. Natl. Acad. Sci. U. S. A. *104*, 15988–15993. 10.1073/pnas.0705062104.
106. Qin, L., Yang, D., Yi, W., Cao, H., and Xiao, G. (2021). Roles of leader and follower cells in collective cell migration. Mol. Biol. Cell *32*, 1267–1272. 10.1091/mbc.E20-10-0681.
107. Rorth, P. (2012). Fellow travellers: Emergent properties of collective cell migration. EMBO Rep. *13*, 984–991. 10.1038/embor.2012.149.
108. Das, T., Safferling, K., Rausch, S., Grabe, N., Boehm, H., and Spatz, J.P. (2015). A molecular mechanotransduction pathway regulates collective migration of epithelial cells.

Nat. Cell Biol. *17*, 276–287. 10.1038/ncb3115.
109. Peglion, F., Llense, F., and Etienne-Manneville, S. (2014). Adherens junction treadmilling during collective migration. Nat. Cell Biol. *16*, 639–651. 10.1038/ncb2985.
110. Tambe, D.T., Corey Hardin, C., Angelini, T.E., Rajendran, K., Park, C.Y., Serra-Picamal, X., Zhou, E.H., Zaman, M.H., Butler, J.P., Weitz, D.A., et al. (2011). Collective cell guidance by cooperative intercellular forces. Nat. Mater. *10*, 469–475. 10.1038/nmat3025.
111. Bui, J., Conway, D.E., Heise, R.L., and Weinberg, S.H. (2019). Mechanochemical Coupling and Junctional Forces during Collective Cell Migration. Biophys. J. *117*, 170–183. 10.1016/j.bpj.2019.05.020.
112. Thomason, H.A., Scothern, A., Harg, S.M.C., and Garrod, D.R. (2010). Desmosomes: adhesive strength and signalling in health and disease. Biochem J. *429*, 419–433. 10.1042/BJ20100567.
113. Green, K.J., Jaiganesh, A., and Broussard, J.A. (2019). Desmosomes: Essential contributors to an integrated intercellular junction network. F1000Research *8*, 1–16. 10.12688/f1000research.20942.1.
114. Wei, Q., and Huang, H. (2013). Insights into the role of cell-cell junctions in physiology and disease 1st ed. (Elsevier Inc.) 10.1016/B978-0-12-407694-5.00005-5.
115. Zihni, C., Mills, C., Matter, K., and Balda, M.S. (2016). Tight junctions: From simple barriers to multifunctional molecular gates. Nat. Rev. Mol. Cell Biol. *17*, 564–580. 10.1038/nrm.2016.80.
116. Kumar, N.M., and Gilula, N.B. (1996). The gap junction communication channel. Cell *84*, 381–388. 10.1016/S0092-8674(00)81282-9.
117. Capaldo, C.T., Farkas, A.E., and Nusrat, A. (2014). Epithelial adhesive junctions. F1000Prime Rep. *6*, 4–7. 10.12703/P6-1.
118. Harris, T.J.C., and Tepass, U. (2010). Adherens junctions: From molecules to morphogenesis. Nat. Rev. Mol. Cell Biol. *11*, 502–514. 10.1038/nrm2927.
119. Troyanovsky, S. (2005). Cadherin dimers in cell-cell adhesion. Eur. J. Cell Biol. *84*, 225–233. 10.1016/j.ejcb.2004.12.009.
120. Meng, W., and Takeichi, M. (2009). Adherens Junction: Molecular Architecture and Regulation. Cold Spring Harb. Perspect. Biol. *1*. 10.1101/cshperspect.a002899.
121. Biswas, K.H. (2020). Molecular Mobility-Mediated Regulation of E-Cadherin Adhesion. Trends Biochem. Sci. *45*, 163–173. 10.1016/j.tibs.2019.10.012.
122. Le Duc, Q., Shi, Q., Blonk, I., Sonnenberg, A., Wang, N., Leckband, D., and De Rooij, J. (2010). Vinculin potentiates E-cadherin mechanosensing and is recruited to actin-anchored sites within adherens junctions in a myosin II-dependent manner. J. Cell Biol. *189*, 1107–1115. 10.1083/jcb.201001149.
123. Nishimura, T., and Takeichi, M. (2009). Remodeling of the Adherens Junctions During Morphogenesis. In Current Topics in Developmental Biology (Elsevier Inc.), pp. 33–54. 10.1016/S0070-2153(09)89002-9.
124. Christofori, G., and Semb, H. (1999). The role of the cell-adhesion molecule E-cadherin as a tumour-suppressor gene. Trends Biochem. Sci. *24*, 73–76. 10.1016/S0968-0004(98)01343-7.
125. Kourtidis, A., Lu, R., Pence, L.J., and Anastasiadis, P.Z. (2017). A central role for cadherin signaling in cancer. Exp. Cell Res. *358*, 78–85. 10.1016/j.yexcr.2017.04.006.
126. Birchmeier, W., and Behrens, J. (1994). Cadherin expression in carcinomas: role in the formation of cell junctions and the prevention of invasiveness. Biochim. Biophys. Acta

1198, 11–26. 10.1016/0304-419x(94)90003-5.
127. Berx, G., and Van Roy, F. (2001). The E-cadherin/catenin complex: An important gatekeeper in breast cancer tumorigenesis and malignant progression. Breast Cancer Res. *3*, 289–293. 10.1186/bcr309.
128. Cowin, P., Rowlands, T.M., and Hatsell, S.J. (2005). Cadherins and catenins in breast cancer. Curr. Opin. Cell Biol. *17*, 499–508. 10.1016/j.ceb.2005.08.014.
129. Berx, G., Cleton-Jansen, A.M., Nollet, F., De Leeuw, W.J.F., Van De Vijver, M.J., Cornelisse, C., and Van Roy, F. (1995). E-cadherin is a tumour/invasion suppressor gene mutated in human lobular breast cancers. EMBO J. *14*, 6107–6115. 10.1002/j.1460-2075.1995.tb00301.x.
130. Bracke, M.E., Van Roy, F.M., and Mareel, M.M. (1996). The E-cadherin/Catenin Complex in Invasion and Metastasis. In Current Topics in Microbiology and Immunology, U. Günthert and W. Birchmeier, eds. (Springer-Verlag), pp. 123–161.
131. Gamallo, C., Palacios, J., Suarez, A., Pizarro, A., Navarro, P., Quintanilla, M., and Cano, A. (1993). Correlation of E-cadherin expression with differentiation grade and histological type in breast carcinoma. Am. J. Pathol. *142*, 987–993.
132. Moll, R., Mitze, M., Frixen, U.H., and Birchmeier, W. (1993). Differential loss of E-cadherin expression in infiltrating ductal and lobular breast carcinomas. Am. J. Pathol. *143*, 1731–1742.
133. Müller, L., Hatzfeld, M., and Keil, R. (2021). Desmosomes as Signaling Hubs in the Regulation of Cell Behavior. Front. Cell Dev. Biol. *9*. 10.3389/fcell.2021.745670.
134. Kowalczyk, A.P., and Green, K.J. (2013). Structure, function, and regulation of desmosomes. Prog. Mol. Biol. Transl. Sci. *116*, 95–118. 10.1016/B978-0-12-394311-8.00005-4.
135. Najor, N.A. (2018). Desmosomes in Human Disease. Annu. Rev. Pathol. Mech. Dis. *13*, 51–70. 10.1146/annurev-pathol-020117-044030.
136. Green, K.J., and Gaudry, C.A. (2000). Are desmosomes more than tethers for intermediate filaments? Nat. Rev. Mol. Cell Biol. *1*, 208–216. 10.1038/35043032.
137. Dusek, R.L., Godsel, L.M., and Green, K.J. (2007). Discriminating roles of desmosomal cadherins: Beyond desmosomal adhesion. J. Dermatol. Sci. *45*, 7–21. 10.1016/j.jdermsci.2006.10.006.
138. Hatzfeld, M. (2007). Plakophilins: Multifunctional proteins or just regulators of desmosomal adhesion? Biochim. Biophys. Acta *1773*, 69–77. 10.1016/J.BBAMCR.2006.04.009.
139. Saito, M., Tucker, D.K., Kohlhorst, D., Niessen, C.M., and Kowalczyk, A.P. (2012). Classical and desmosomal cadherins at a glance. J. Cell Sci. *125*, 2547–2552. 10.1242/JCS.066654/-/DC1.
140. Sonnenberg, A., and Liem, R.K.H. (2007). Plakins in development and disease. Exp. Cell Res. *313*, 2189–2203. 10.1016/j.yexcr.2007.03.039.
141. Yin, T., Getsios, S., Caldelari, R., Godsel, L.M., Kowalczyk, A.P., Müller, E.J., and Green, K.J. (2005). Mechanisms of plakoglobin-dependent adhesion: Desmosome-specific functions in assembly and regulation by epidermal growth factor receptor. J. Biol. Chem. *280*, 40355–40363. 10.1074/jbc.M506692200.
142. Zhou, G., Yang, L., Gray, A., Srivastava, A.K., Li, C., Zhang, G., and Cui, T. (2017). The role of desmosomes in carcinogenesis. Onco. Targets. Ther. *10*, 4059–4063. 10.2147/OTT.S136367.

143. Mosaddeghzadeh, N., and Ahmadian, M.R. (2021). The RHO Family GTPases: Mechanisms of Regulation and Signaling. Cells *10*, 1831. 10.3390/CELLS10071831.
144. Porter, A.P., Papaioannou, A., and Malliri, A. (2016). Deregulation of Rho GTPases in cancer. Small GTPases *7*, 123–138. 10.1080/21541248.2016.1173767.
145. Zegers, M.M., and Friedl, P. (2014). Rho GTPases in collective cell migration. Small GTPases *5*. 10.4161/sgtp.28997.
146. Lawson, C.D., and Ridley, A.J. (2018). Rho GTPase signaling complexes in cell migration and invasion. J. Cell Biol. *217*, 447–457.
147. Boureux, A., Vignal, E., Faure, S., and Fort, P. (2007). Evolution of the Rho Family of Ras-Like GTPases in Eukaryotes. Mol. Biol. Evol. *24*, 203–216. 10.1093/molbev/msl145.
148. Haga, R.B., and Ridley, A.J. (2016). Rho GTPases: Regulation and roles in cancer cell biology. Small GTPases *7*, 207–221. 10.1080/21541248.2016.1232583.
149. Aspenström, P. (2020). Fast-cycling Rho GTPases. Small GTPases *11*, 248–255. 10.1080/21541248.2017.1391365.
150. Hall, A. (1998). Rho GTpases and the actin cytoskeleton. Science *279*, 509–514. 10.1126/science.279.5350.509.
151. Ueyama, T. (2019). Rho-Family Small GTPases: From Highly Polarized Sensory Neurons to Cancer Cells. Cells *8*. 10.3390/cells8020092.
152. Wittinghofer, A., and Vetter, I.R. (2011). Structure-Function Relationships of the G Domain, a Canonical Switch Motif. Annu. Rev. Biochem. *80*, 943–971. 10.1146/annurev-biochem-062708-134043.
153. Roberts, P.J., Mitin, N., Keller, P.J., Chenette, E.J., Madigan, J.P., Currin, R.O., Cox, A.D., Wilson, O., Kirschmeier, P., and Der, C.J. (2008). Rho family GTPase modification and dependence on CAAX motif-signaled posttranslational modification. J. Biol. Chem. *283*, 25150–25163. 10.1074/jbc.M800882200.
154. Wirth, A., Chen-Wacker, C., Wu, Y., Gorinski, N., Filippov, M.A., Pandey, G., and Ponimaskin, E. (2013). Dual lipidation of the brain-specific Cdc42 isoform regulates its functional properties. Biochem J. *456*, 311–322. 10.1042/BJ20130788.
155. Bishop, A.L., and Hall, A. (2000). Rho GTPases and their effector proteins. Biochem. J. *348*, 241–255. 10.1042/0264-6021:3480241.
156. Cherfils, J., and Zeghouf, M. (2013). Regulation of small GTPases by GEFs, GAPs, and GDIs. Physiol. Rev. *93*, 269–309. 10.1152/physrev.00003.2012.
157. Müller, P.M., Rademacher, J., Bagshaw, R.D., Wortmann, C., Barth, C., van Unen, J., Alp, K.M., Giudice, G., Eccles, R.L., Heinrich, L.E., et al. (2020). Systems analysis of RhoGEF and RhoGAP regulatory proteins reveals spatially organized RAC1 signalling from integrin adhesions. Nat. Cell Biol. *22*, 498–511. 10.1038/s41556-020-0488-x.
158. Hodge, R.G., and Ridley, A.J. (2016). Regulating Rho GTPases and their regulators. Nat. Rev. Mol. Cell Biol. *17*. 10.1038/nrm.2016.67.
159. Cook, D.R., Rossman, K.L., and Der, C.J. (2013). Rho guanine nucleotide exchange factors: regulators of Rho GTPase activity in development and disease. Oncogene *33*, 4021–4035. 10.1038/onc.2013.362.
160. Rossman, K.L., Der, C.J., and Sondek, J. (2005). GEF means go: turning on RHO GTPases with guanine nucleotide-exchange factors. Nat. Rev. Mol. Cell Biol. *6*, 167–180. 10.1038/nrm1587.
161. Moon, S.Y., and Zheng, Y. (2003). Rho GTPase-activating proteins in cell regulation. Trends Cell Biol. *13*, 13–22. 10.1016/S0962-8924(02)00004-1.

162. Dovas, A., and Couchman, J.R. (2005). RhoGDI: Multiple functions in the regulation of Rho family GTPase activities. Biochem. J. *390*, 1–9. 10.1042/BJ20050104.
163. Garcia-Mata, R., Boulter, E., and Burridge, K. (2011). The "invisible hand": Regulation of RHO GTPases by RHOGDIs. Nat. Rev. Mol. Cell Biol. *12*, 493–504. 10.1038/nrm3153.
164. Boulter, E., Garcia-Mata, R., Guilluy, C., Dubash, A., Rossi, G., Brennwald, P.J., and Burridge, K. (2010). Regulation of Rho GTPase crosstalk, degradation and activity by RhoGDI1. Nat. Cell Biol. *12*, 477–483. 10.1038/ncb2049.
165. Tcherkezian, J., and Lamarche-Vane, N. (2007). Current knowledge of the large RhoGAP family of proteins. Biol. Cell *99*, 67–86. 10.1042/bc20060086.
166. Vega, F.M., and Ridley, A.J. (2008). Rho GTPases in cancer cell biology. FEBS Lett. *582*, 2093–2101. 10.1016/j.febslet.2008.04.039.
167. Svensmark, J.H., and Brakebusch, C. (2019). Rho GTPases in cancer: friend or foe? Oncogene *38*, 7447–7456. 10.1038/s41388-019-0963-7.
168. Wheeler, A.P., and Ridley, A.J. (2004). Why three Rho proteins? RhoA, RhoB, RhoC, and cell motility. Exp. Cell Res. *301*, 43–49. 10.1016/j.yexcr.2004.08.012.
169. Prendergast, G.C. (2001). Actin' up: RhoB in cancer and apoptosis. Nat. Rev. Cancer *1*, 162–168. 10.1038/35101096.
170. MacHacek, M., Hodgson, L., Welch, C., Elliott, H., Pertz, O., Nalbant, P., Abell, A., Johnson, G.L., Hahn, K.M., and Danuser, G. (2009). Coordination of Rho GTPase activities during cell protrusion. Nature *461*, 99–103. 10.1038/nature08242.
171. Michaelson, D., Silletti, J., Murphy, G., D'Eustachio, P., Rush, M., and Philips, M.R. (2001). Differential localization of Rho GTPases in live cells: Regulation by hypervariable regions and RhoGDI binding. J. Cell Biol. *152*, 111–126. 10.1083/jcb.152.1.111.
172. Adamson, P., Paterson, H.F., and Hall, A. (1992). Intracellular Localization of the P21 Rho Proteins. J. Cell Biol. *119*, 617–627.
173. Lessey, E.C., Guilluy, C., and Burridge, K. (2012). From mechanical force to RhoA activation. Biochemistry *51*, 7420–7432. 10.1021/bi300758e.
174. Matsui, T., Amano, M., Yamamoto, T., Chihara, K., Nakafuku, M., Ito, M., Nakano, T., Okawa, K., Iwamatsu, A., and Kaibuchi, K. (1996). Rho-associated kinase, a novel serine/threonine kinase, as a putative target for small GTP binding protein Rho. EMBO J. *15*, 2208–2216. 10.1002/J.1460-2075.1996.TB00574.X.
175. Amano, M., Ito, M., Kimura, K., Fukata, Y., Chihara, K., Nakano, T., Matsuura, Y., and Kaibuchi, K. (1996). Phosphorylation and Activation of Myosin by Rho-associated Kinase (Rho-kinase). J. Biol. Chem. *271*, 20246–20249. 10.1074/JBC.271.34.20246.
176. Kureishi, Y., Kobayashi, S., Amano, M., Kimura, K., Kanaide, H., Nakano, T., Kaibuchi, K., and Ito, M. (1997). Rho-associated kinase directly induces smooth muscle contraction through myosin light chain phosphorylation. J. Biol. Chem. *272*, 12257–12260. 10.1074/JBC.272.19.12257.
177. Maekawa, M., Ishizaki, T., Boku, S., Watanabe, N., Fujita, A., Iwamatsu, A., Obinata, T., Ohashi, K., Mizuno, K., and Narumiya, S. (1999). Signaling from Rho to the actin cytoskeleton through protein kinases ROCK and LIM-kinase. Science *285*, 895–898. 10.1126/science.285.5429.895.
178. Ohashi, K., Nagata, K., Maekawa, M., Ishizaki, T., Narumiya, S., and Mizuno, K. (2000). Rho-associated Kinase ROCK Activates LIM-kinase 1 by Phosphorylation at Threonine 508 within the Activation Loop. J. Biol. Chem. *275*, 3577–3582. 10.1074/JBC.275.5.3577.

179. Kimura, K., Ito, M., Amano, M., Chihara, K., Fukata, Y., Nakafuku, M., Yamamori, B., Feng, J., Nakano, T., Okawa, K., et al. (1996). Regulation of Myosin Phosphatase by Rho and Rho-Associated Kinase (Rho-Kinase). Science *273*, 245–248. 10.1126/SCIENCE.273.5272.245.
180. Riento, K., and Ridley, A.J. (2003). Rocks: multifunctional kinases in cell behaviour. Nat. Rev. Mol. Cell Biol. *4*, 446–456. 10.1038/NRM1128.
181. Okumura, N., Fujii, K., Kagami, T., Makiko, N., Kitahara, M., Kinoshita, S., and Koizumi, N. (2016). Activation of the Rho/Rho Kinase Signaling Pathway Is Involved in Cell Death of Corneal Endothelium. Invest. Ophthalmol. Vis. Sci. *57*, 6843–6851. 10.1167/IOVS.16-20123.
182. Saadeldin, I.M., Tukur, H.A., Aljumaah, R.S., and Sindi, R.A. (2021). Rocking the Boat: The Decisive Roles of Rho Kinases During Oocyte, Blastocyst, and Stem Cell Development. Front. Cell Dev. Biol. *8*, 1–10. 10.3389/fcell.2020.616762.
183. Schofield, A. V., Steels, R., and Bernard, O. (2012). Rho-associated coiled-coil kinase (ROCK) protein controls microtubule dynamics in a novel signaling pathway that regulates cell migration. J. Biol. Chem. *287*, 43620–43629. 10.1074/jbc.M112.394965.
184. Goto, H., Kosako, H., Tanabe, K., Yanagida, M., Sakurai, M., Amano, M., Kaibuchi, K., and Inagakii, M. (1998). Phosphorylation of vimentin by RHO-associated kinase at a unique amino- terminal site that is specifically phosphorylated during cytokinesis. J. Biol. Chem. *273*, 11728–11736. 10.1074/jbc.273.19.11728.
185. Kosako, H., Amano, M., Yanagida, M., Tanabe, K., Nishi, Y., Kaibuchi, K., and Inagaki, M. (1997). Phosphorylation of glial fibrillary, acidic protein at the same sites by cleavage furrow kinase and Rho-associated kinase. J. Biol. Chem. *272*, 10333–10336. 10.1074/jbc.272.16.10333.
186. Amano, M., Kaneko, T., Maeda, A., Nakayama, M., Ito, M., Yamauchi, T., Goto, H., Fukata, Y., Oshiro, N., Shinohara, A., et al. (2003). Identification of Tau and MAP2 as novel substrates of Rho-kinase and myosin phosphatase. J. Neurochem. *87*, 780–790. 10.1046/j.1471-4159.2003.02054.x.
187. Yasui, Y., Amano, M., Nagata, K.I., Inagaki, N., Nakamura, H., Saya, H., Kaibuchi, K., and Inagaki, M. (1998). Roles of Rho-associated kinase in cytokinesis; mutations in Rho-associated kinase phosphorylation sites impair cytokinetic segregation of glial filaments. J. Cell Biol. *143*, 1249–1258. 10.1083/jcb.143.5.1249.
188. Newell-Litwa, K.A., Badoual, M., Asmussen, H., Patel, H., Whitmore, L., and Horwitz, A.R. (2015). ROCK 1 and 2 differentially regulate actomyosin organization to drive cell and synaptic polarity. J. Cell Biol. *210*, 225–242. 10.1083/JCB.201504046.
189. Nakagawa, O., Fujisawa, K., Ishizaki, T., Saito, Y., Nakao, K., and Narumiya, S. (1996). ROCK-I and ROCK-II, two isoforms of Rho-associated coiled-coil forming protein serine/threonine kinase in mice. FEBS Lett *392*, 189–193. 10.1016/0014-5793(96)00811-3.
190. Leung, T., Chen, X.-Q., Manser, E., and Lim, L. (1996). The p160 RhoA-Binding Kinase ROKα Is a Member of a Kinase Family and Is Involved in the Reorganization of the Cytoskeleton. Mol. Cell. Biol. *16*, 5313–5327. 10.1128/mcb.16.10.5313.
191. Julian, L., and Olson, M.F. (2014). Rho-associated coiled-coil containing kinases (ROCK). Small GTPases *5*. 10.4161/SGTP.29846.
192. Surma, M., Wei, L., and Shi, J. (2011). Rho kinase as a therapeutic target in cardiovascular disease. Future Cardiol. *7*, 657–671. 10.2217/FCA.11.51.

193. Shi, J., Zhang, L., and Wei, L. (2011). Rho-kinase in development and heart failure: Insights from genetic models. Pediatr. Cardiol. *32*, 297–304. 10.1007/s00246-011-9920-0.
194. Shi, J., Wu, X., Surma, M., Vemula, S., Zhang, L., Yang, Y., Kapur, R., and Wei, L. (2013). Distinct roles for ROCK1 and ROCK2 in the regulation of cell detachment. Cell Death Dis. *4*. 10.1038/cddis.2013.10.
195. Ishizaki, T., Maekawa, M., Fujisawa, K., Okawa, K., Iwamatsu, A., Fujita, A., Watanabe, N., Saito, Y., Kakizuka, A., Morii, N., et al. (1996). The small GTP-binding protein Rho binds to and activates a 160 kDa Ser/Thr protein kinase homologous to myotonic dystrophy kinase. EMBO J. *15*, 1885–1893. 10.1002/J.1460-2075.1996.TB00539.X.
196. Toksoz, D., and Merdek, K.D. (2002). The Rho small GTPase : Functions in health and disease Review Histology and. 915–927. 10.14670/HH-17.915.
197. Sahai, E., and Marshall, C.J. (2002). RHO-GTPASES AND CANCER. Nat. Rev. Cancer *2*, 133–142. 10.1038/nrc725.
198. Hanahan, D., and Weinberg, R.A. (2011). Hallmarks of cancer: The next generation. Cell *144*, 646–674. 10.1016/j.cell.2011.02.013.
199. Forbes, S.A., Bindal, N., Bamford, S., Cole, C., Kok, C.Y., Beare, D., Jia, M., Shepherd, R., Leung, K., Menzies, A., et al. (2011). COSMIC: Mining complete cancer genomes in the catalogue of somatic mutations in cancer. Nucleic Acids Res. *39*, 945–950. 10.1093/nar/gkq929.
200. Hodis, E., Watson, I.R., Kryukov, G. V, Arold, S.T., Imielinski, M., Theurillat, J., Nickerson, E., Auclair, D., Li, L., Place, C., et al. (2012). A Landscape of Driver Mutations in Melanoma. Cell *150*, 251–263. 10.1016/j.cell.2012.06.024.
201. Krauthammer, M., Kong, Y., Ha, B.H., Evans, P., Bacchiocchi, A., Mccusker, J.P., Cheng, E., Davis, M.J., Goh, G., Choi, M., et al. (2012). Exome sequencing identifies recurrent somatic RAC1 mutations in melanoma. Nat. Genet. *44*. 10.1038/ng.2359.
202. Alan, J.K., and Lundquist, E.A. (2013). Mutationally activated Rho GTPases in cancer. Small GTPases *4*, 159–163. 10.4161/sgtp.26530.
203. Cook, D.R., Rossman, K.L., and Der, C.J. (2014). Rho guanine nucleotide exchange factors: Regulators of Rho GTPase activity in development and disease. Oncogene *33*, 4021–4035. 10.1038/onc.2013.362.
204. Gadea, G., and Blangy, A. (2014). Dock-family exchange factors in cell migration and disease. Eur. J. Cell Biol. *93*, 466–477. 10.1016/j.ejcb.2014.06.003.
205. Fritz, G., Just, I., and Kaina, B. (1999). Rho GTPases are over-expressed in human tumors. Int. J. Cancer *81*, 682–687. 10.1002/(sici)1097-0215(19990531)81:5<682::aid-ijc2>3.0.co;2-b.
206. Fritz, G., Brachetti, C., Bahlmann, F., Schmidt, M., and Kaina, B. (2002). Rho GTPases in human breast tumours: Expression and mutation analyses and correlation with clinical parameters. Br. J. Cancer *87*, 635–644. 10.1038/sj.bjc.6600510.
207. Gómez Del Pulgar, T., Benitah, S.A., Valerón, P.F., Espina, C., and Lacal, J.C. (2005). Rho GTPase expression in tumourigenesis: Evidence for a significant link. BioEssays *27*, 602–613. 10.1002/bies.20238.
208. Tanaka, K., Matsumoto, Y., Ishikawa, H., Fukumitsu, N., Numajiri, H., Murofushi, K., Oshiro, Y., Okumura, T., Satoh, T., and Sakurai, H. (2020). Impact of RhoA overexpression on clinical outcomes in cervical squamous cell carcinoma treated with concurrent chemoradiotherapy. J. Radiat. Res. *61*, 221–230. 10.1093/jrr/rrz093.
209. Kamai, T., Kawakami, S., Koga, F., Arai, G., Takagi, K., Arai, K., Tsujii, T., and

Yoshida, K.I. (2003). RhoA is associated with invasion and lymph node metastasis in upper urinary tract cancer. BJU Int. *91*, 234–238. 10.1046/j.1464-410X.2003.03063.x.
210. Abraham, M.T., Kuriakose, M.A., Sacks, P.G., Yee, H., Chiriboga, L., Bearer, E.L., and Delacure, M.D. (2001). Motility-Related Proteins as Markers for Head and Neck Squamous Cell Cancer. Laryngoscope *111*, 1285–1289. 10.1097/00005537-200107000-00027.
211. Pan, Y., Bi, F., Liu, N., Xue, Y., Yao, X., Zheng, Y., and Fan, D. (2004). Expression of seven main Rho family members in gastric carcinoma. Biochem. Biophys. Res. Commun. *315*, 686–691. 10.1016/j.bbrc.2004.01.108.
212. Kamai, T., Yamanishi, T., Shirataki, H., Takagi, K., Asami, H., Ito, Y., and Yoshida, K.I. (2004). Overexpression of RhoA, Rac1, and Cdc42 GTPases is associated with progression in testicular cancer. Clin. Cancer Res. *10*, 4799–4805. 10.1158/1078-0432.CCR-0436-03.
213. Sakata-Yanagimoto, M., Enami, T., Yoshida, K., Shiraishi, Y., Ishii, R., Miyake, Y., Muto, H., Tsuyama, N., Sato-Otsubo, A., Okuno, Y., et al. (2014). Somatic RHOA mutation in angioimmunoblastic T cell lymphoma. Nat. Genet. *46*, 171–175. 10.1038/ng.2872.
214. Yoo, H.Y., Sung, M.K., Lee, S.H., Kim, S., Lee, H., Park, S., Kim, S.C., Lee, B., Rho, K., Lee, J.E., et al. (2014). A recurrent inactivating mutation in RHOA GTPase in angioimmunoblastic T cell lymphoma. Nat. Genet. *46*, 371–375. 10.1038/ng.2916.
215. Palomero, T., Couronné, L., Khiabanian, H., Kim, M., Ambesi-impiombato, A., Perez-garcia, A., Carpenter, Z., Abate, F., Allegretta, M., Haydu, J.E., et al. (2014). Recurrent mutations in epigenetic regulators , RHOA and FYN kinase in peripheral T cell lymphomas. Nat. Publ. Gr. *46*. 10.1038/ng.2873.
216. Manso, R., Sánchez-Beato, M., Monsalvo, S., Gómez, S., Cereceda, L., Llamas, P., Rojo, F., Mollejo, M., Menárguez, J., Alves, J., et al. (2014). The RHOA G17V gene mutation occurs frequently in peripheral T-cell lymphoma and is associated with a characteristic molecular signature. Blood *123*, 2893–2894.
217. Hayre, M.O., Inoue, A., Kufareva, I., Wang, Z., Mikelis, C.M., Drummond, R.A., Avino, S., Finkel, K., Kalim, K.W., Dipasquale, G., et al. (2016). Inactivating mutations in GNA13 and RHOA in Burkitt's lymphoma and diffuse large B-cell lymphoma: a tumor suppressor function for the Gα13/RhoA axis in B cells. Oncogene *35*, 3771–3780. 10.1038/onc.2015.442.
218. Kakiuchi, M., Nishizawa, T., Ueda, H., Gotoh, K., Tanaka, A., Hayashi, A., Yamamoto, S., Tatsuno, K., Katoh, H., Watanabe, Y., et al. (2014). Recurrent gain-of-function mutations of RHOA in diffuse-type gastric carcinoma. Nat. Genet. *46*, 583–587. 10.1038/ng.2984.
219. Wang, K., Yuen, S.T., Xu, J., Lee, S.P., Yan, H.H.N., Shi, S.T., Siu, H.C., Deng, S., Chu, K.M., Law, S., et al. (2014). Whole-genome sequencing and comprehensive molecular profiling identify new driver mutations in gastric cancer. Nat. Genet. *46*, 573–582. 10.1038/ng.2983.
220. Walma, D.A.C., and Yamada, K.M. (2020). The extracellular matrix in development. Development *147*. 10.1242/dev.175596.
221. Levental, K.R., Yu, H., Kass, L., Lakins, J.N., Egeblad, M., Erler, J.T., Fong, S.F.T., Csiszar, K., Giaccia, A., Weninger, W., et al. (2009). Matrix Crosslinking Forces Tumor Progression by Enhancing Integrin Signaling. Cell *139*, 891–906.

10.1016/j.cell.2009.10.027.
222. Agudelo-Garcia, P.A., de Jesus, J.K., Williams, S.P., Nowicki, M.O., Chiocca, E.A., Liyanarachchi, S., Li, P.K., Lannutti, J.J., Johnson, J.K., Lawler, S.E., et al. (2011). Glioma cell migration on three-dimensional nanofiber scaffolds is regulated by substrate topography and abolished by inhibition of STAT3 signaling. Neoplasia *13*, 831–840. 10.1593/neo.11612.
223. Nelson, M.T., Short, A., Cole, S.L., Gross, A.C., Winter, J., Eubank, T.D., and Lannutti, J.J. (2014). Preferential, enhanced breast cancer cell migration on biomimetic electrospun nanofiber "cell highways." BMC Cancer *14*, 1–16. 10.1186/1471-2407-14-825.
224. Park, J.S., Kim, D.H., and Levchenko, A. (2018). Topotaxis: A New Mechanism of Directed Cell Migration in Topographic ECM Gradients. Biophys. J. *114*, 1257–1263. 10.1016/j.bpj.2017.11.3813.
225. Provenzano, P.P., Inman, D.R., Eliceiri, K.W., Knittel, J.G., Yan, L., Rueden, C.T., White, J.G., and Keely, P.J. (2008). Collagen density promotes mammary tumor initiation and progression. BMC Med. *6*, 1–15. 10.1186/1741-7015-6-11.
226. Cheung, K.J., Gabrielson, E., Werb, Z., and Ewald, A.J. (2013). Collective invasion in breast cancer requires a conserved basal epithelial program. Cell *155*, 1639–1651. 10.1016/j.cell.2013.11.029.
227. Dekoninck, S., and Blanpain, C. (2019). Stem cell dynamics, migration and plasticity during wound healing. Nat. Cell Biol. *21*, 18–24. 10.1038/s41556-018-0237-6.
228. Deryugina, E.I., and Bourdon, M.A. (1996). Tenascin mediates human glioma cell migration and modulates cell migration on fibronectin. J. Cell Sci. *109*, 643–652. 10.1242/jcs.109.3.643.
229. Vinci, M., Gowan, S., Boxall, F., Patterson, L., Zimmermann, M., Court, W., Lomas, C., Mendiola, M., Hardisson, D., and Eccles, S.A. (2012). Advances in establishment and analysis of three-dimensional tumor spheroid-based functional assays for target validation and drug evaluation. BMC Biol. *10*. 10.1186/1741-7007-10-29.
230. Vinci, M., Box, C., Zimmermann, M., and Eccles, S.A. (2013). Tumor spheroid-based migration assays for evaluation of therapeutic agents. Methods Mol. Biol. *986*, 253–266. 10.1007/978-1-62703-311-4_16.
231. Labernadie, A., Kato, T., Brugués, A., Serra-Picamal, X., Derzsi, S., Arwert, E., Weston, A., González-Tarragó, V., Elosegui-Artola, A., Albertazzi, L., et al. (2017). A mechanically active heterotypic E-cadherin/N-cadherin adhesion enables fibroblasts to drive cancer cell invasion. Nat. Cell Biol. *19*, 224–237. 10.1038/ncb3478.
232. McKenzie, A.J., Hicks, S.R., Svec, K. V., Naughton, H., Edmunds, Z.L., and Howe, A.K. (2018). The mechanical microenvironment regulates ovarian cancer cell morphology, migration, and spheroid disaggregation. Sci. Rep. *8*, 1–20. 10.1038/s41598-018-25589-0.
233. Cuenca, M.B., Canedo, L., Perez-Castro, C., and Grecco, H.E. (2020). An Integrative and Modular Framework to Recapitulate Emergent Behavior in Cell Migration. Front. Cell Dev. Biol. *8*, 1–12. 10.3389/fcell.2020.615759.
234. Islam, M.S., Ang, B.C., Andriyana, A., and Afifi, A.M. (2019). A review on fabrication of nanofibers via electrospinning and their applications. SN Appl. Sci. *1*, 1–16. 10.1007/s42452-019-1288-4.
235. Huang, Z.M., Zhang, Y.Z., Kotaki, M., and Ramakrishna, S. (2003). A review on polymer nanofibers by electrospinning and their applications in nanocomposites. Compos. Sci. Technol. *63*, 2223–2253. 10.1016/S0266-3538(03)00178-7.

236. Davidson, C.D., Jayco, D.K.P., Matera, D.L., DePalma, S.J., Hiraki, H.L., Wang, W.Y., and Baker, B.M. (2020). Myofibroblast activation in synthetic fibrous matrices composed of dextran vinyl sulfone. Acta Biomater. *105*, 78–86. 10.1016/j.actbio.2020.01.009.
237. DePalma, S.J., Davidson, C.D., Stis, A.E., Helms, A.S., and Baker, B.M. (2021). Microenvironmental determinants of organized iPSC-cardiomyocyte tissues on synthetic fibrous matrices. Biomater. Sci. *9*, 93–107. 10.1039/d0bm01247e.
238. Bishop, J.R., Schuksz, M., and Esko, J.D. (2007). Heparan sulphate proteoglycans fine-tune mammalian physiology. Nature *446*, 1030–1037. 10.1038/nature05817.
239. Tinevez, J.Y., Perry, N., Schindelin, J., Hoopes, G.M., Reynolds, G.D., Laplantine, E., Bednarek, S.Y., Shorte, S.L., and Eliceiri, K.W. (2017). TrackMate: An open and extensible platform for single-particle tracking. Methods *115*, 80–90. 10.1016/j.ymeth.2016.09.016.
240. Riching, K.M., Cox, B.L., Salick, M.R., Pehlke, C., Riching, A.S., Ponik, S.M., Bass, B.R., Crone, W.C., Jiang, Y., Weaver, A.M., et al. (2015). 3D collagen alignment limits protrusions to enhance breast cancer cell persistence. Biophys. J. *107*, 2546–2558. 10.1016/j.bpj.2014.10.035.
241. Richard Brown (2022). nearestneighbour.m (https://www.mathworks.com/matlabcentral/fileexchange/12574-nearestneighbour-m), MATLAB Central File Exchange. Retrieved March 4, 2022.
242. Pelham, R.J., and Wang, Y.L. (1997). Cell locomotion and focal adhesions are regulated by substrate flexibility. Proc. Natl. Acad. Sci. U. S. A. *94*, 13661–13665. 10.1073/pnas.94.25.13661.
243. Lo, C.M., Wang, H.B., Dembo, M., and Wang, Y.L. (2000). Cell movement is guided by the rigidity of the substrate. Biophys. J. *79*, 144–152. 10.1016/S0006-3495(00)76279-5.
244. Chan, C.E., and Odde, D.J. (2008). Traction dynamics of filopodia on compliant substrates. Science *322*, 1687–1691. 10.1126/science.1163595.
245. Rens, E.G., and Merks, R.M.H. (2020). Cell Shape and Durotaxis Explained from Cell-Extracellular Matrix Forces and Focal Adhesion Dynamics. iScience *23*, 101488. 10.1016/j.isci.2020.101488.
246. Matera, D.L., Wang, W.Y., Smith, M.R., Shikanov, A., and Baker, B.M. (2019). Fiber Density Modulates Cell Spreading in 3D Interstitial Matrix Mimetics. ACS Biomater. Sci. Eng. *5*, 2965–2975. 10.1021/acsbiomaterials.9b00141.
247. Su, C.Y., Burchett, A., Dunworth, M., Choi, J.S., Ewald, A.J., Ahn, E.H., and Kim, D.H. (2021). Engineering a 3D collective cancer invasion model with control over collagen fiber alignment. Biomaterials *275*, 120922. 10.1016/j.biomaterials.2021.120922.
248. Hiraki, H.L., Matera, D.L., Wang, W.Y., Zarouk, A.A., Argento, A.E., Buschhaus, J.M., Humphries, B.A., Luker, G.D., Baker, B.M., Prabhu, E.S., et al. (2022). Fiber density and matrix stiffness modulate distinct cell migration modes in a 3D stroma mimetic composite hydrogel. Acta Biomater. 10.1016/j.actbio.2022.09.043.
249. Hiraki, H.L., Matera, D.L., Rose, M.J., Kent, R.N., Todd, C.W., Stout, M.E., Wank, A.E., Schiavone, M.C., DePalma, S.J., Zarouk, A.A., et al. (2021). Magnetic Alignment of Electrospun Fiber Segments Within a Hydrogel Composite Guides Cell Spreading and Migration Phenotype Switching. Front. Bioeng. Biotechnol. *9*, 1–14. 10.3389/fbioe.2021.679165.
250. Nam, K.H., Kim, P., Wood, D.K., Kwon, S., Provenzano, P.P., and Kim, D.H. (2016). Multiscale Cues Drive Collective Cell Migration. Sci. Rep. *6*, 1–13. 10.1038/srep29749.

251. Brownfield, D.G., Venugopalan, G., Lo, A., Mori, H., Tanner, K., Fletcher, D.A., and Bissell, M.J. (2013). Patterned collagen fibers orient branching mammary epithelium through distinct signaling modules. Curr. Biol. *23*, 703–709. 10.1016/j.cub.2013.03.032.
252. Weiss, P., and Garber, B. (1952). Shape and Movement of Mesenchyme Cells as Functions of the Physical Structure of the Medium: Contributions to a Quantitative Morphology. Proc. Natl. Acad. Sci. *38*, 264–280. 10.1073/pnas.38.3.264.
253. Nakatsuji, N., Gould, A.C., and Johnson, K.E. (1982). Movement and guidance of migrating mesodermal cells in Ambystoma maculatum gastrulae. J. Cell Sci. *56*, 207–222. 10.1242/jcs.56.1.207.
254. Lecaudey, V., and Gilmour, D. (2006). Organizing moving groups during morphogenesis. Curr. Opin. Cell Biol. *18*, 102–107. 10.1016/J.CEB.2005.12.001.
255. Kimura, K., Ito, M., Amano, M., Chihara, K., Fukata, Y., Nakafuku, M., Yamamori, B., Feng, J., Nakano, T., Okawa, K., et al. (1996). Regulation of Myosin Phosphatase by Rho and Rho-Associated Kinase (Rho-Kinase). Science *273*, 245–248. 10.1126/science.273.5272.245.
256. Amano, M., Nakayama, M., and Kaibuchi, K. (2010). Rho-kinase/ROCK: A key regulator of the cytoskeleton and cell polarity. Cytoskeleton *67*, 545–554. 10.1002/CM.20472.
257. Ridley, A.J., and Hall, A. (1992). The small GTP-binding protein rho regulates the assembly of focal adhesions and actin stress fibers in response to growth factors. Cell *70*, 389–399. 10.1016/0092-8674(92)90163-7.
258. Lawson, C.D., and Burridge, K. (2014). The on-off relationship of Rho and Rac during integrin-mediated adhesion and cell migration. Small GTPases *5*. 10.4161/sgtp.27958.
259. Takaishi, K., Sasaki, T., Kotani, H., Nishioka, H., and Takai, Y. (1997). Regulation of cell-cell adhesion by Rac and Rho small G proteins in MDCK cells. J. Cell Biol. *139*, 1047–1059. 10.1083/jcb.139.4.1047.
260. Priya, R., Yap, A.S., and Gomez, G.A. (2013). E-cadherin supports steady-state Rho signaling at the epithelial zonula adherens. Differentiation *86*, 133–140. 10.1016/J.DIFF.2013.01.002.
261. Gupta, S., Duszyc, K., Verma, S., Budnar, S., Liang, X., Gomez, G.A., Marcq, P., Noordstra, I., and Yap, A.S. (2021). Enhanced RhoA signalling stabilizes E-cadherin in migrating epithelial monolayers. J. Cell Sci. *134*, 1–16. 10.1242/jcs.258767.
262. Ershov, D., Phan, M.S., Pylvänäinen, J.W., Rigaud, S.U., Le Blanc, L., Charles-Orszag, A., Conway, J.R.W., Laine, R.F., Roy, N.H., Bonazzi, D., et al. (2022). TrackMate 7: integrating state-of-the-art segmentation algorithms into tracking pipelines. Nat. Methods *19*, 829–832. 10.1038/s41592-022-01507-1.
263. Loesel, K.E., Hiraki, H.L., Baker, B.M., and Parent, C.A. (2023). An adaptive and versatile method to quantitate and characterize collective cell migration behaviors on complex surfaces. Front. Cell Dev. Biol. Signal. *11*. 10.3389/fcell.2023.1106653.
264. Santner, S.J., Dawson, P.J., Tait, L., Soule, H.D., Eliason, J., Mohamed, A.N., Wolman, S.R., Heppner, G.H., and Miller, F.R. (2001). Malignant MCF10CA1 cell lines derived from premalignant human breast epithelial MCF10AT cells. Breast Cancer Res. Treat. *65*, 101–110. 10.1023/A:1006461422273.
265. Dawson, P.J., Wolman, S.R., Tait, L., Heppner, G.H., and Miller, F.R. (1996). MCF10AT: A model for the evolution of cancer from proliferate breast disease. Am. J. Pathol. *148*, 313–319.
266. Neve, R.M., Chin, K., Fridlyand, J., Yeh, J., Baehner, F.L., Fevr, T., Clark, L., Bayani, N.,

Coppe, J.P., Tong, F., et al. (2006). A collection of breast cancer cell lines for the study of functionally distinct cancer subtypes. Cancer Cell *10*, 515–527. 10.1016/J.CCR.2006.10.008.
267. SenGupta, S., Hein, L.E., Xu, Y., Zhang, J., Konwerski, J.R., Li, Y., Johnson, C., Cai, D., Smith, J.L., and Parent, C.A. (2021). Triple-Negative Breast Cancer Cells Recruit Neutrophils by Secreting TGF-β and CXCR2 Ligands. Front. Immunol. *12*, 1–20. 10.3389/fimmu.2021.659996.
268. Hughes, L., Malone, C., Chumsri, S., Burger, A.M., and McDonnell, S. (2008). Characterisation of breast cancer cell lines and establishment of a novel isogenic subclone to study migration, invasion and tumourigenicity. Clin. Exp. Metastasis *25*, 549–557. 10.1007/S10585-008-9169-Z.
269. Petersen, O.W., Ronnov-Jessen, L., Howlett, A.R., and Bissell, M.J. (1992). Interaction with basement membrane serves to rapidly distinguish growth and differentiation pattern of normal and malignant human breast epithelial cells. Proc. Natl. Acad. Sci. U. S. A. *89*, 9064–9068. 10.1073/pnas.89.19.9064.
270. Lasfargues, E.Y., Coutinho, W.G., and Redfield, E.S. (1978). Isolation of two human tumor epithelial cell lines from solid breast carcinomas. J. Natl. Cancer Inst. *61*, 967–973. 10.1093/jnci/61.4.967.
271. Iorns, E., Drews-Elger, K., Ward, T.M., Dean, S., Clarke, J., Berry, D., Ashry, D. El, and Lippman, M. (2012). A New Mouse Model for the Study of Human Breast Cancer Metastasis. PLoS One *7*. 10.1371/journal.pone.0047995.
272. Cailleau, R., Young, R., Olivé, M., and Reeves, W.J. (1974). Breast tumor cell lines from pleural effusions. J. Natl. Cancer Inst. *53*, 661–674. 10.1093/jnci/53.3.661.
273. Price, J.E., Polyzos, A., Zhang, R.D., and Daniels, L.M. (1990). Tumorigenicity and Metastasis of Human Breast Carcinoma Cell Lines in Nude Mice. Cancer Res. *50*, 717–721.
274. Kranenburg, O., Poland, M., Van Horck, F.P.G., Drechsel, D., Hall, A., and Moolenaar, W.H. (1999). Activation of RhoA by Lysophosphatidic Acid and G 12/13 Subunits in Neuronal Cells: Induction of Neurite Retraction. Mol. Biol. Cell *10*, 1851–1857.
275. Ren, X.-D., Kiosses, W.B., and Schwartz, M.A. (1999). Regulation of the small GTP-binding protein Rho by cell adhesion and the cytoskeleton. EMBO J. *18*, 578–585.
276. Stuelten, C.H., Lee, R.M., Losert, W., and Parent, C.A. (2018). Lysophosphatidic acid regulates the motility of MCF10CA1a breast cancer cell sheets via two opposing signaling pathways. Cell. Signal. *45*, 1–11. 10.1016/j.cellsig.2018.01.005.
277. Narumiya, S., Ishizaki, T., and Uehata, M. (2000). Use and properties of ROCK-specific inhibitor Y-27632. Methods Enzymol. *325*, 273–284. 10.1016/S0076-6879(00)25449-9.
278. Ishizaki, T., Uehata, M., Tamechika, I., Keel, J., Nonomura, K., Maekawa, M., and Narumiya, S. (2000). Pharmacological properties of Y-27632, a specific inhibitor of Rho-associated kinases. Mol. Pharmacol. *57*, 976–983.
279. Uehata, M., Ishizaki, T., Satoh, H., Ono, T., Kawahara, T., Morishita, T., Yamagami, K., Inui, J., Maekawa, M., and Narumiya, S. (1997). Calcium sensitization of smooth muscle mediated by a Rho-associated protein kinase in hypertension. Nature *389*.
280. Tkach, V., Bock, E., and Berezin, V. (2005). The role of RhoA in the regulation of cell morphology and motility. Cell Motil. Cytoskeleton *61*, 21–33. 10.1002/CM.20062.
281. Ghosh, P.M., Ghosh-Choudhury, N., Moyer, M.L., Mott, G.E., Thomas, C.A., Foster, B.A., Greenberg, N.M., and Kreisberg, J.I. (1999). Role of RhoA activation in the growth

and morphology of a murine prostate tumor cell line. Oncogene *18*, 4120–4130. 10.1038/sj.onc.1202792.
282. Vega, F.M., Fruhwirth, G., Ng, T., Ridley, A.J., Wu, M., Wu, Z.F., Kumar-Sinha, C., Chinnaiyan, A., Merajver, S.D., Vega, F.M., et al. (2011). RhoA and RhoC have distinct roles in migration and invasion by acting through different targets. J. Cell Biol. *193*, 655–665. 10.1083/jcb.201011038.
283. Wang, W.Y., Pearson, A.T., Kutys, M.L., Choi, C.K., Wozniak, M.A., Baker, B.M., and Chen, C.S. (2018). Extracellular matrix alignment dictates the organization of focal adhesions and directs uniaxial cell migration. APL Bioeng. *2*, 1–16. 10.1063/1.5052239.
284. Turner, C.E. (2000). Paxillin and focal adhesion signalling. Nat. Cell Biol. *2*, 231–236. 10.1038/35046659.
285. Pinon, P., Pärssinen, J., Vazquez, P., Bachmann, M., Rahikainen, R., Jacquier, M.C., Azizi, L., Määttä, J.A., Bastmeyer, M., Hytönen, V.P., et al. (2014). Talin-bound NPLY motif recruits integrin-signaling adapters to regulate cell spreading and mechanosensing. J. Cell Biol. *205*, 265–281. 10.1083/JCB.201308136.
286. Partridge, M.A., and Marcantonio, E.E. (2006). Initiation of Attachment and Generation of Mature Focal Adhesions by Integrin-containing Filopodia in Cell Spreading. Mol. Biol. Cell *17*, 4237–4248. 10.1091/mbc.E06.
287. Schaller, M.D., and Parsons, J.T. (1995). pp125FAK-dependent tyrosine phosphorylation of paxillin creates a high-affinity binding site for Crk. Mol. Cell. Biol. *15*, 2635–2645. 10.1128/mcb.15.5.2635.
288. Petit, V., Boyer, B., Lentz, D., Turner, C.E., Thiery, J.P., and Valles, A.M. (2000). Phosphorylation of tyrosine residues 31 and 118 on paxillin regulates cell migration through an association with CRK in NBT-II cells. J. Cell Biol. *148*, 957–969. 10.1083/jcb.148.5.957.
289. Bellis, S.L., Perrotta, J.A., Curtis, M.S., and Turner, C.E. (1997). Adhesion of fibroblasts to fibronectin stimulates both serine and tyrosine phosphorylation of paxillin. Biochem. J. *325*, 375–381. 10.1042/bj3250375.
290. Arganda-Carreras, I., Kaynig, V., Rueden, C., Eliceiri, K.W., Schindelin, J., Cardona, A., and Seung, H.S. (2017). Trainable Weka Segmentation: A machine learning tool for microscopy pixel classification. Bioinformatics *33*, 2424–2426. 10.1093/bioinformatics/btx180.
291. Choi, C.K., Vicente-Manzanares, M., Zareno, J., Whitmore, L.A., Mogilner, A., and Horwitz, A.R. (2008). Actin and α-actinin orchestrate the assembly and maturation of nascent adhesions in a myosin II motor-independent manner. Nat Cell Biol *10*, 1039–1050.
292. Vicente-Manzanares, M., and Horwitz, A.R. (2011). Adhesion dynamics at a glance. J. Cell Sci. *124*, 3923–3927. 10.1242/jcs.095653.
293. Parsons, J.T., Horwitz, A.R., and Schwartz, M.A. (2010). Cell adhesion: integrating cytoskeletal dynamics and cellular tension. Nat. Rev. Mol. Cell Biol. *11*, 633. 10.1038/NRM2957.
294. Laukaitis, C.M., Webb, D.J., Donais, K., and Horwitz, A.F. (2001). Differential dynamics of α5 integrin, paxillin, and α-actinin during formation and disassembly of adhesions in migrating cells. J. Cell Biol. *153*, 1427–1440. 10.1083/jcb.153.7.1427.
295. Kaibuchi, K., Kuroda, S., Fukata, M., and Nakagawa, M. (1999). Regulation of cadherin-mediated cell-cell adhesion by the rho family GTPases. Curr. Opin. Cell Biol. *11*, 591–

596. 10.1016/S0955-0674(99)00014-9.
296. Fukata, M., Nakagawa, M., Kuroda, S., and Kaibuchi, K. (1999). Cell adhesion and Rho small GTPases. J. Cell Sci. *112*, 4491–4500. 10.1242/jcs.112.24.4491.
297. Pinheiro, D., and Bellaïche, Y. (2018). Mechanical Force-Driven Adherens Junction Remodeling and Epithelial Dynamics. Dev. Cell *47*, 3–19. 10.1016/j.devcel.2018.09.014.
298. Braga, V.M.M., Machesky, L.M., Hall, A., and Hotchin, N.A. (1997). The small GTPases Rho and Rac are required for the establishment of cadherin-dependent cell-cell contacts. J. Cell Biol. *137*, 1421–1431. 10.1083/jcb.137.6.1421.
299. Ratheesh, A., Gomez, G.A., Priya, R., Verma, S., Kovacs, E.M., Jiang, K., Brown, N.H., Akhmanova, A., Stehbens, S.J., and Yap, A.S. (2012). Centralspindlin and α-catenin regulate Rho signalling at the epithelial zonula adherens. Nat. Cell Biol. *14*, 818–828. 10.1038/ncb2532.
300. Jones, J.C.R. (1988). Characterization of a 125K glycoprotein associated with bovine epithelial desmosomes. J. Cell Sci. *89*, 207–216.
301. Amagai, M., Fujimori, T., Masunaga, T., Shimizu, H., Nishikawa, T., Shimizu, N., Takeichi, M., and Hashimoto, T. (1995). Delayed assembly of desmosomes in keratinocytes with disrupted classic-cadherin-mediated cell adhesion by a dominant negative mutant. J. Invest. Dermatol. *104*, 27–32. 10.1111/1523-1747.ep12613462.
302. Michels, C., Buchta, T., Bloch, W., Krieg, T., and Niessen, C.M. (2009). Classical cadherins regulate desmosome formation. J. Invest. Dermatol. *129*, 2072–2075. 10.1038/jid.2009.17.
303. Derksen, P.W.B., and van de Ven, R.A.H. (2020). Shared mechanisms regulate spatiotemporal RhoA-dependent actomyosin contractility during adhesion and cell division. Small GTPases *11*, 113–121. 10.1080/21541248.2017.1366966.
304. Smith, A.L., Dohn, M.R., Brown, M. V., and Reynolds, A.B. (2012). Association of Rho-associated protein kinase 1 with E-cadherin complexes is mediated by p120-catenin. Mol. Biol. Cell *23*, 99–110. 10.1091/mbc.E11-06-0497.
305. Anastasiadis, P.Z., Moon, S.Y., Thoreson, M.A., Mariner, D.J., Crawford, H.C., Zheng, Y., and Reynolds, A.B. (2000). Inhibition of RhoA by p120 catenin. Nat. Cell Biol. *2*, 637–644. 10.1038/35023588.
306. Sheu, H.M., Kitajima, Y., and Yaoita, H. (1989). Involvement of protein kinase C in translocation of desmoplakins from cytosol to plasma membrane during desmosome formation in human squamous cell carcinoma cells grown in low to normal calcium concentration. Exp. Cell Res. *185*, 176–190. 10.1016/0014-4827(89)90047-5.
307. Bass-Zubek, A.E., Hobbs, R.P., Amargo, E. V., Garcia, N.J., Hsieh, S.N., Chen, X., Wahl, J.K., Denning, M.F., and Green, K.J. (2008). Plakophilin 2: A critical scaffold for PKCα that regulates intercellular junction assembly. J. Cell Biol. *181*, 605–613. 10.1083/jcb.200712133.
308. Thomason, H.A., Cooper, N.H., Ansell, D.M., Chiu, M., Merrit, A.J., Hardman, M.J., and Garrod, D.R. (2012). Direct evidence that PKCα positively regulates wound re-epithelialization: Correlation with changes in desmosomal adhesiveness. J. Pathol. *227*, 346–356. 10.1002/path.4016.
309. Wallis, S., Lloyd, S., Wise, I., Ireland, G., Fleming, T.P., and Garrod, D. (2000). The α isoform of protein kinase C is involved in signaling the response of desmosomes to wounding in cultured epithelial cells. Mol. Biol. Cell *11*, 1077–1092. 10.1091/mbc.11.3.1077.

310. Kröger, C., Loschke, F., Schwarz, N., Windoffer, R., Leube, R.E., and Magin, T.M. (2013). Keratins control intercellular adhesion involving PKC-α-mediated desmoplakin phosphorylation. J. Cell Biol. *201*, 681–692. 10.1083/jcb.201208162.
311. Jackson, B., Peyrollier, K., Pedersen, E., Basse, A., Karlsson, R., Wang, Z., Lefever, T., Ochsenbein, A.M., Schmidt, G., Aktories, K., et al. (2011). RhoA is dispensable for skin development, but crucial for contraction and directed migration of keratinocytes. Mol. Biol. Cell *22*, 593–605. 10.1091/mbc.E09-10-0859.
312. Arthur, W.T., Burridge, K., Carolina, N., Hill, C., and Carolina, N. (2001). RhoA Inactivation by p190RhoGAP Regulates Cell Spreading and Migration by Promoting Membrane Protrusion and Polarity. Mol. Biol. Cell *12*, 2711–2720.
313. Totsukawa, G., Wu, Y., Sasaki, Y., Hartshorne, D.J., Yamakita, Y., Yamashiro, S., and Matsumura, F. (2004). Distinct roles of MLCK and ROCK in the regulation of membrane protrusions and focal adhesion dynamics during cell migration of fibroblasts. J. Cell Biol. *164*, 427–439. 10.1083/jcb.200306172.
314. Reeb, T., Rhea, L., Adelizzi, E., Garnica, B., Dunnwald, E., and Dunnwald, M. (2023). ARHGAP29 is required for keratinocyte proliferation and migration. bioRxiv, 1–26.
315. Wojciak-Stothard, B., and Ridley, A.J. (2003). Shear stress–induced endothelial cell polarization is mediated by Rho and Rac but not Cdc42 or PI 3-kinases. J. Cell Biol. *161*, 429–439. 10.1083/jcb.200210135.
316. Vega, F.M., Fruhwirth, G., Ng, T., and Ridley, A.J. (2011). RhoA and RhoC have distinct roles in migration and invasion by acting through different targets. J. Cell Biol. *193*, 655–665. 10.1083/JCB.201011038.
317. Hotchin, N.A., and Hall, A. (1995). The Assembly of Integrin Adhesion Complexes Requires Both Extracellular Matrix and Intracellular rho/rac GTPases. J. Cell Biol. *131*, 1857–1865.
318. Rooij, J. De, Kerstens, A., Danuser, G., Schwartz, M.A., and Waterman-storer, C.M. (2005). Integrin-dependent actomyosin contraction regulates epithelial cell scattering. J. Cell Biol. *171*, 153–164. 10.1083/jcb.200506152.
319. Yano, H., Mazaki, Y., Kurokawa, K., Hanks, S.K., Matsuda, M., and Sabe, H. (2004). Roles played by a subset of integrin signaling molecules in cadherin-based cell–cell adhesion. J. Cell Biol. *166*, 283–295. 10.1083/jcb.200312013.
320. Martinez-Rico, C., Pincet, F., Thiery, J.-P., and Dufour, S. (2010). Integrins stimulate E-cadherin-mediated intercellular adhesion by regulating Src-kinase activation and actomyosin contractility. J. Cell Sci. *123*, 712–722. 10.1242/jcs.047878.
321. Dupin, I., Camand, E., and Etienne-Manneville, S. (2009). Classical cadherins control nucleus and centrosome position and cell polarity. J. Cell Biol. *185*, 779–786. 10.1083/jcb.200812034.
322. Camand, E., Peglion, F., Sanson, M., and Etienne-Manneville, S. (2012). N-cadherin expression level modulates integrin- mediated polarity and strongly impacts on the speed and directionality of glial cell migration. J. Cell Sci. *125*, 844–857. 10.1242/jcs.087668.
323. Quadri, S.K. (2012). Cross talk between focal adhesion kinase and cadherins: Role in regulating endothelial barrier function. Microvasc. Res. *83*, 3–11. 10.1016/j.mvr.2011.08.001.
324. Nobes, C.D., and Hall, A. (1995). Rho, Rac, and Cdc42 GTPases Regulate the Assembly of Multimolecular Focal Complexes Associated with Actin Stress Fibers, Lamellipodia, and Filopodia. Cell *81*, 53–62.

325. Kuo, J.-C., Han, X., Hsiao, C.-T., Yates III, J.R., and Waterman, C.M. (2011). Analysis of the myosin-II-responsive focal adhesion proteome reveals a role for β-Pix in negative regulation of focal adhesion maturation. Nat. Cell Biol. *13*. 10.1038/ncb2216.
326. Totsukawa, G., Yamakita, Y., Yamashiro, S., Hartshorne, D.J., Sasaki, Y., and Matsumura, F. (2000). Distinct roles of ROCK (Rho-kinase) and MLCK in spatial regulation of MLC phosphorylation for assembly of stress fibers and focal adhesions in 3T3 fibroblasts. J. Cell Biol. *150*, 797–806. 10.1083/jcb.150.4.797.
327. Ridley, A.J., Paterson, H.F., Johnston, C.L., Diekmann, D., and Hall, A. (1992). The small GTP-binding protein rac regulates growth factor-induced membrane ruffling. Cell *70*, 401–410. 10.1016/0092-8674(92)90164-8.
328. Jacquemet, G., Morgan, M.R., Byron, A., Humphries, J.D., Choi, C.K., Chen, C.S., Caswell, P.T., and Humphries, M.J. (2013). Rac1 is deactivated at integrin activation sites through an IQGAP1–filamin-A–RacGAP1 pathway. J. Cell Sci. *126*, 4121–4135. 10.1242/jcs.121988.
329. Lim, Y., Lim, S.T., Tomar, A., Gardel, M., Bernard-Trifilo, J.A., Xiao, L.C., Uryu, S.A., Canete-Soler, R., Zhai, J., Lin, H., et al. (2008). PyK2 and FAK connections to p190Rho guanine nucleotide exchange factor regulate RhoA activity, focal adhesion formation, and cell motility. J. Cell Biol. *180*, 187–203. 10.1083/jcb.200708194.
330. Miyauchi, M., Matsumura, R., Kawahara, H., and Gupton, S. (2023). BAG6 supports stress fiber formation by preventing the ubiquitin-mediated degradation of RhoA. Mol. Cell. Biol. *34*, 1–17. 10.1091/mbc.E22-08-0355.
331. Ren, X., Kiosses, W.B., Sieg, D.J., Otey, C.A., Schlaepfer, D.D., and Schwartz, M.A. (2000). Focal adhesion kinase suppresses Rho activity to promote focal adhesion turnover. J. Cell Biol. *113*, 3673–3678.
332. Chen, B.-H., Tzen, J.T.C., Bresnick, A.R., and Chen, H.-C. (2002). Roles of Rho-associated Kinase and Myosin Light Chain Kinase in Morphological and Migratory Defects of Focal Adhesion Kinase-null Cells. J. Biol. Chem. *277*, 33857–33863. 10.1074/jbc.M204429200.
333. Dubash, A.D., Wennerberg, K., García-Mata, R., Menold, M.M., Arthur, W.T., and Burridge, K. (2007). A novel role for Lsc/p115 RhoGEF and LARG in regulating RhoA activity downstream of adhesion to fibronectin. J. Cell Sci. *120*, 3989–3998. 10.1242/jcs.003806.
334. Koetsier, J.L., Amargo, E. V, Todorovic, V., Green, K.J., and Godsel, L.M. (2013). Plakophilin 2 Affects Cell Migration by Modulating Focal Adhesion Dynamics and Integrin Protein Expression. Soc. Investig. Dermatology *134*, 112–122. 10.1038/jid.2013.266.
335. Yamana, N., Arakawa, Y., Nishino, T., Kurokawa, K., Tanji, M., Itoh, R.E., Monypenny, J., Ishizaki, T., Bito, H., Nozaki, K., et al. (2006). The Rho-mDia1 Pathway Regulates Cell Polarity and Focal Adhesion Turnover in Migrating Cells through Mobilizing Apc and c-Src. Mol. Cell. Biol. *26*, 6844–6858. 10.1128/mcb.00283-06.
336. Chrzanowska-Wodnicka, M., and Burridge, K. (1996). Rho-stimulated Contractility Drives the Formation of Stress Fibers and Focal Adhesions. J. Cell Biol. *133*, 1403–1415. 10.1083/jcb.133.6.1403.
337. De Pascalis, C., and Etienne-Manneville, S. (2017). Single and collective cell migration: The mechanics of adhesions. Mol. Biol. Cell *28*, 1833–1846. 10.1091/mbc.E17-03-0134.
338. Katayama, K.I., Melendez, J., Baumann, J.M., Leslie, J.R., Chauhan, B.K., Nemkul, N.,

Lang, R.A., Kuan, C.Y., Zheng, Y., and Yoshida, Y. (2011). Loss of RhoA in neural progenitor cells causes the disruption of adherens junctions and hyperproliferation. Proc. Natl. Acad. Sci. U. S. A. *108*, 7607–7612. 10.1073/pnas.1101347108.

339. Priya, R., Yap, A.S., and Gomez, G.A. (2013). E-cadherin supports steady-state Rho signaling at the epithelial zonula adherens. Differentiation *86*, 133–140. 10.1016/j.diff.2013.01.002.
340. Yamada, S., and Nelson, W.J. (2007). Localized zones of Rho and Rac activities drive initiation and expansion of epithelial cell-cell adhesion. J. Cell Biol. *178*, 517–527. 10.1083/jcb.200701058.
341. Acharya, B.R., Nestor-Bergmann, A., Liang, X., Gupta, S., Duszyc, K., Gauquelin, E., Gomez, G.A., Budnar, S., Marcq, P., Jensen, O.E., et al. (2018). A Mechanosensitive RhoA Pathway that Protects Epithelia against Acute Tensile Stress Article A Mechanosensitive RhoA Pathway that Protects Epithelia against Acute Tensile Stress. Dev. Cell *47*, 439–452. 10.1016/j.devcel.2018.09.016.
342. Wójciak-Stothard, B., Potempa, S., Eichholtz, T., and Ridley, A.J. (2001). Rho and Rac but not Cdc42 regulate endothelial cell permeability. J. Cell Sci. *114*, 1343–1355. 10.1242/jcs.114.7.1343.
343. Walsh, S. V., Hopkins, A.M., Chen, J., Narumiya, S., Parkos, C.A., and Nusrat, A. (2001). Rho kinase regulates tight junction function and is necessary for tight junction assembly in polarized intestinal epithelia. Gastroenterology *121*, 566–579. 10.1053/gast.2001.27060.
344. Anderson, S.C., Stone, C., Tkach, L., and SundarRaj, N. (2002). Rho and rho-kinase (ROCK) signaling in adherens and gap junction assembly in corneal epithelium. Investig. Ophthalmol. Vis. Sci. *43*, 978–986.
345. Carramusa, L., Ballestrem, C., Zilberman, Y., and Bershadsky, A.D. (2007). Mammalian diaphanous-related formin Dia1 controls the organization of E-cadherin-mediated cell-cell junctions. J. Cell Sci. *120*, 3870–3882. 10.1242/jcs.014365.
346. Ryu, J.R., Echarri, A., Li, R., and Pendergast, A.M. (2009). Regulation of Cell-Cell Adhesion by Abi/Diaphanous Complexes. Mol. Cell. Biol. *29*, 1735–1748. 10.1128/mcb.01483-08.
347. Thumkeo, D., Shinohara, R., Watanabe, K., Takebayashi, H., Toyoda, Y., Tohyama, K., Ishizaki, T., Furuyashiki, T., and Narumiya, S. (2011). Deficiency of mDia, an actin nucleator, disrupts integrity of neuroepithelium and causes periventricular dysplasia. PLoS One *6*. 10.1371/journal.pone.0025465.
348. Wheelock, M.J., and Jensen, P.J. (1992). Regulation of Keratinocyte Intercellular Junction Organization and Epidermal Morphogenesis by E-Cadherin. J. Cell Biol. *117*, 415–425.
349. Lewis, J.E., James K, W.I., Sass, K.M., Jensen, P.J., Johnson, K.R., and Wheelock, M.J. (1997). Cross-Talk between Adherens Junctions and Desmosomes Depends on Plakoglobin. J. Cell Biol. *136*, 919–934.
350. Norvell, S.M., and Green, K.J. (1998). Contributions of extracellular and intracellular domains of full length and chimeric cadherin molecules to junction assembly in epithelial cells. J. Cell Sci. *111*, 1305–1318.
351. Shafraz, O., Rübsam, M., Stahley, S.N., Caldara, A.L., Kowalczyk, A.P., Niessen, C.M., and Sivasankar, S. (2018). E-cadherin binds to desmoglein to facilitate desmosome assembly. Elife *7*, 1–18.
352. Godsel, L.M., Dubash, A.D., Bass-Zubek, A.E., Amargo, E. V., Klessner, J.L., Hobbs, R.P., Chen, X., and Green, K.J. (2010). Plakophilin 2 couples actomyosin remodeling to

desmosomal plaque assembly via RhoA. Mol. Biol. Cell *21*, 2844–2859. 10.1091/mbc.E10-02-0131.
353. Nanavati, B.N., Noordstra, I., Verma, S., Duszyc, K., Green, K.J., and Yap, A.S. (2023). Desmosome-anchored intermediate filaments facilitate tension-sensitive RhoA signaling for epithelial homeostasis. bioRxiv. 10.1101/2023.02.23.529786.
354. Anear, E., and Parish, R.W. (2012). The effects of modifying RhoA and Rac1 activities on heterotypic contact inhibition of locomotion. FEBS Lett. *586*, 1330–1335. 10.1016/j.febslet.2012.03.044.
355. García-Mariscal, A., Li, H., Pedersen, E., Peyrollier, K., Ryan, K.M., Stanley, A., Quondamatteo, F., and Brakebusch, C. (2018). Loss of RhoA promotes skin tumor formation and invasion by upregulation of RhoB. Oncogene *37*, 847–860. 10.1038/onc.2017.333.
356. Ho, T.T.G., Merajver, S.D., Lapière, C.M., Nusgens, B. V., and Deroanne, C.F. (2008). RhoA-GDP regulates rhob protein stability potential involvement of RhoGDIα. J. Biol. Chem. *283*, 21588–21598. 10.1074/jbc.M710033200.
357. Simpson, K.J., Dugan, A.S., and Mercurio, A.M. (2004). Functional analysis of the contribution of RhoA and RhoC GTPases to invasive breast carcinoma. Cancer Res. *64*, 8694–8701. 10.1158/0008-5472.CAN-04-2247.
358. Pertz, O., Hodgson, L., Klemke, R.L., and Hahn, K.M. (2006). Spatiotemporal dynamics of RhoA activity in migrating cells. Nature *440*, 1069–1072. 10.1038/nature04665.
359. Vega, F.M., Colomba, A., Reymond, N., Thomas, M., and Ridley, A.J. (2012). RhoB regulates cell migration through altered focal adhesion dynamics. Open Biol. *2*. 10.1098/rsob.120076.
360. Vega, F.M., Thomas, M., Reymond, N., and Ridley, A.J. (2015). The Rho GTPase RhoB regulates cadherin expression and epithelial cell-cell interaction. Cell Commun. Signal. *13*, 1–9. 10.1186/s12964-015-0085-y.
361. Moolenaar, W.H., Kranenburg, O., Postma, F.R., and Zondag, G.C.M. (1997). Lysophosphatidic acid: G-protein signalling and cellular responses. Curr. Opin. Cell Biol. *9*, 168–173. 10.1016/S0955-0674(97)80059-2.
362. Fernandez-Gonzalez, R., Balaghi, N., Wang, K., Hawkins, R., Rothenberg, K., Mcfaul, C., Schimmer, C., Ly, M., Do Carmo, A.M., Scepanovic, G., et al. (2022). PyJAMAS: open-source, multimodal segmentation and analysis of microscopy images. Bioinformatics *38*, 594–596. 10.1093/bioinformatics/btab589.
363. Farrell, D.L., Weitz, O., Magnasco, M.O., and Zallen, J.A. (2017). SEGGA: A toolset for rapid automated analysis of epithelial cell polarity and dynamics. Dev. *144*, 1725–1734. 10.1242/dev.146837.
364. Mashburn, D.N., Lynch, H.E., Ma, X., and Hutson, M.S. (2012). Enabling user-guided segmentation and tracking of surface-labeled cells in time-lapse image sets of living tissues. Cytom. Part A *81 A*, 409–418. 10.1002/cyto.a.22034.
365. Breitsprecher, D., and Goode, B.L. (2013). Formins at a glance. J. Cell Sci. *126*, 1–7. 10.1242/jcs.107250.
366. Rizvi, S.A., Neidt, E.M., Cui, J., Feiger, Z., Skau, C.T., Gardel, M.L., Kozmin, S.A., and Kovar, D.R. (2009). Identification and Characterization of a Small Molecule Inhibitor of Formin-Mediated Actin Assembly. Chem. Biol. *16*, 1158–1168. 10.1016/J.CHEMBIOL.2009.10.006.
367. Nishimura, Y., Shi, S., Zhang, F., Liu, R., Takagi, Y., Bershadsky, A.D., Viasnoff, V., and

Sellers, J.R. (2021). The formin inhibitor SMIFH2 inhibits members of the myosin superfamily. J. Cell Sci. *134*. 10.1242/JCS.253708/237818.
368. Isogai, T., Van Der Kammen, R., and Innocenti, M. (2015). SMIFH2 has effects on Formins and p53 that perturb the cell cytoskeleton. Sci. Reports 2015 51 *5*, 1–15. 10.1038/srep09802.
369. Priya, R., Gomez, G.A., Budnar, S., Verma, S., Cox, H.L., Hamilton, N.A., and Yap, A.S. (2015). Feedback regulation through myosin II confers robustness on RhoA signalling at E-cadherin junctions. Nat. Cell Biol. *17*, 1282–1293. 10.1038/ncb3239.
370. Benink, H.A., and Bement, W.M. (2005). Concentric zones of active RhoA and Cdc42 around single cell wounds. J. Cell Biol. *168*, 429. 10.1083/JCB.200411109.
371. Mahlandt, E.K., Arts, J.J.G., Van Der Meer, W.J., Van Der Linden, F.H., Tol, S., Van Buul, J.D., Gadella, T.W.J., and Goedhart, J. (2021). Visualizing endogenous Rho activity with an improved localization-based, genetically encoded biosensor. 10.1242/jcs.258823.
372. Capuana, L., Boström, A., and Etienne-Manneville, S. (2020). Multicellular scale front-to-rear polarity in collective migration. Curr. Opin. Cell Biol. *62*, 114–122. 10.1016/J.CEB.2019.10.001.
373. Stuelten, C.H. (2017). Using the dot assay to analyze migration of cell sheets. J. Vis. Exp. *2017*, 1–7. 10.3791/56451.
374. Brown, J.M., and Giaccia, A.J. (1998). The unique physiology of solid tumors: Opportunities (and problems) for cancer therapy. Cancer Res. *58*, 1408–1416.
375. Vaupel, P., Kallinowski, F., and Okunieff, P. (1990). Blood flow, oxygen consumption and tissue oxygenation of human tumors. Adv. Exp. Med. Biol. *277*, 895–905. 10.1007/978-1-4684-8181-5_103.
376. Quail, D.F., and Joyce, J.A. (2013). Microenvironmental regulation of tumor progression and metastasis. Nat. Med. *19*, 1423–1437. 10.1038/nm.3394.
377. Hayes, J.D., Dinkova-Kostova, A.T., and Tew, K.D. (2020). Oxidative Stress in Cancer. Cancer Cell *38*, 167–197. 10.1016/j.ccell.2020.06.001.